Geochemical techniques for the exploration and exploitation of geothermal energy

Luigi Marini

Dipartimento per lo Studio del Territorio e delle sue Risorse, Università degli Studi di Genova, Corso Europa 26, 16132 Genova, Italia

Tel 0039-10-3538307

Fax 0039-10352169

e-mail luigi@ugo.dipteris.unige.it

Genova, Ottobre 2000

1. Introduction

Before discussing the geochemical techniques applied in the exploration and exploitation of geothermal resources, it is convenient to recall few general concepts.

Geothermal energy is the natural heat of the earth, which is transferred towards the surface through conductive and convective processes. Because of these processes, the temperature within the earth crust generally increases with depth of ~30 °C/km. Assuming that the yearly average temperature at the earth surface is 15°C, a temperature close to 105°C should be found at ~3 km depth. However, in the present economic and technologic framework, it is generally not convenient to extract these relatively low-temperature fluids from these comparatively great depths. From this simple consideration, it is clear that geothermal energy can be economically exploited in geologically favorable contexts, where a natural thermal engine, which is generally represented by the heat released from magma batches situated at depths of few kilometers, is present. This natural thermal engine triggers the convective circulation of the waters contained in the overlaying rocks. Thus, these fluids ascend towards the earth surface and are stored in relatively shallow reservoirs. These geothermal reservoirs are separated from cold waters, which are generally present at shallow depths, by either primarily impervious layers or by rocks whose poor permeability is due to seal-sealing phenomena.

Since the energy contained in geothermal fluids is much smaller than that contained in the same amount of oil, a further requirement for the economic exploitation of geothermal energy is the storage of geothermal fluids into reservoirs of comparatively high permeability.

Exploitable geothermal systems can be divided in the two following groups, based on their geological setting:

(1) systems situated in areas of either active volcanism or recent magmatism;
(2) systems located in other geological frameworks.

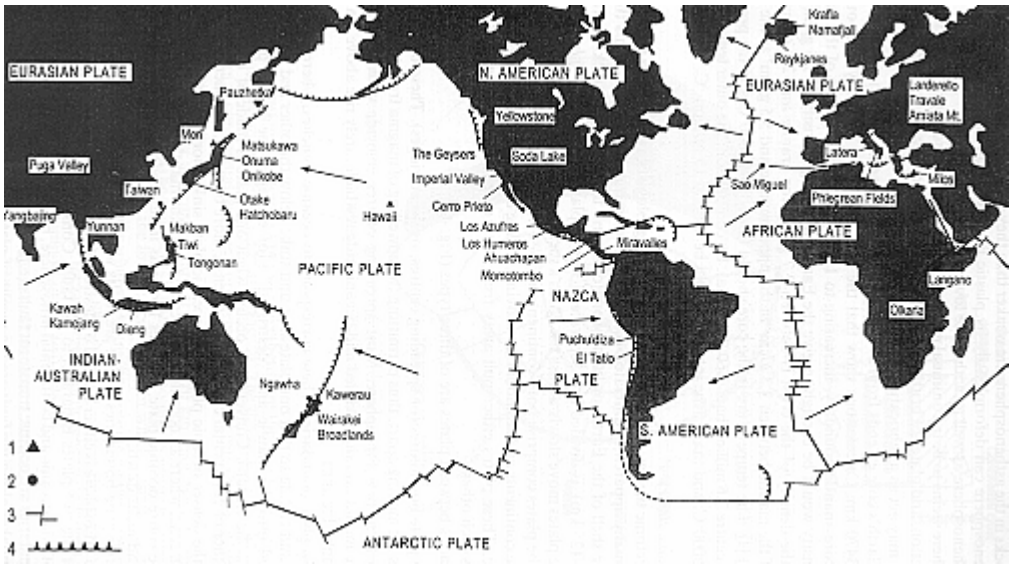

Fig. 1.1. Geographical distribution of high-temperature geothermal systems, compared with lithospheric plate boundaries. 1= fields exploited for electrical production; 2=identified high-temperature fields; 3=mid-ocean ridges and transform faults; 4=convergent plate boundaries (from Barbier, 1997).

The high-temperature (> ~180°C) geothermal systems, which are under exploitation for the conventional generation of electric energy, mostly belong to the first

group, whereas the geothermal systems exploited for direct uses belong to both groups. Since most active volcanoes are situated along the margins of crustal and oceanic plates, high-temperature geothermal systems are also found close to these plate margins (Fig. 1.1). Since Chile is also located in such a tectonic plate context, reference will be made here to high-temperature geothermal systems, starting with a short review of the present knowledge on the origin and evolution of the fluids circulating in active volcanic areas (from Brombach, 2000).

However, geochemical techniques are very important also in investigating low-temperature geothermal systems, such as those of the Alps, as shown, for instance, by Martinotti et al. (1999), Pastorelli et al. (1999), Marini et al. (2000), Pastorelli et al. (2000), and Perello et al. (2000).

2. The origin and evolution of volcanic and geothermal fluids: a review

The study of the origin and evolution of volcanic and geothermal fluids is one of the main concerns of geoscientists since years. Possible sources contributing major and trace elements to these discharges include the magma, the host rocks and the fluids circulating in the subsurface.

Craig (1963) found that the deuterium content of thermal waters was always close to that of local groundwaters (Fig. 2.1). On the basis of these isotopic measurements he suggested that by far the major proportions of water in hydrothermal discharges are of local meteoric origin. About then, Ellis and Mahon (1964) showed that most of the chemical constituents of geothermal waters could simply be leached from crustal rocks. Based on these findings, the formation of hydrothermal solutions was explained largely in terms of the interaction of meteoric waters with crustal rocks at elevated temperatures, with magmatic contributions limited to the supply of heat.

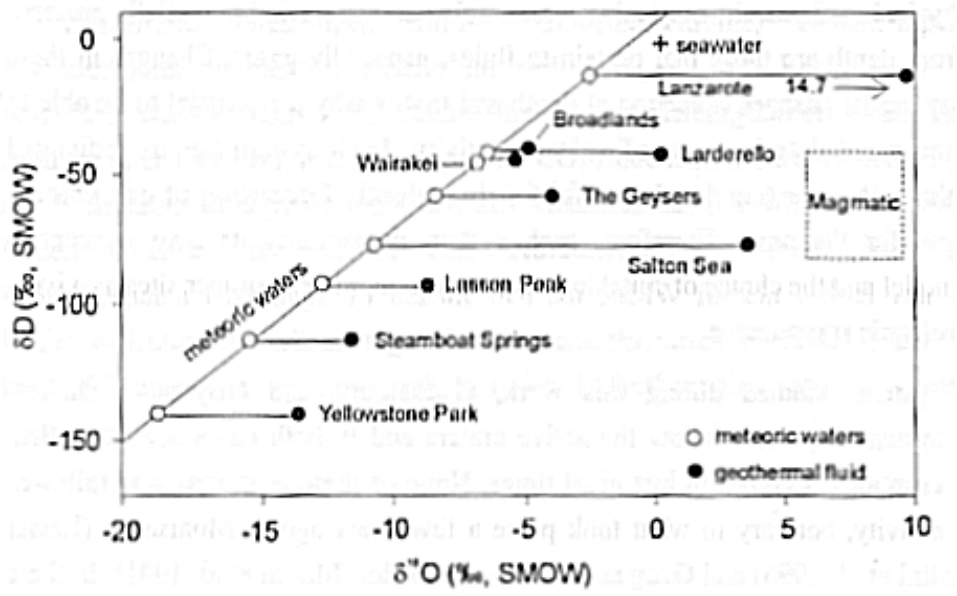

Fig. 2.1 Oxygen isotope shifts of geothermal fluids relative to local meteoric waters. After data of Craig (1963).

Giggenbach (1987), by studying White Island volcano over a long time period and its changes from typically volcanic discharges to "geothermal" discharges got convinced that magmatic contributions to "geothermal" discharges may be much more important than generally assumed. In the meantime, this idea was pronounced by

exploration geologists (Bonham, 1986; Hedenquist, 1987; White and Hedenquist, 1990), who found increasingly convincing evidence of a magmatic connection to ore deposition. Giggenbach (1992a), studied a big number of geothermal systems in volcanic island arcs at different latitudes and stated that the "horizontal"^{18}O shifts, interpreted by Craig as due to water-rock interaction, are rather the exception than the rule. In fact, he found that significant hydrogen shifts from local meteoric water values are common in fluid discharges from island arc volcanoes and proposed a common magmatic endmember for these systems (Fig. 2.2).

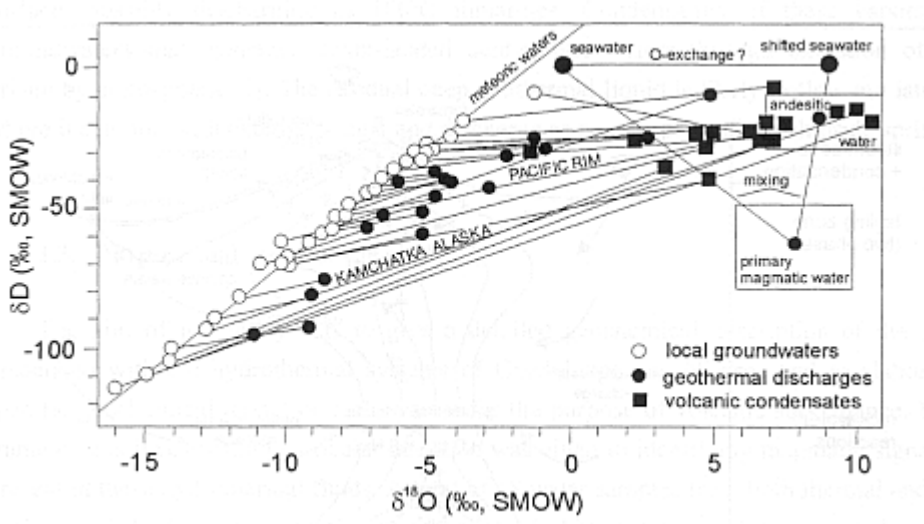

Fig. 2.2 Isotopic composition of geothermal and volcanic water discharges and associated local groundwaters (from Giggenbach, 1992a).

He termed this latter "andesitic" water and suggested that it originated as seawater that was altered during diagenesis and subduction. As shown in Fig. 2.2, volcanic condensates plot close to the andesitic end member indicating high contributions of this latter, whereas the geothermal discharges are in general characterized by much higher proportions in local groundwater.

Besides H_2O, excess amounts of CO_2 and N_2 are also a characteristic of many vapor discharges along convergent plate boundaries (Marty et al. 1989; Varekamp et al. 1992; Kita et al, 1993; Giggenbach and Poreda, 1993; Sano et Marty, 1995; Giggenbach, 1997a). They are generally explained as being derived from the subducted slab. This same origin was proposed for a considerable part of the S and Cl in vapor discharges (Giggenbach, 1996).

In summary, the origin of hydrothermal fluids in volcanic island arcs is depicted in the generally proposed diagram of Fig. 2.3. The generation of a H_2O-rich fluid phase (Stolper and Newman, 1994) initiates partial melting of the mantle wedge in the vicinity of the subduction slab. Dehydration of the sediments that accompany the subducting slab and melting of the slab add components to the melt. The melt thus formed rises through the crust, which may act as another potential source for adding components to the magma. Fluids produced through the degassing of a magma consist mainly of water vapor, CO_2, SO_2 and/or H_2S and HCl (Giggenbach, 1987). Variations in their relative concentrations depend mainly on differences in magmatic volatile solubility and degree of degassing of the magma (Giggenbach, 1996). Absorption of these gases into deep circulating groundwater and cooling leads to the formation of acid, relatively oxidized, and highly reactive solutions. These are reduced and neutralized through the interaction with wall rocks in a zone of primary neutralization, whereby major cations are leached

and added to the fluid (Giggenbach, 1988, 1997a; Reed, 1997). Boiling of the geothermal liquid thus formed, liberates the dissolved gases, which fractionate into the vapor phase that ascends to the surface, discharging at 100ºC fumaroles. Condensation of these vapors into groundwaters may generate steam-heated acid-sulfate waters from atmospheric oxidation of H_2S. The residual deep geothermal liquid is likely to flow out laterally where it can mix with external waters and discharge as neutral-pH chloride springs.

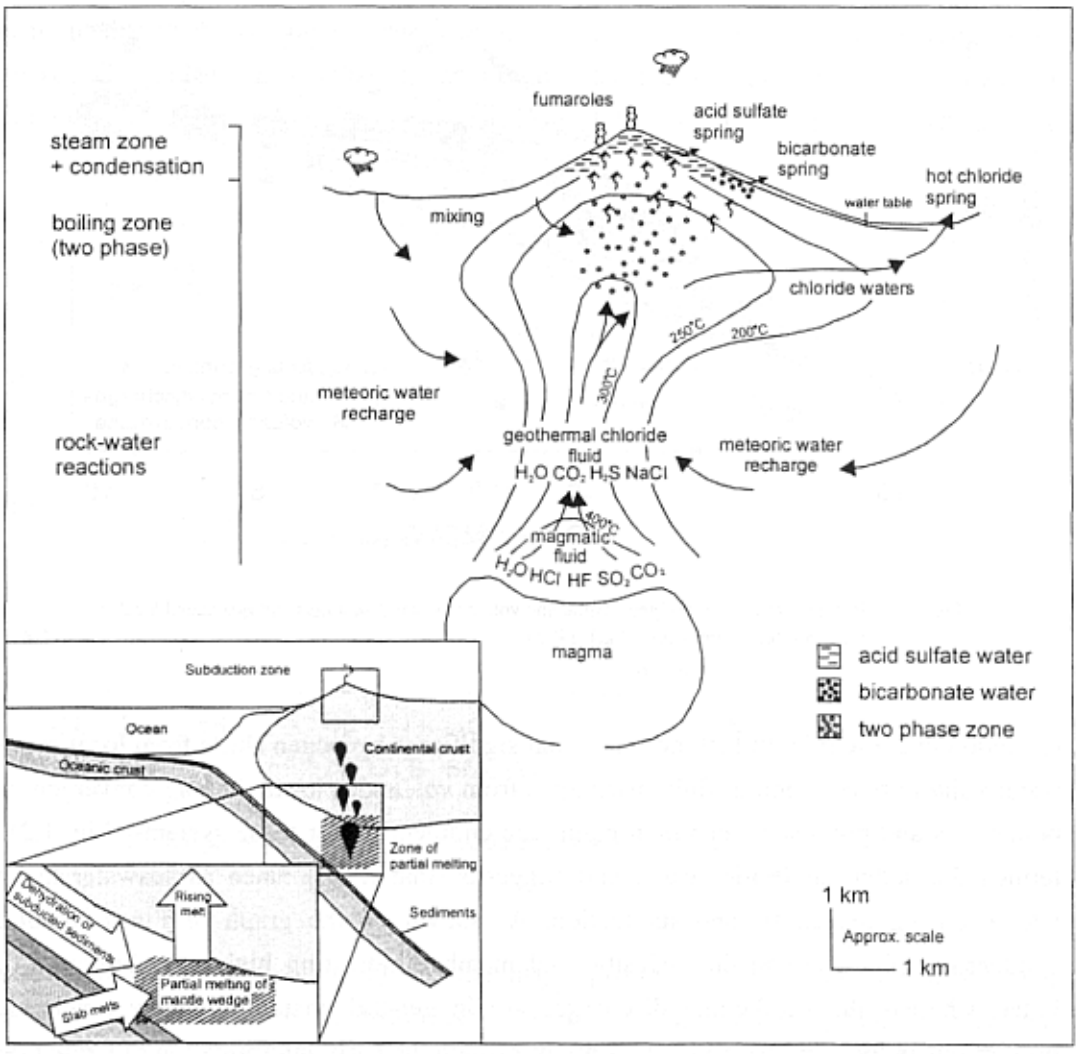

Fig. 2.3 Schematic cross section of a typical hydrothermal-volcanic system in active island-arc andesite volcanoes. Modified, after Hedenquist (1986) and Hedenquist and Lowenstein (1994).

3. Sampling and analysis of geothermal fluids

3.1. Geothermal liquids

The strategies of sampling and analysis of the natural waters circulating in the geothermal area to be investigated (i.e., the number of samples to be collected and the analytical routine) chiefly depend on the scale and state of advancement of each specific project, the available funds, and logistic constraints. In general, it is not advisable either to analyze a large number of chemical and isotopic parameters in a small number of samples nor to determine a small number of chemical parameters in a huge number of

samples. Besides, oversampling is not possible because water samples are stable for limited periods of time.

The best strategy is to collect samples from a reasonable number of thermal and non thermal waters, distributed all over the investigated area, to be analyzed, as soon as possible, for the following constituents: Li, Na, K, Mg, Ca, alkalinity, SO_4, Cl, F, B, SiO_2 and NH_3. Additional constituents useful to investigate specific problems are Al (total and monomeric), H_2S, Rb, Cs, Br, As, and Hg.

If possible, the hydrogeochemical survey should be carried out at the end of the dry season, to get water samples least affected by mixing with surface (rain) water.

3.1.1. Field work

In order to simplify logistics, field operations must be minimized. However, because some species are unstable, they must either be analyzed in the field or preserved by means of simple treatments, such as filtration, acidification, and dilution.

Filtration must be carried out to prevent algal growth, which may bring about removal of dissolved chemical constituents, such as NH_3 and SO_4, and clogging of laboratory instruments during water analysis. Filtration is usually carried out through a 0.45 μm membrane filter, although use of this size does not assure complete removal of suspended solids; in fact, finely dispersed Al-oxyhydroxides may pass through the 0.45 μm membrane filters (Kennedy and Zellweger, 1974; Laxen and Chandler, 1982).

Acidification is needed to preserve cation contents of high-temperature waters, which become supersaturated upon cooling, and to prevent precipitation of trace metals from both high-temperature and low-temperature waters. Acidification is usually done by the addition of either HCl (e.g., 1 ml HCl 1:1 [~6 N] to 50 ml of sample) or HNO_3 (e.g., 0.5 ml HNO_3 1:3 [~4 N] to 50 ml of sample). In order to avoid dissolution of suspended solids, never acidify unfiltered water !

Since precipitation of SiO_2 from supersaturated waters, accompanied by co-precipitation of trace elements (e.g., Al), takes place even at pH as low as 1.5, dilution of filtered or filtered-acidified samples is advisable for silica determination.

Based on previous observations, the following sample aliquots are usually collected:

- a filtered aliquot for the analysis of anions, $D/^1H$ and $^{18}O/^{16}O$ isotopic ratios and ^3H activity;
- a filtered-acidified aliquot for the determination of cations;
- a filtered-diluted (1:10) aliquot for the determination of silica.

Other sample aliquots have to be collected for specific purposes, e.g., complexing with 8-hydroxy-quinoline and extraction in methyl-isobutyl-ketone is needed for the determination of monomeric Al. Sample size depends on the number of constituents to be determined and on laboratory requirements. Large water amounts are generally needed for tritium determination and when trace elements are analyzed after a pre-concentration step. Polyethylene bottles are generally preferred to fragile glass bottles, but acid-cleaned glass bottles are sometimes needed, e.g., for Hg determination.

The field measurements to be carried out are:

- temperature, which is generally measured by means of a digital thermometer; however, normal- and maximum-glass thermometers are also needed for calibration and measurement of hot, unapproachable springs;
- pH by means of a portable, digital mV-pH-meter equipped with a glass electrode;
- Eh by means of a portable, digital mV-pH-meter equipped with a Pt electrode;
- conductivity by means of a portable, digitable conductivity-meter equipped with a suitable cell (range 0.1-100,000 μS/cm);

- alkalinity by acidimetric titration using HCl 0.1 or 0.01 N and methyl orange as indicator; utilization of a microdosimeter (minimum added HCl volume 0.5 μL) allows to work with 200-1000 μL of water. It must be noted that the parameter measured in this way is total alkalinity, Alk_t, although in most non-thermal waters this is practically equal to carbonate alkalinity, Alk_c, i.e., the sum of bicarbonate + carbonate contents (in equivalents). In most geothermal waters and high-pH, high-salinity waters, Alk_t is greater than Alk_c, since other species, mainly $H_2BO_3^-$, $H_3SiO_4^-$, and NH_3, are also titrated. The effects of these species may be corrected carrying out an alkalinity titration followed by CO_2 removal and by a back titration in the laboratory, or by means of speciation calculations. Determination of Alk_t in the field is needed to calculate reliable P_{CO2} values, which are of upmost importance in geothermal prospecting.
- H_2S by addition of a known amount of iodine and titration of excess iodine with sodium thiosulfate; addition of a few drops of starch indicator just before the end point is needed; alternatively, H_2S can be measured by means of the methylene blue colorimetric method; the analysis of H_2S is generally performed for environmental purposes and is not part of the standard analytical routine.

Flowrate of springs can be roughly evaluated by measuring the time needed by a leaf or some other floating object to travel a known distance along the flow channel. The distance/time ratio represents the average water velocity. The flowrate is then obtained by multiplying the average water velocity times the average cross-section of the channel. Consistent units have to be used.

Sample number and other details have to be written on bottles by using indelible marker pen. Results of field analyses and other sampling details have to be written in a field note book.

3.1.2. Geothermal wells

The geothermal wells, which tap a single liquid phase at temperatures > 100°C under reservoir conditions, obviously discharge two-phase liquid + vapor mixtures, which are generated through boiling of the original single liquid phase (incidentally, it must be noted that the term “vapor” is commonly used in the geothermal slang instead of the proper term “gas”).

Sampling and analysis of both liquid and vapor phases, separated at known P,T conditions, are required to recalculate the composition of the original single liquid phase. The two phases can be separated by means of either a wellhead pressure separator, if available, or a small-scale sampling line, comprising a small Webre-type separator, a cooler for the separated liquid, a cooler-condenser for the separated vapor, and a gas/condendate separator (e.g., Fig. 3.1).

A similar equipment (Fig. 3.2) was earlier described by Ellis and Mahon (1977) and Giggenbach and Goguel (1989) and references therein, where operating procedures are also found.

The composition of the single liquid phase under reservoir conditions is then calculated by means of the simple mass balance:

$$C_O = C_L (1 - y) + y C_V \qquad (3.1)$$

Indices O, L, V refer to the single liquid phase initially present in the geothermal reservoir, the liquid phase at separation conditions, and the vapor phase (see below) at separation conditions, respectively, and y is the steam fraction.

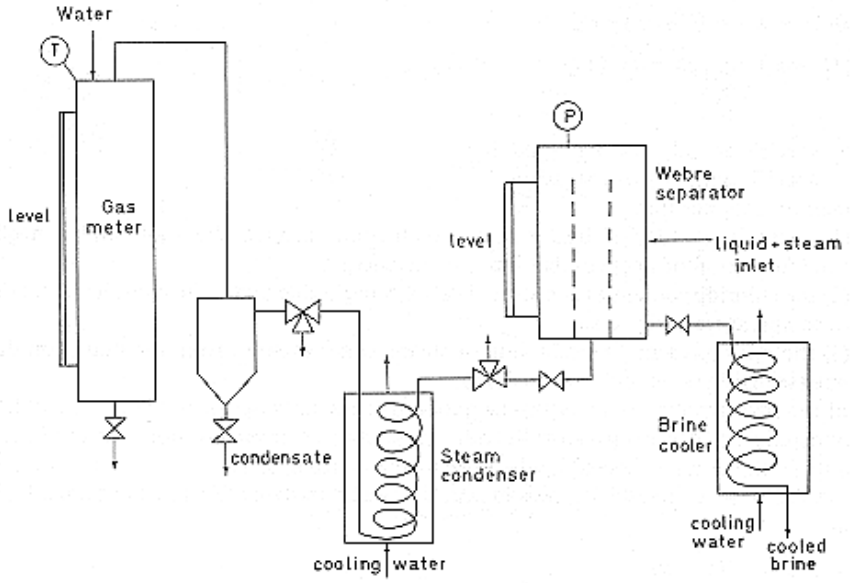

Fig. 3.1. Small-scale sampling line for geothermal well discharges (Marini and Cioni, 1985).

From the previous discussion it is clear that when samples of separated liquid and vapor phases are collected from a geothermal well, it is necessary to know:

- separation temperature and/or pressure (specifying if bar-g or bar-a);
- well-bottom temperature and/or pressure and total discharge enthalpy.

Above it was hypothesized the presence of a single liquid phase in the geothermal reservoir. Although this is the most frequent situation, it is not the only one, since either a biphase liquid + vapor mixture or a single vapor phase can also be present in the reservoir. These possibilities can be ascertained by accurate enthalpy data or by gas geochemistry (Giggenbach, 1980; Bertrami et al., 1985).

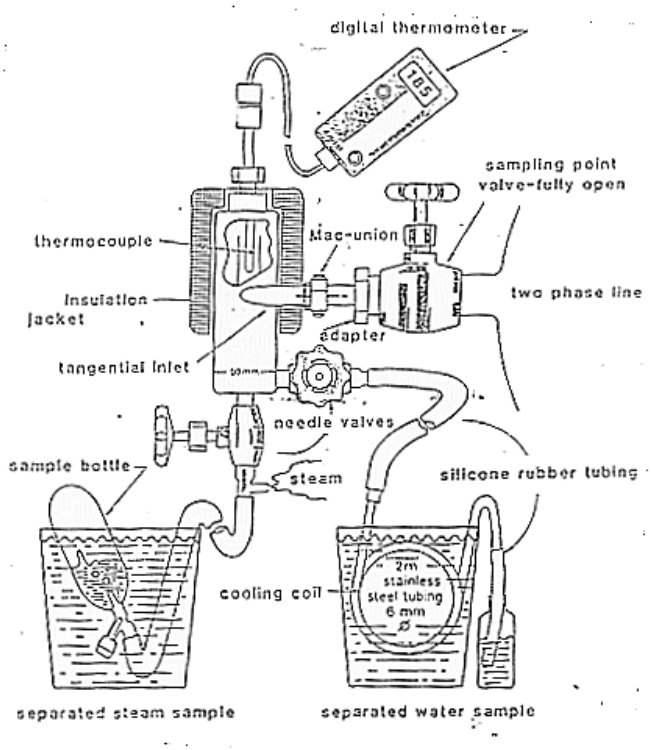

Fig. 3.2. Sampling line for two-phase geothermal discharges (from Giggenbach and Goguel, 1989).

3.1.3. Laboratory analyses

The standard instruments required in the analysis of geothermal samples includes:

- double beam or modern single beam atomic absorption spectrophotometer for the determination of cations, as well as boron (> 10 mg/kg) and silica;
- ionic chromatograph for the analysis of most anions, except fluoride and bicarbonate;
- visible-UV spectrophotometer for the colorimetric determination of boron (curcumine method) and silica (ammonium molybdate method);
- automatic titrator for the determination of alkalinity;
- pH-mV-meter which allows one to read 0.001 pH-unit and 0.1 mV, equipped with glass-electrodes for pH determination, and fluoride- and ammonia- specific electrodes.

Giggenbach and Goguel (1989) give a detailed description of the instruments and methods, which are usually used for the analysis of geothermal liquids.

In order to reduce errors in laboratory analyses, it is advisable to prepare concentrated standards from commercial solutions, to prepare diluted standards daily, to introduce frequently diluted standards in the analytical routine (to get rid of instrumental drifts), to repeat the analysis of a given sample (stored in sufficient amount in the lab), although the concentration of some solutes may change with time.

The quality of water analysis is usually checked computing the ionic balance; however, possible errors for minor constituents (e.g., Li, F, etc., but also Mg and SO_4 in high-temperature geothermal liquids) or neutral species (e.g., SiO_2, H_3BO_3, NH_3) cannot be detected in this way. At best, ionic balance gives an indication on the analytical accuracy of major constituents.

3.2. Geothermal gases

Gothermal gas samples are usually analysed for H_2O, CO_2, H_2S, NH_3, He, Ar, O_2, N_2, H_2, CH_4, and CO; in addition to these constituents, HCl, HF and oxidized S species (mainly SO_2, and subordinately S_2 and SO_3) have to be taken into account too in high-temperature volcanic gases.

3.2.1 Sampling of geothermal gases

Geothermal and volcanic gases are commonly sampled into ~250 ml bottles equipped with one or two Torion or Rotaflo valves (Giggenbach, 1975a; Giggenbach and Goguel, 1989). In the laboratory, ~50 ml of a 4N NaOH solution are fed into these partly evacuated bottles, which are then evacuated by means of a rotary oil pump, and weighted. The low pressure inside the bottle is indicated by the characteristic clicking sound upon shaking. Since the NaOH solution has to be carbonate free, it is advisable to quickly wash the NaOH pellets with distilled water. Besides one bottle have to be stored to determine the analytical blank.

For fumarole sampling a glass tube or a glass funnel is inserted into the vent; the discharge end of the apparatus is equipped with a short rubber pipe, where the bottle will be connected, after a given time, which must be sufficient to heat the sampling train and purge it from air (Fig. 3.3).

The fumarolic gas is allowed to enter the bottle by slowly opening the valve. Then, the valve must be regulated to have a high gas flow entering the bottle, to minimize water loss due to condensation. Condensation cannot be avoided, but the drops of steam condensate, which form in the pipes, have to be transferred to the bottle. The bottle must be held with the entrance down, in order to allow interaction between the gas and the alkaline solution.

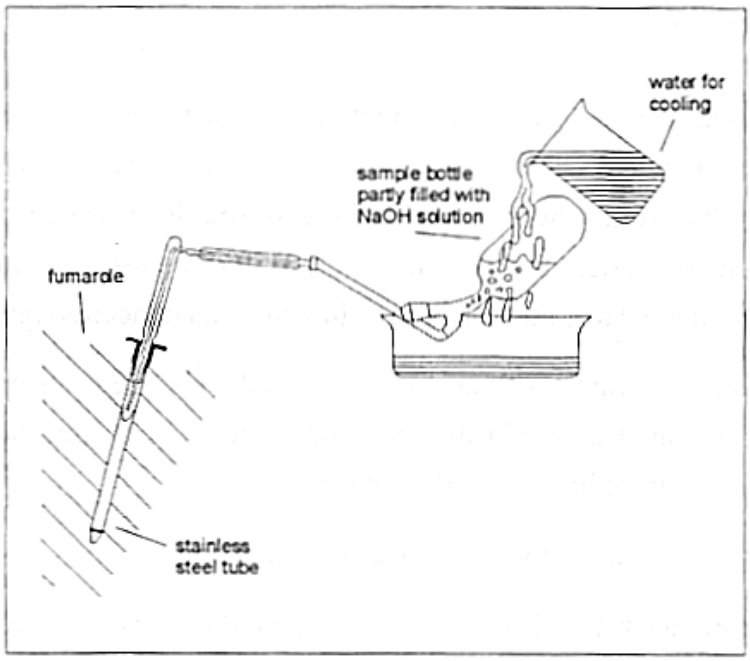

Fig. 3.3. Sampling of fumarolic gases by use of a NaOH charged bottle (from Brombach, 2000).

This interaction brings about condensation of water vapor (the process has to be favored by cooling the bottle with cold water) while the acidic gases (CO_2 and H_2S in geothermal gases, plus SO_2, HCl, and HF in volcanic gases) are absorbed in the alkaline solution, according to the following reactions:

$$CO_{2(g)} + 2\ OH^- = CO_3^{2-} + H_2O \quad (3.2)$$

$$H_2S_{(g)} + OH^- = HS^- + H_2O \quad (3.3)$$

$$4\ SO_{2(g)} + 7\ OH^- = 3\ SO_4^{2-} + HS^- + 3\ H_2O \quad (3.4)$$

$$HCl_{(g)} + OH^- = Cl^- + H_2O \quad (3.5)$$

$$HF_{(g)} + OH^- = F^- + H_2O \quad (3.6)$$

The non-absorbed gases (N_2, O_2, H_2, CH_4, He, Ar, ...) dissolve subordinately in the alkaline solution liquid phase and are chiefly collected in the head space above it. Therefore the flowrate of fumarolic gases entering the bottle will slow due to increasing pressure of the gases accumulating in the head space (the gas flow is obviously driven by the pressure difference between the vent and the bottle itself). If the bottle is not properly cooled also water participates significantly to gas pressure. When the flowrate slows the valve must be closed. The amount of gases that can be sampled is limited by either: (1) exhaustion of NaOH, for fluids rich in acid gases ; (2) exhaustion of vacuum, for fluids rich in non-absorbed gases; (3) exhaustion of the liquid space, for fluids rich in water. If the chemical characteristics of the discharged fluids are known, the amount of NaOH can be adjusted accordingly.

Steam or gas discharges from a pool are collected following the same procedure of fumarole sampling. In this case a glass or plastic funnel is attached to the sampling line (Fig. 3.4). Metals should be avoided, to prevent H_2 production through reaction with acidic solutions, which are common in steam-heated pools. The funnel must be placed near the point where gas or steam enters the pool to prevent air contamination (pool water is aerated), which brings about addition of atmospheric gases, e.g., N_2, O_2 and Ar and consequent removal of H_2S and other reduced species through reaction with O_2.

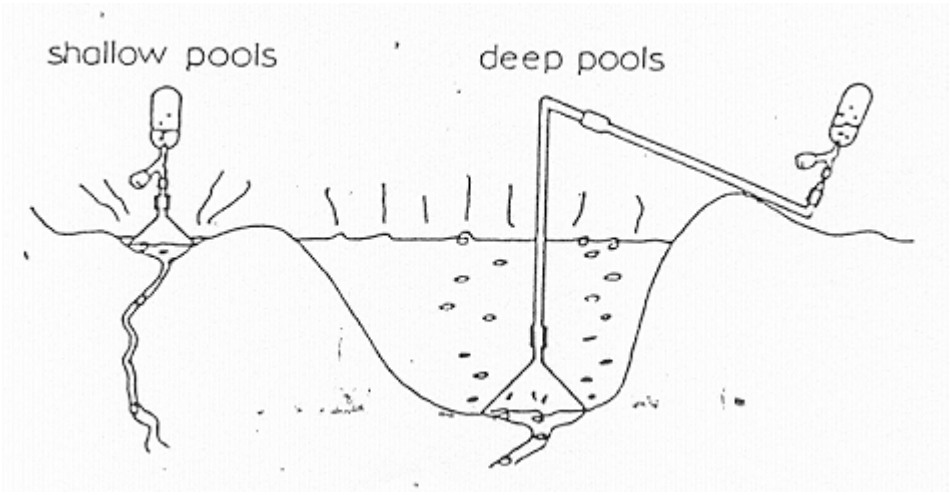

Fig. 3.4. Sampling of geothermal gases from pools (from Giggenbach and Goguel, 1989).

The same NaOH charged bottles can be used also to collect steam samples from geothermal well discharges, either from a steam line downstream of the wellhead pressure separator (in this case a T-piece should be used for safety reason) or by means of a small-scale sampling line (see above).

Use of NaOH charged bottles allows representative sampling of both geothermal and volcanic gases. The only disadvantage of this procedure is the reaction of excess NaOH with CO to produce sodium formate, whose kinetics is described by Giggenbach and Matsuo (1991). For CO determination, separate samples have to be collected, downstream of a condenser-separator (Fig. 3.5), which is cooled with either boiling diethyl ether or ice + liquid water or just water. Use of ether or ice maintains condensation temperature constant at 38°C or 0°C, respectively, whereas if water is used, condensation temperature must be checked and kept constant by regulating the water flow. Use of this equipment allows one to collect also samples of steam condensates (for the determination of the $D/^{1}H$ and $^{18}O/^{16}O$ ratios of H_2O). Uncondensable gases can also be used for isotopic analyses, e.g., the $^{13}C/^{12}C$ and $^{18}O/^{16}O$ ratios of CO_2.

3.2.1 Laboratory analysis of geothermal gases

As indicated by Giggenbach and Goguel (1989), in the laboratory, NaOH charged bottles are weighted again to determine the total amount of collected gases, A_c.

Then the first analytical step is the chemical (and eventually isotopic) analysis of non-absorbed gases, to avoid air contamination. Chemical analysis of non-absorbed gases, including CH_4 but excluding higher hydrocarbons, is performed by gas chromatography, for instance by employing two distinct gas chromatographs (Giggenbach and Goguel, 1989; Fig. 3.6).

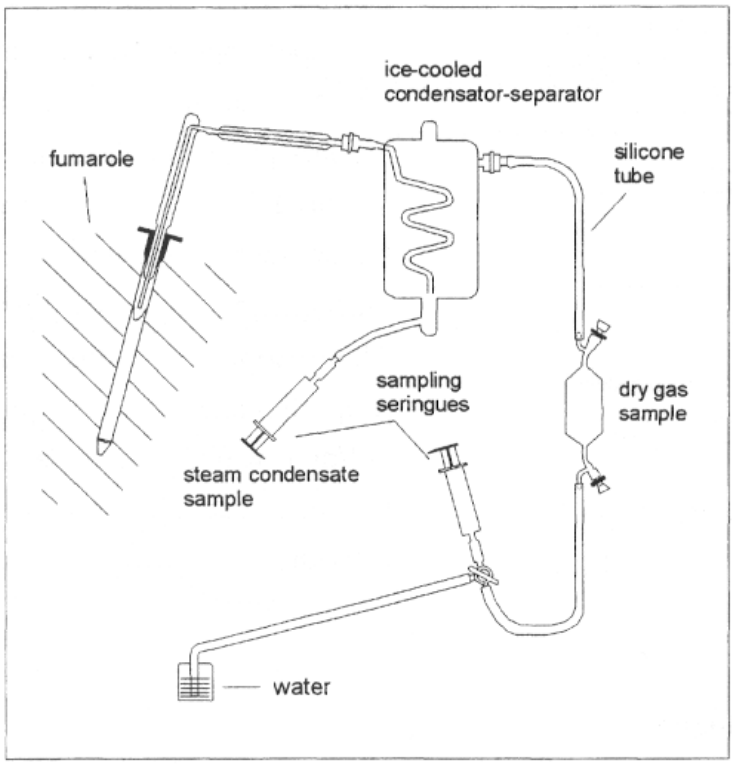

Fig. 3.5 Sampling of fumarolic gases by use of a condenser-separator (from Brombach, 2000).

High sensitivity determinations of He and H_2, and lower sensitivity analyses of O_2, N_2 and CH_4 are carried out by using a gas chromatograph equipped with a thermal conductivity detector (TCD). Gases are separated on a column packed with 5 Å molecular sieves, at 30°C, employing Ar as gas carrier.

High sensitivity determinations of Ar, N_2, and CH_4 are performed by using an other GC equipped with TCD, after separation on a first column packed with 5 Å molecular sieves, at 80°C, and combustion of O_2 in a second column also packed with 5 Å molecular sieves, but kept at 220°C, employing H_2 as gas carrier.

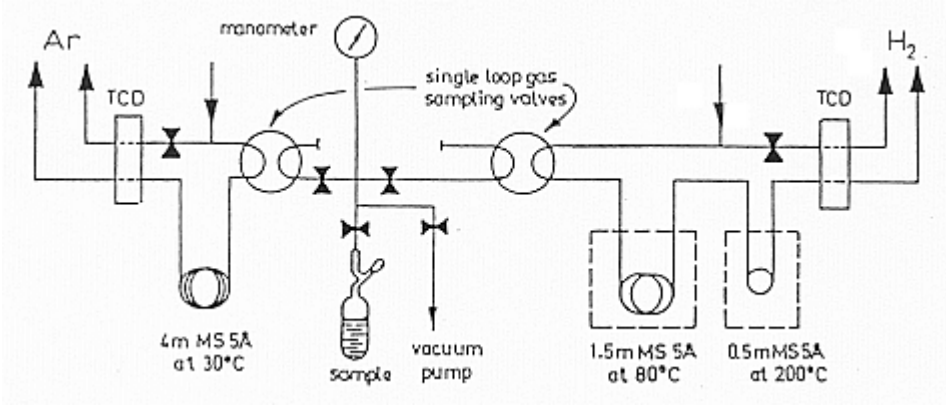

Fig. 3.6 Plumbing of the two gas-chromatograph used for chemical analysis of non-absorbed gases (from Giggenbach and Goguel, 1989)

For calibration, a series of gas mixtures are introduced in the gas chromatographs at known pressure (sample injection pressure must be noted too). The partial pressure of

the gases refers to the volume constituted by the head space in the bottle and the gas inlet system, which is equal to $V_f - V_c + V_g$, where V_c is the condensate volume in the bottle, V_g the volume of the gas inlet system, and V_f the volume of the empty bottle, which was previously determined by difference between the weight of the bottle filled with water and the weight of the empty bottle.

Upon completion of chemical (and eventually isotopic) analysis of non-absorbed gases, the condensate is collected into a cylinder and its volume V_c (in ml) is measured. Different portions of the condensate are then analyzed for:

(1) ammonia, as soon as possible, by means of a gas sensing ammonia electrode;

(2) hydrogen sulfide, as soon as possible, by addition of a known amount of iodine and titration of excess iodine by using sodium thiosulfate; alternatively, H_2S can be analyzed by ionic chromatography, after peroxide oxidation of sulfide to sulfate;

(3) carbon dioxide, through acidimetric titration; first H_2S must be removed, either through peroxide oxidation of sulfide to sulfate or precipitation of sulfide with $AgNO_3$; then a glass pH electrode is inserted in the solution and the pH is brought to 8.3, through careful addition of 0.1 N HCl, in order to convert carbonate to bicarbonate; finally the true titration is carried out from pH 8.3 to pH 3.8, where the bicarbonate is totally converted to carbonic acid (Fig. 3.7).

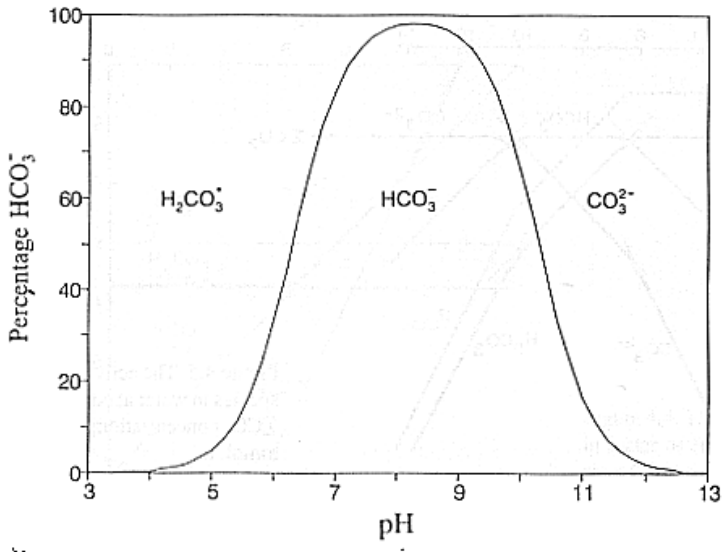

Fig. 3.7 Distribution of dissolved carbonate species as a function of pH (from Appelo and Postma, 1996)

The amount W_i (in mg) and M_i (in mmol) of each component is then calculated on the basis of the concentrations C_i (in mg/L) obtained by wet chemistry analyses, by means of the relationships:

$$W_i = C_i V_c /1000, \quad (3.7)$$

$$M_i = W_i / MWi, \quad (3.8)$$

where MWi is the molecular weight of the i-th component.

Following Giggenbach and Goguel (1989), the amounts of "nonabsorbed " gases M_i, in mmol, are calculated taking into account the dissolution of each component in the alkaline solution:

$$M_i = P_i (((V_f - V_c + V_g)/22400) + (Vc/18\ K_i)) \quad (3.9)$$

Where P_i is the gas pressure in mbar measured by gas chromatography (see above) and K_i is the Henry's Law constant at 20°C, in bars (mole fraction)$^{-1}$:

$K_{He} = 142{,}900$ $K_{O2} = 39{,}840$

K_{N2} = 78,740 K_{Ar} = 36,400

K_{H2} = 65,500 K_{CH4}= 36,100

The moles of water collected are then obtained as follows:

$$M_{H2O} = (W_c - W_{CO2} - W_{H2S} - W_{NH3} - 4\,M_{He} - 2\,M_{H2} - 40\,M_{Ar} - 32\,M_{O2} - 28\,M_{N2} - 16\,M_{CH4}) / 18000, \quad (3.10)$$

where W_c is the amount of sample collected in mg.

The individual gas fractions of all components except H_2O, X_i, in mmol/mol dry gas are computed by means of:

$$X_i = 1000\,M_i / \Sigma M_i \quad (3.11)$$

Finally the gas fraction, in mmol/mol total vapor is computed as follows:

$$Xg = 1000\,\Sigma M_i / (M_{H2O} + \Sigma M_i) \quad (3.12)$$

Carbon monoxide and hydrogen are analyzed, by means of a gaschromatograph fitted with a Reduced Gas Detector (HgO), in the separated sample of dry gas. Hydrogen is used as reference component to calculate the CO fraction in total vapor.

4. Types of waters generally present in high-enthalpy geothermal areas

The waters circulating in high-enthalpy geothermal areas are generally ascribable to the four types described below (e.g., Ellis and Mahon, 1977; Henley et al., 1984; Giggenbach, 1988). It must be underscored, however, that each of these waters may mix with each other giving rise to hybrid water types. The usual location of the different types of waters is sketched in Fig. 4.1.

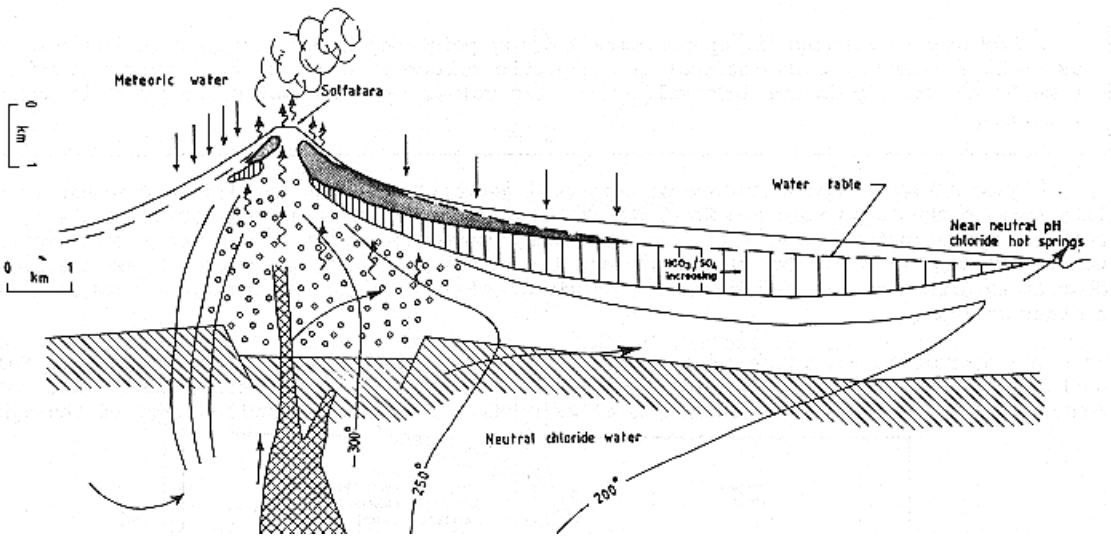

Fig. 4.1. Sketch of a geothermal system typical of active island-arc andesite volcanoes, showing the usual location of the different types of waters (from Henley and Ellis, 1983).

4.1. Sodium-chloride waters

Waters circulating in deep, high-enthalpy geothermal reservoirs usually have sodium-chloride composition and chloride contents ranging up to ten thousand mg/kg, although in some systems (e.g., Salton Sea, California) chloride may be as high as 155,000 mg/kg.

The pH of these waters is close (± 1 or 2 units) to the neutral pH for the temperatures of the waters (e.g., 5.5-5.6 at 200-300 °C). Silica, potassium, lithium, boron, fluoride are much higher than in cold waters. The high chloride waters also

contain appreciable calcium. Magnesium is instead much lower than in cold waters. The main dissolved gases are CO_2 and H_2S.

In general, the waters circulating in deep, high-enthalpy geothermal reservoirs are mainly of meteoric origin, but in some systems connate or other saline waters may be present. In geothermal systems with close volcanic-magmatic association and located along convergent plate boundaries, the deep, magmatic heat source may add acid gases like HCl, HF, SO_2, H_2S and CO_2 as well as some 'andesitic' water (Giggenbach, 1992a). Conversion of the initially acid aqueous solutions to neutral sodium-chloride waters requires extensive rock-water interaction and virtually complete removal of magmatic sulfur species in the form of sulfates and sulfides.

The deep sodium-chloride waters may flow directly to the surface and discharge from boiling, high chloride springs, whose pH ranges from near neutral to alkaline; alternatively they may mix with shallow, low-salinity waters to give relatively diluted chloride waters.

Because of the morphologic-hydrologic structure of the volcanoes distributed along convergent plate boundaries, in these areas sodium-chloride waters frequently discharge from springs located several kilometers away from the upflow part of the geothermal systems (Fig. 4.1).

4.2. Acid-sulfate waters

Acid-sulfate waters are typically found above the upflow part of the geothermal systems, where steam separation takes place. Boiling results in the transfer of gas species, mainly CO_2 and H_2S, into the vapor phase. This vapor phase can reach the surface without any interaction with shallow or surface waters, in the form of fumaroles and steam jets. Alternatively, separated vapor may condensate, at least partly, in shallow groundwaters or surface waters to form steam-heated waters. In this environment, atmospheric oxygen oxidizes H_2S to sulfuric acid producing acid-sulfate waters. These are characterized by low chloride contents and low pH values (0 to 3) and react quickly with host rocks to give advanced argillic alteration parageneses, which are dominated by kaolinite and alunite. Dissolved cations and silica are mainly leached from the surrounding rocks, whose compositions may be approached by these acid waters.

Shallow steam-heated waters may themselves boil, separating secondary steam, which reaches the surface in the form of low-pressure steaming grounds.

4.3. Sodium-bicarbonate waters

Bicarbonate-rich waters originate through either dissolution of CO_2-bearing gases or condensation of geothermal steam in relatively deep, oxygen-free groundwaters. Because the absence of oxygen prevents oxidation of H_2S, the acidity of these aqueous solutions is due to dissociation of H_2CO_3. Although it is a weak acid, it converts feldspars to clays, generating neutral aqueous solutions, which are typically rich in sodium and bicarbonate, particularly at medium-high temperature. In fact:

(1) the low solubility of calcite prevents the aqueous solution to increase in calcium content;
(2) potassium and magnesium are fixed in clays and chlorites, respectively;
(3) sulfate concentration is limited by the low solubility of anhydrite.

Sodium-bicarbonate waters are generally found in the 'condensation zone' of vapor-dominated systems and in the marginal parts of liquid-dominated systems. However, sodium-bicarbonate waters are also present in deep geothermal reservoirs hosted in metamorphic and/or sedimentary rocks (e.g. Kizildere, Turkey).

4.4. Acid chloride-sulfate waters

This type of waters is commonly found in crater lakes such as El Chichón (Casadevall et al. 1984), Kawah Ijen (Delmelle and Bernard, 1994), Poás (Brantley et al., 1987; Rowe et al., 1992), Ruapehu (Giggenbach, 1975b; Christenson and Wood, 1993), Sirung (Poorter et al., 1989), Yugama and Yakeyama (Takano and Watanuki, 1990). The chemistry of crater lakes' waters, especially during periods of intense volcanic activity, is obviously dominated by inflow and absorption of magmatic gases rich in HCl and S species, mainly SO_2 and H_2S (e.g., Aguilera et al., 2000 and references therein), leading to the production of strongly reactive aqueous solutions. In fact, through dissolution in liquid water, SO_2 disproportionates as specified by the following reaction (Murray and Cubicciotti, 1983):

$$4\ SO_2 + 4\ H_2O \Rightarrow H_2S + 3\ H_2SO_4. \qquad (4.1)$$

In crater lakes these highly acid oxidized solutions are very reactive with respect to cation leaching or rock dissolution, leading to deposition of alunite, anhydrite, pyrite, and kaolinite. Nevertheless the low availability of rocks in lacustrine environments often prevents the neutralization of the acid aqueous solutions. At greater depths, magmatic gases interact with water and masses of rocks much larger than in crater lakes, and at higher temperatures and for longer periods of time, with respect to crater lakes, thus leading to higher extents of neutralization and ultimately to the formation of neutral NaCl waters (Giggenbach, 1997a; Reed, 1997).

Consistently, acid Cl-SO_4 to SO_4-Cl waters are rare in geothermal reservoirs associated with recent volcanism, as pointed out by Truesdell (1991) who reports the best documented examples of deep geothermal wells producing acid waters, i.e., Tatun, Sumikawa and Miravalles, and discusses their origin.

At Tatun, acid Cl-SO_4 waters come from a geothermal reservoir which is mostly developed within a 900 m-thick sequence of orthoquartzitic sandstones (containing only quartz, kaolinite, and minor alunite, and elemental sulfur) and subordinately within highly altered andesites. The HCl introduced in the Tatun reservoir water, most probably from a volcanic source, is not neutralized through water-rock interaction because no minerals capable of neutralizing acids are present in the reservoir rocks.

Both well S-2 at Sumikawa and well PGM-2 at Miravalles started to produce acid SO_4-Cl waters after deepening. The pH of the brine of well PGM-2, separated at atmospheric pressure and cooled at 25°C is 2.2-2.4. This acidity is governed by dissociation of bisulfate ion, HSO_4^-. Because this acid is more strongly associated at high temperature than at low temperature, the decrease in temperature driven by iso-enthalpic boiling causes the dissociation of HSO_4^- and the consequent production of H^+. Since the supply of H^+ ion from dissociation of bisulfate exceeds the removal of protons by CO_2 loss, the pH value decreases. Therefore the pH under reservoir conditions is higher, probably close to 3.3 at 230°C, as indicated by chemical modeling.

The most likely hypotheses to explain the origin of these waters are: (a) mixing of shallow acid SO_4 waters with neutral NaCl waters and (b) inflow of magmatic gases in the geothermal reservoir and incomplete neutralization of such fluids. The first hypothesis requires very high concentrations of SO_4 to be present in the acid SO_4 waters, close to 65,000 mg/kg at Miravalles and 130,000 mg/kg at Sumikawa (see Truesdell, 1991 for further details). Since these concentrations are unrealistically high, hypothesis (a) appears to be very unlikely, although not impossible. Mechanism (b) is considered to be most likely (Truesdell, 1991; Giggenbach and Corrales Soto, 1992) and is also consistent with the general conceptual geochemical model of the hydrothermal systems with close volcanic-magmatic association (Giggenbach, 1988, 1997a; Reed, 1997).

Corrosive acid SO_4-Cl waters were also found in some geothermal fields of the Philippines, such as Tiwi, Mt. Labo, Cagua, and Mt. Pinatubo (Sussman et al., 1993). Again, these acid waters do not come from separate reservoirs, but are produced through inflow of acid magmatic gases into the deepest portions of convecting neutral-pH, NaCl systems (Delfin et al., 1992; Reyes, 1990; Reyes and Giggenbach, 1992). In particular, at Mt. Pinatubo, the high-temperature (>350°C), corrosive fluids were encountered by three wells drilled a few years before the 1991 volcanic eruption. These data testify, once more, that the acidity and the chemistry of the aqueous solution depends on the extent of water-rock "titration", which is also a function of the amount of magmatic gases added to the water and of the availability of minerals which are able to neutralize acids.

5. The chemical classification of waters

The chemical classification of waters is essential for a correct utilization of geochemical techniques, which can be confidently applied only to particular kinds of fluids with limited ranges of composition, reflecting the environment of provenance.

For instance, most ionic solute geothermometers (see below) can be applied only to the samples representative of water-rock equilibrium at depth. This assumption is usually fulfilled for neutral sodium-chloride waters only. Therefore these samples have to be properly identified and selected. Furthermore, possible phenomena affecting the original characteristics of sodium-chloride waters (i.e., addition of cold, shallow groundwaters, boiling, dissolution or precipitation of mineral phases) have to be recognized and evaluated.

The chemical classification of waters can be carried out following different techniques, some of which are listed below.

5.1. The Schoeller plot

It displays the log contents of several constituents for each water sample; these values are connected with a line, whose shape allows an "eyeball" comparison of the different waters plotted.

As an example, in Fig. 5.1 thermal waters exhibit higher concentrations of Li, Na, K, F, Cl, SO_4 and B, than cold waters, which have higher contents of Mg and Ca. Bicarbonate is similar in cold and thermal waters.

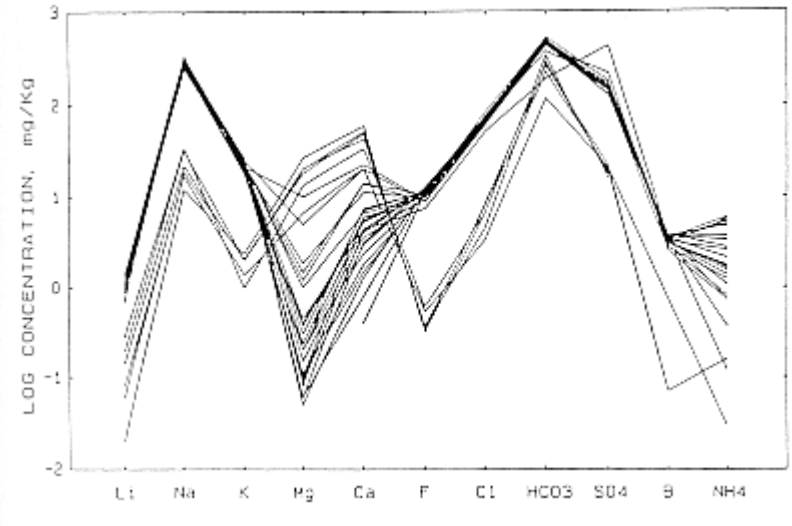

Fig. 5.1 The Schoeller plot of hot and cold waters from San Ignacio, Honduras (from Truesdell, 1991)

Because logarithmic values are used, a wide range of contents can be arranged in this plot. The effect of mixing with dilute water, as well as gain or loss of steam, is to move the line representing a sample vertically without changing its shape.

The main disadvantage of this procedure is that when many samples are represented on the same plot, individual patterns are lost.

5.2. The Cl-SO_4-HCO_3 triangular plot

The Cl-SO_4-HCO_3 triangular plot is used for an initial classification of geothermal water samples (Giggenbach, 1988; Giggenbach and Goguel, 1989). The position of a data point in this plot is obtained by first calculating the sum Σ_{an} of the concentrations c_i (in mg/kg) of all three species involved:

$$\Sigma_{an} = c_{Cl} + c_{SO4} + c_{HCO3} \quad (5.1)$$

Then the percentages of chloride, %Cl, and bicarbonate, %HCO_3, are evaluated according to:

$$\%Cl = 100\ c_{Cl} / \Sigma_{an} \quad (5.2)$$

$$\%HCO_3 = 100\ c_{HCO3} / \Sigma_{an} \quad (5.3)$$

In this plot (Fig. 5.2) are indicated the compositional ranges for the different kinds of waters typically found in geothermal areas, such as:

(1) mature NaCl waters of neutral pH, which are rich in Cl and plot near the Cl vertex;
(2) Na-HCO_3 waters, here indicated as peripheral waters
(3) volcanic and steam-heated waters, generated through absorption into groundwater of either high-temperature, HCl-bearing volcanic gases or lower-temperature H_2S-bearing geothermal vapors.

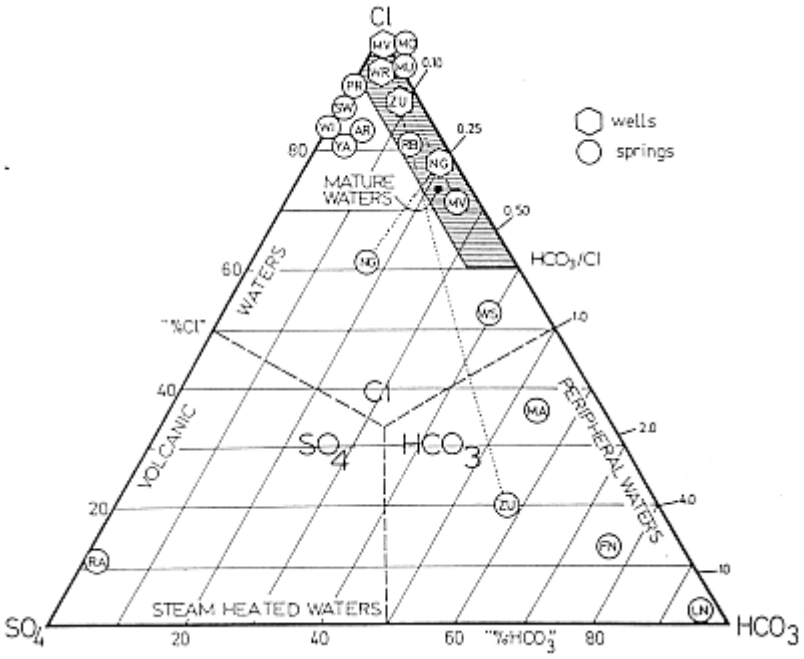

Fig. 5.2 Relative Cl, SO_4 and HCO_3 contents of thermal waters on weight basis (from Giggenbach and Goguel, 1989)

The advantages of this diagram are:

- the three main anion are plotted separately on the three vertices of the plot;

- mixing lines are straight lines;
- all available samples can be plotted; groupings and trends can be evaluated.

Its limitations are:

- relative ratios between Cl, SO_4 and HCO_3 are displayed; the content of each species relative to water is obliterated in this plot;
- apparent correlations may be accidental; correlations have to be checked by means of additional independent data.

5.3. The Langelier-Ludwig square diagram

This diagram is a sort of square version of the more popular diamond-shaped Piper plot. The position of a sample in the Langelier-Ludwig (or LL) plot is obtained by first calculating the sum of main anions, Σ_{an}, and of main cations, Σ_{cat}, by means of the following equations:

$$\Sigma_{an} = e_{Cl} + e_{SO4} + e_{HCO3} \quad (5.4)$$

$$\Sigma_{cat} = e_{Ca} + e_{Mg} + e_{Na} + e_{K}, \quad (5.5)$$

where e_i refer to the concentration of the i-th component in eq/l or meq/l. Then the percentages of each cation, e.g., Na, and each anion, e.g., Cl, are evaluated according to:

$$\%Na = 50\ e_{Na} / \Sigma_{cat} \quad (5.6)$$

$$\%Cl = 50\ e_{Cl} / \Sigma_{an}. \quad (5.7)$$

Suitable groupings of cations and anions are selected (inspection of correlation coefficients may be useful) and plotted as percentages. Generally %Na is grouped with %K and plotted on the Y-axis, while the sum % HCO_3 plus %SO_4 is plotted on the X-axis. In such a diagram %Ca+%Mg and %Cl are also fixed by the following equations:

$$\%Ca+\%Mg = 50 - (\%Na + \%K) \quad (5.8)$$

$$\%Cl = 50 - (\%HCO_3 + \%\ SO_4)\ . \quad (5.9)$$

The identification of peculiar chemical types of waters is often improved by changing the groupings of anions and cations. For instance:

- plotting the sum %Na+%K+%Mg against % HCO_3 helps to identify cold, low-salinity calcium bicarbonate waters circulating in limestones;
- plotting the sum %Na+%K+%Ca against % HCO_3 helps to identify cold, low-salinity magnesium bicarbonate waters typically originating by interaction with mafic and ultramafic rocks;
- plotting the sum %Na+%K+%Mg against % HCO_3 + %Cl helps to identify cold, calcium sulfate waters produced by interaction with gypsum and/or anhydrite.

The advantages of this diagram are:

- mixing lines are straight lines;
- all available samples can be plotted; grouping and trends can be evaluated;
- the vertices display the composition of salts present in nature, e.g., calcite, anhydrite, halite, ...; dissolution or precipitation of these salts are suggested by trends mowing towards or away from the pertinent vertex.

Its limitations are:

- both anions and cations must be grouped; the use of sums of species obliterates any information carried out by individual species;
- relative ratios are displayed; the content of each species relative to water is also obliterated in this plot;
- apparent correlations may be accidental; correlations have to be checked by means of additional independent data.

According to Tonani (unpublished reports) the square LL plot represents the base of a compositional pyramid whose edges are the chemical concentrations, in eq/l or meq/l, and whose axis express the total ionic salinity (TIS, in the same unit).

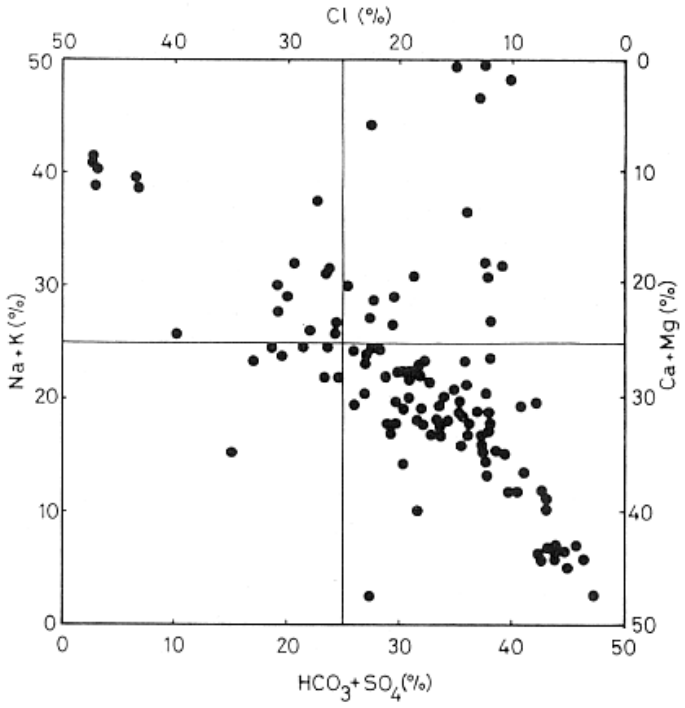

Fig. 5.3 Square Langelier-Ludwig diagram for the thermal waters of Lesbos Island, Greece (Fytikas et al, 1989).

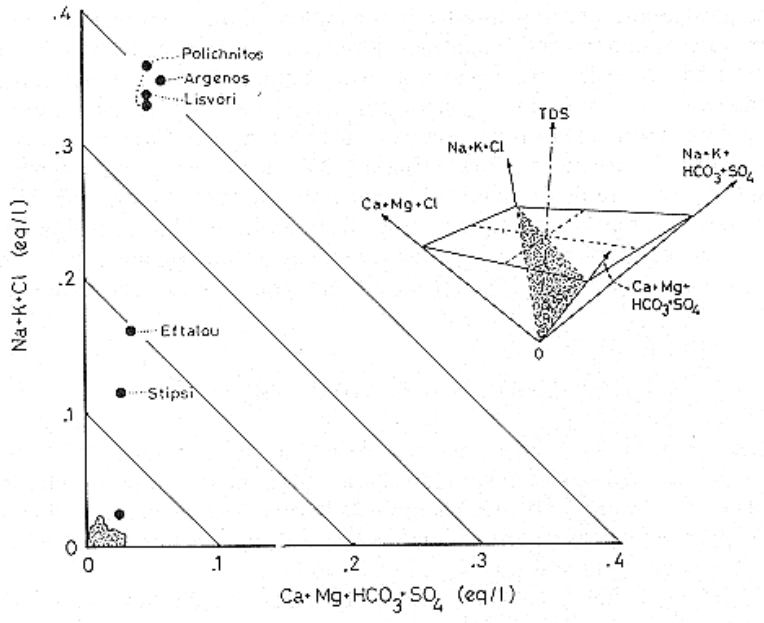

Fig. 5.4 $e_{Na} + e_K + e_{Cl}$ vs. $e_{Ca} + e_{Mg} + e_{SO4} + e_{HCO3}$ correlation plot with isosalinity lines for the thermal waters of Lesbos Island, Greece (Fytikas et al, 1989). Most waters fall in the shaded area near the origin. The diagram is equivalent to the triangular cross-section of the LL pyramid sketched on the right.

The triangular cross-sections of this pyramid allow one to recover the information provided by TIS. Some of these cross-sections are equivalent to peculiar binary

correlation plots. For instance, referring to the pyramid whose base is the above mentioned %Na + %K vs. % HCO_3 + %SO_4 square LL plot, it can be demonstrated that:
the cross-sections of this pyramid, whose trace is the diagonal connecting the vertex X=0, Y = 50 with the vertex X = 50, Y = 0 of the square LL plot, is equivalent to the $e_{Na} + e_K + e_{Cl}$ vs. $e_{Ca} + e_{Mg} + e_{SO4} + e_{HCO3}$ diagram;
the cross-sections of this pyramid, whose trace is the diagonal connecting the vertex X = 0, Y = 0 with the vertex X = 50, Y = 50 of the square LL plot, is equivalent to the $e_{Ca} + e_{Mg} + e_{Cl}$ vs. $e_{Na} + e_K + e_{SO4} + e_{HCO3}$ diagram;
the cross-section of this pyramid, whose trace parallels the X-axis of the square LL plot, is equivalent to the e_{Cl} vs. $e_{SO4} + e_{HCO3}$ diagram;
the cross-section of this pyramid, whose trace parallels the Y-axis of the square LL plot, is equivalent to the $e_{Ca} + e_{Mg}$ vs. $e_{Na} + e_K$ diagram.
In these cross-sections the lines with slope -1 are isosalinity lines; in the latter two cross-sections isosalinity lines refer to TIS/2.

5.4. Principal Component Analysis (PCA)

In general, chemical variables are intercorrelated, but these correlations are not easily discernible and raw data are therefore difficult to be interpreted. The purpose of PCA is to reduce the chemical variables to a smaller set of principal components (PC's). PC's group together correlated chemical variables and they can be, therefore, associated with sources or processes, i.e., they are interpretable.

The mathematics of PCA is beyond the scope of this brief presentation, and the reader is referred to Davis (1973) for further details.

First, chemical variables are standardized, subtracting the average and dividing by the standard deviation. The standardized variables, Z_i, have therefore average equal to zero and standard deviation equal to 1. They have the same "weight" in the subsequent procedure.

The PCA then expresses the ***n*** standardized variables in terms of ***n*** PC's, which are linear combination of the standardized variables, that is:

$$PC_1 = a_1 Z_1 + a_2 Z_2 + a_3 Z_3 + ... + a_n Z_n \quad (5.10)$$
$$PC_2 = b_1 Z_1 + b_2 Z_2 + b_3 Z_3 + ... + b_n Z_n$$
$$PC_3 = c_1 Z_1 + c_2 Z_2 + c_3 Z_3 + ... + c_n Z_n$$
$$.$$
$$.$$
$$PC_n = n_1 Z_1 + n_2 Z_2 + n_3 Z_3 + ... + n_n Z_n$$

the coefficients a_1, a_2, a_3, a_n... n_1, n_2, n_3, n_n are called *loadings*. They are a measure of the extent to which each chemical variable contributes to a given PC. Loadings have values between +1 and -1. Loadings are the key to interpret PC's. PCA is carried out in such a way that each new PC is much efficient as possible in terms of accounting for the total variance. When the ***n*** PC's have been calculated all the original variance will be accounted for.

When PCA is applied to a set of water analyses from a given area, taking into account the seven main dissolved constituents (i.e., Ca, Mg, Na, K, HCO_3, SO_4, Cl), few PC's (sometimes only two) are generally sufficient to explain a significant proportion of the total variance. The correlation plot between these PC's often looks very similar to one cross-section of the L-L compositional pyramid, substantiating the water classification carried out in a deterministic way.

6. Mixing and boiling

Before discussing the influence of mixing and boiling processes on geothermal liquids, it is convenient to clarify what is the meaning of mobile and compatible dissolved constituents.

6.1. Mobile and compatible dissolved constituents

Dissolved constituents may be subdivided into two major groups according to their behavior:

- *mobile* or *conservative* constituents are those whose activity is not limited by saturation with respect to a solid or a gas phase; comparatively mobile constituents in geothermal waters (and in most natural waters as well) are Cl, Br, B and, to a minor extent, Li, Rb and Cs; once they have been added to a geothermal water through a complex history, their contents along the upflow path are changed only by mixing and steam loss;
- *compatible* constituents are those whose activity is controlled by saturation with respect to a solid or a gas phase; they equilibrate under reservoir conditions and may respond to termochemical changes along the upflow path of the geothermal water; Ca, Mg, Na, K, HCO_3, SO_4, F, SiO_2,.. usually have compatible behavior in geothermal environments.

The limits between these two groups are not absolute; for instance Cs is mobile at temperatures > 250°C, but it is taken up in hydrothermal zeolites at lower temperatures. Also the other rare alkalies are not truly mobile constituents, since Rb is incorporated in K-bearing alteration minerals (e.g., illite) already at temperatures > 300°C and Li enters authigenic quartz and chlorite (Goguel, 1983; Giggenbach and Goguel, 1989). Boric acid distributes between steam and liquid phases, especially at high temperature (Tonani, 1970).

6.2. Correlation plots of dissolved constituents versus chloride

Chloride has mobile behavior in most natural waters. Saturation with respect to halite, which determines a compatible behavior of chloride, is in fact attained only in very peculiar natural environments. Therefore chloride can be confidently used as the mobile species of reference to investigate the behavior of other dissolved constituents.

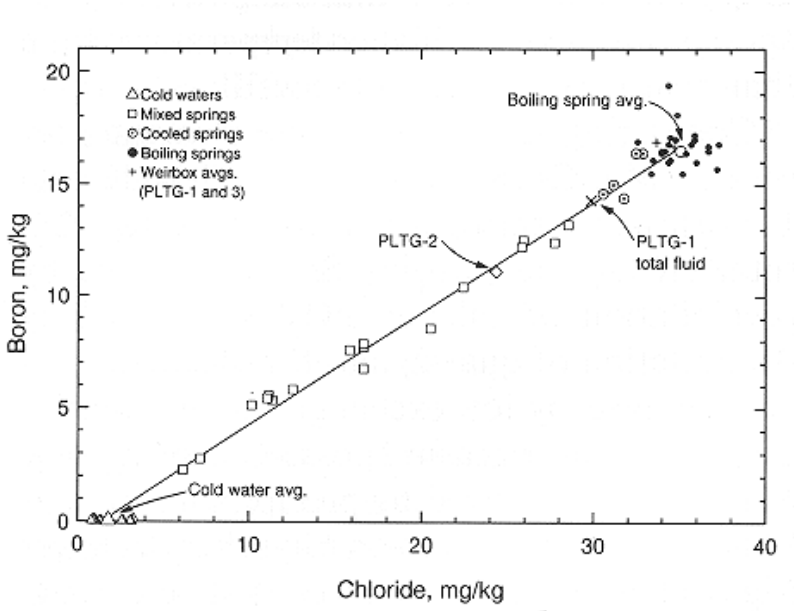

Fig. 6.1 Boron vs. chloride plots for the hot springs of Platanares, Honduras (from Janik et al., 1991)

Such an investigation is conveniently carried out by means of binary diagrams, where each chemical species of interest is plotted against chloride. These diagrams are particularly useful to detect mixing and boiling processes. Water points moves away from the origin of the axis (which is representative of pure water, i.e., of separated steam) due to boiling. Binary mixing causes, instead, tight linear trends linking the geothermal endmember and the cold endmember. However, if a Cl-poor water mixes with a Cl-rich geothermal water whose chemistry is poorly constrained, the effects of mixing are very similar to and not easily discernible from boiling effects (Fig. 6.1).

The enthalpy vs. chloride plot is very useful in this respect.

6.3. Enthalpy vs. chloride plot

The use of enthalpy vs. chloride plots is thoroughly discussed by Fournier (1979a) and references therein. The enthalpy vs. chloride plot is a suitable tool to distinguish the effects of boiling and mixing, since both steam and cold waters, which generally have low chloride contents, are characterized by very different enthalpy values.

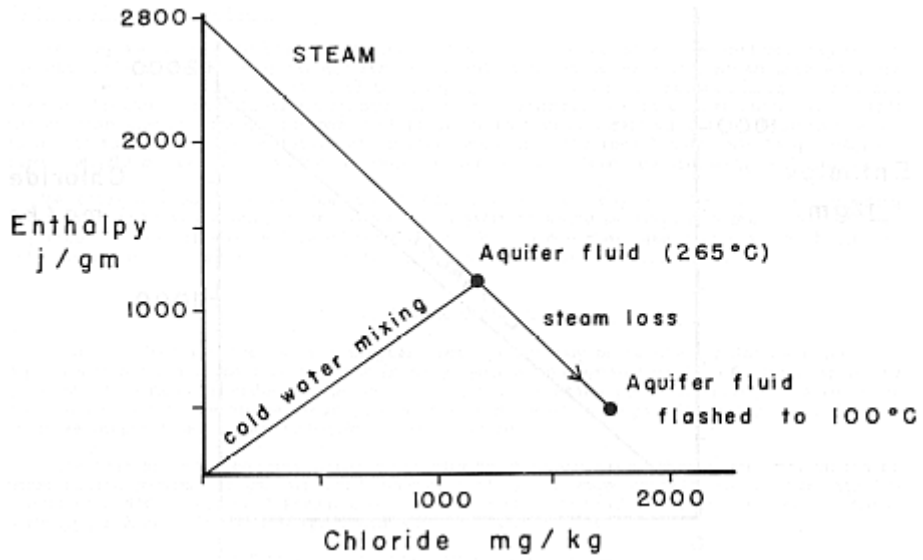

Fig. 6.2 Enthalpy vs. chloride plot showing the effects of boiling and dilution on a geothermal aquifer liquid at 265°C

The enthalpy - chloride plot of Fig. 6.2 shows that boiling (steam loss) moves the liquid from the point representative of the 265°C geothermal liquid towards higher chloride contents and lower enthalpies, whereas addition of cold, dilute waters determine a decrease in both enthalpy and chloride.

If a spring water is cooled mainly through conductive heat loss, the chloride concentration of the deep hot water remains unchanged.

6.4. Two-components mixing equations for conservative constituents

In a binary mixture the concentration, C_M, of any conservative constituent is given by the following equation:

$$C_M = C_A\, x + C_B\, (1 - x) \qquad (6.1)$$

where subscripts A and B refer to the two endmembers and x is the weight fraction of endmember A in the mixture. If mixing occurs without loss or gain of heat, then the following relationship holds true:

$$H_{L,M} = H_{L,A}\ x + H_{L,B}\ (1 - x) \qquad (6.2)$$

where H_L stands for the specific enthalpy of liquid water.

6.5. Boiling equations for non-volatile constituents

Two limiting mechanisms of boiling (steam separation) can be recognized:

(1) *single-step separation*: the steam, continuously produced by decompression of the uprising liquid, remains in contact and in equilibrium with the liquid until it is separated in a unique separation event;

(2) *continuous separation*: the steam is continuously separated from the liquid as soon as it forms.

An infinite number of intermediate mechanisms can exist; they are characterized by a finite number of separation steps (*multi-step separation*).

It is assumed that steam is separated in a single step at pressure P. The concentration, C_L, of any constituent, which does not enter the steam phase, at separation pressure P is fixed by the following relationship:

$$C_L = C_O /(1 - y) \qquad (6.3)$$

where C_O is the concentration of that constituent in the deep water and y is the steam fraction. If boiling is isoenthalpic, which is a realistic assumption for the irreversible adiabatic processes taking place in geothermal wells and high-flow rate natural geothermal manifestations, y can be obtained by means of the following isoenthalpic balance:

$$H_O = H_L\ (1 - y) + H_V\ y, \qquad (6.4)$$

which can be rearranged to give:

$$y = (H_O - H_L) / (H_V - H_L) \qquad (6.5)$$

where H indicates the specific enthalpy of the specified phase and subscript V stands for vapor. Since water is by far the major constituent of geothermal fluids, the specific enthalpies of pure water (tabulated by Keenan et al., 1969) are generally used in these calculations. However, if the aqueous solution has a relatively high salinity (NaCl > 5 wt%), specific enthalpies of the liquid and vapor phases differ significantly from those of pure water and should be suitably computed (e.g., Dittman, 1977).

6.6. Boiling equations for volatile constituents

When steam separation takes place, the less soluble gases (e.g. N_2, H_2, CH_4, and CO) enter preferentially the vapor phase, while the more soluble gases (CO_2, H_2S, and NH_3) are retained in part in the liquid phase. Early vapors are richer in gas, especially in the low-solubility constituents, whereas late vapors are relatively gas-poor and contain preferentially high-solubility constituents.

The kind of separation mechanism, either single-step, continuous or multi-step, has a dramatic influence on the composition of the separated vapor.

The distribution of gases between liquid and vapor is conveniently expressed by the gas distribution coefficient, B_j, which is defined as the ratio between the concentration of gas j in the vapor phase and the concentration of the same gas in the liquid phase:

$$B_j = (n_j/n_{H2O})_V / (n_j/n_{H2O})_L = C_V / C_L \cong x_V / x_L \qquad (6.6)$$

where n indicates the number of moles and x the mole fraction; the latter unit may be used at low gas concentration without any significant error.

Giggenbach (1980) derived the following regression equations (which are valid from 100 to 340°C) for most gas constituents of geothermal interest:

$$\log B_{NH3} = 1.4113 - .00292\ t \qquad (6.7)$$

$$\log B_{H2S} = 4.0547 - .00981\ t \qquad (6.8)$$

$$\log B_{CO2} = 4.7593 - .01092\ t \qquad (6.9)$$

$$\log B_{CH4} = 6.0783 - .01383\ t \quad (6.10)$$
$$\log B_{H2} = 6.2283 - .01403\ t \quad (6.11)$$
$$\log B_{N2} = 6.4426 - .01416\ t \quad (6.12)$$

where t is the temperature in °C. Bertrami et al. (1985) obtained the following temperature dependence for CO:

$$\log B_{CO} = 6.3173 - .01388\ t. \quad (6.13)$$

It should be noted that the logarithm of the distribution coefficient varies linearly with temperature (Fig. 6.3), while the temperature dependence of the Henry's Law constant is far from linear (Fig. 6.4). Fig. 6.4 shows also that gas solubility is a function of the salt content.

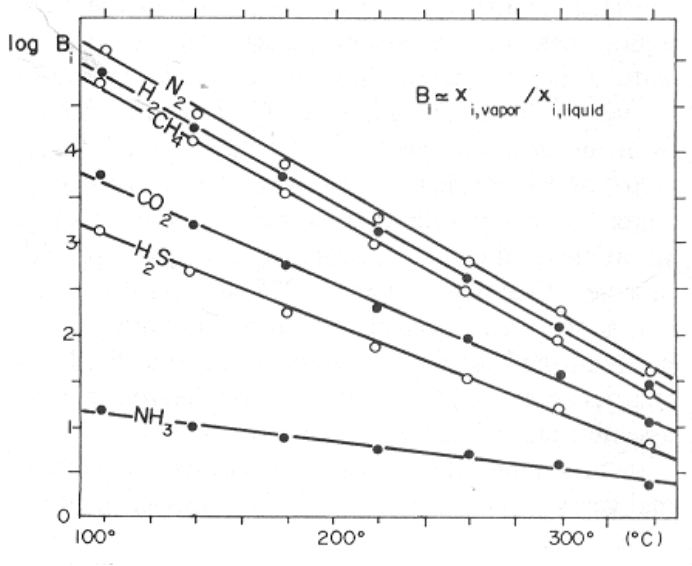

Fig. 6.3. Temperature dependence of the vapor-liquid distribution coefficient for different gases (from Giggenbach, 1980).

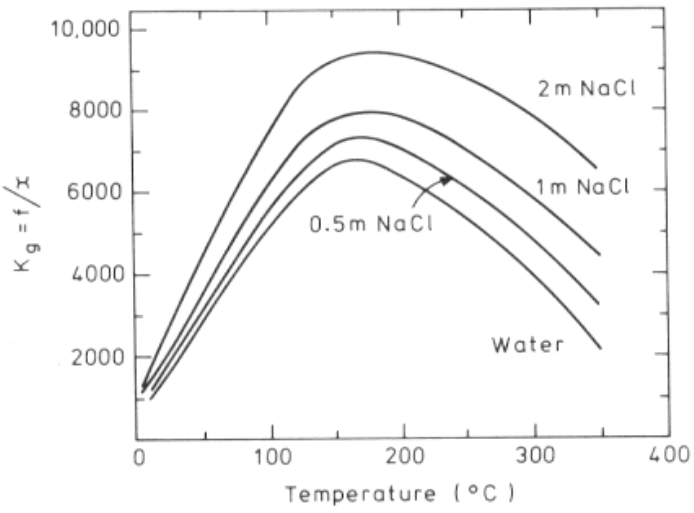

Fig. 6.4 Values of the Henry's Law constant for CO_2 in water and in 0.5 NaCl solution (data from Ellis and Golding, 1963).

If steam is separated in a single step, the concentrations of any volatile constituent at separation pressure P, in the liquid phase, C_L, and in the vapor phase, C_V, are linked to the concentration in the initial liquid, C_O, by the following mass balance:

$$C_O = C_L (1 - y) + C_V y. \quad (6.14)$$

This is equal to equation (3.1), which we used above to calculate the composition of the single liquid phase under reservoir conditions. If we are interested in calculating the concentration of gases in the vapor phase, the following expression is obtained by substituting equation (6.6) in (6.14):

$$C_V = B C_O / (1 - y + y B) \quad (6.15)$$

In multi-step separation the composition of the residual liquid at any step may be taken to be representative of that of the initial liquid of the subsequent step. If a large number of steps is taken, and each step is characterized by very small, constant steam fractions, then the continuous separation mechanism is satisfactorily approached.

The influence of steam separation processes on gas composition is suitably displayed in triangular plots, such as the H_2O-CO_2-N_2 and H_2O-H_2S-N_2 plots (Fig. 6.5). Let us recall that both H_2S and CO_2 are more soluble than N_2.

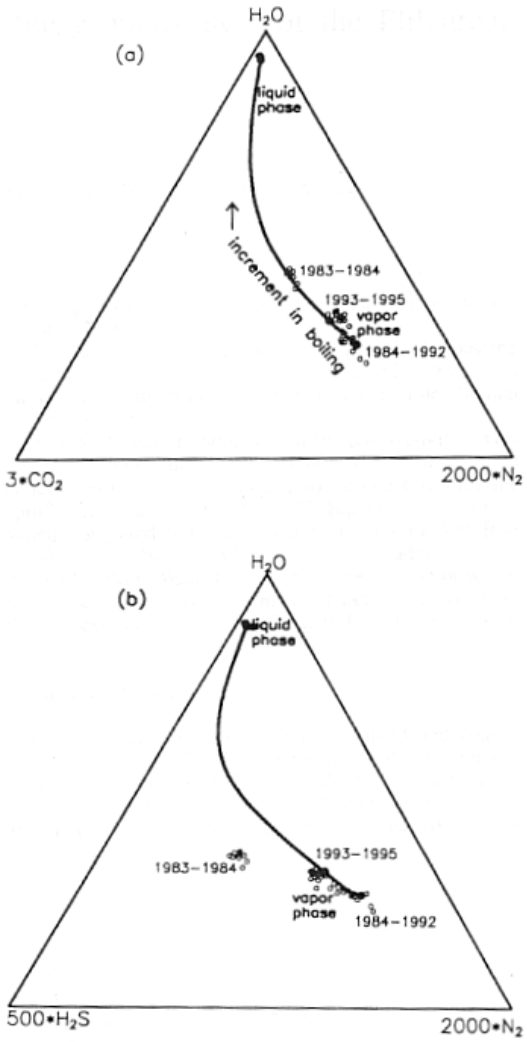

Fig. 6.5 Triangular plots H_2O-CO_2-N_2 and H_2O-H_2S-N_2 for fluids discharges by the Bocca Grande fumarole, Solfatara volcano, Campi Flegrei, Italy, also showing the theoretical curves of steam separation (from Chiodini et al., 1996b).

In single-step separation, early vapors are close to the vertex of N_2, the least soluble gas, while later vapors move towards the H_2O vertex and get progressively close to the composition of the initial liquid (which obviously limits the process); the trend bends slightly towards the vertex of CO_2, the more soluble gas. Multi-step separation (not shown) is outlined by a compositional trend that moves towards the vertex of H_2O, bending strongly towards the vertex of CO_2.

7. Hydrothermal alteration minerals in high-temperature geothermal systems

Several geochemical methods are based on the relationships between hydrothermal alteration minerals occurring in high-temperature geothermal systems and fluids circulating within these systems. These methods include not only the popular chemical geothermometers and other techniques focusing on water-rock interaction (or mineral-solution equilibrium), but also the evaluation of irreversible mass transfer taking place during water-rock interaction, which represents a powerful tool to reconstruct the origin of geothermal fluids (e.g., Reed, 1997).

Therefore, knowledge of hydrothermal alteration mineralogy developing in high-temperature geothermal systems is of upmost importance for fluid geochemistry. Luckily, hydrothermal alteration minerals, which are present within the cuttings and the less frequent cores collected during drilling, have been the subject of many investigations (e.g., Browne, 1970, 1977, 1982; Heald et al., 1987; Steiner, 1977).

Browne (1970), studying the Broadlands geothermal field, New Zealand, pointed out that some hydrothermal minerals (e.g., pyrite, calcite, and quartz) are of little use for evaluating deep temperatures and permeabilities. The reason for this is that these minerals are stable over large temperature intervals. He found that the most informative minerals are the authigenic feldspars, which are sensitive to both temperature and permeability. At Broadlands, the most common primary feldspar mineral is andesine and it is altered to quartz, clay, calcite, albite, or adularia at temperatures of 70-290°C, depending on permeability. Albite replaces andesine above 230°C. Production zones contain abundant adularia, associated with quartz and calcite.

Browne (1977) described 51 hydrothermal minerals typical of active geothermal systems, whose occurrence depends on several factors, such as temperature, pressure, fluid composition, and permeability. For instance, epidote is an indicator of high temperature, whereas adularia, again, indicates both high temperature and high permeability.

Although the sequence of alteration minerals varies from system to system, there is a general relationship between hydrothermal alteration minerals and temperature ranges, as summarized by Henley and Ellis (1983; Fig. 7.1). The same mineral parageneses were also recognized in fossil geothermal systems, i.e., in hydrothermal ore deposits.

Figure 7.1 does not report the mineral phases which forms in near-surface steam-heated zones, where acid-sulfate waters are produced through absorption of H_2S-bearing vapors in shallow groundwaters or surface waters, followed by oxidation, driven by atmospheric oxygen, of H_2S to sulfuric acid. Interaction of these acidic solutions with rocks determines the formation of kaolinite, alunite, gypsum, opal, and hydrated iron oxides (Steiner, 1977). These are the typical phases of the so-called **advanced argillic alteration**.

Among the minerals reported in Fig. 7.1, only quartz, calcite, adularia, and albite can be considered as relatively pure phases. Several minerals (e.g., epidote and chlorites) exhibit, instead, compositional changes due to solid phase mixing. Further complications are due to the development of mixed-layer minerals, involving clays and chlorites. Moreover, chlorites show a transition, with increasing temperature, from

swelling chlorites through mixed swelling and non-swelling chlorites to non-swelling chlorites, as indicated in Fig. 7.1.

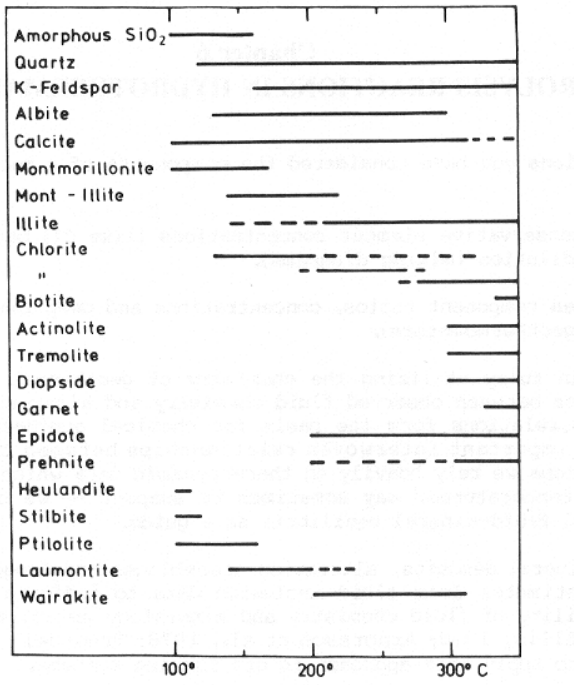

Fig. 7.1. Temperature ranges for typical hydrothermal alteration minerals. Solid and dashed lines indicate the most and less frequent temperature ranges of occurrence, respectively (from Henley and Ellis, 1983).

In spite of these complications, the geothermal systems explored through deep drilling have shown a thermal zoning of the hydrothermal alteration mineralogy, which has led to the identification of the following hydrothermal alteration zones.

The shallowest zone is the **argillic** zone, which is characterized by the presence of montmorillonite, eventually accompanied by illite, chlorites and low-temperature zeolites (e.g., heulandite, stilbite). This zone develops up to temperatures of 150-160°C, above which montmorillonite becomes unstable.

The strong increase in chlorite and illite contents and the appearance of mixed-layer clays characterize the transition to the **phyllitic zone**, also termed illite-chlorite zone, which develops up to temperatures close to 200-250°C. The zeolite mineral typical of this zone is laumontite.

The following zone, called **propylitic zone** or zone of Ca-Al-silicates, is characterized by the presence of secondary minerals, which are close to equilibrium with neutral, sodium-chloride aqueous solution. This zone develops up to temperatures of 300°C. Epidote, the most typical mineral, can start to form in small amounts within the phyllitic zone, but it becomes abundant in the propylitic zone. Epidote is usually accompanied by abundant adularia, albite, and sulfide minerals (e.g., pyrite, pyrrhotite, and sphalerite). The zeolite mineral typical of this zone is wairakite. Chlorite and illite are also stable within this zone, but are less abundant than in the phyllitic zone.

The deepest zone is the **thermo-metamorphic zone**, which is characterized by remarkable textural re-organizations of the original lithotypes and by the appearance of high-temperature mineral phases, such as amphiboles (e.g., actinolite and tremolite), pyroxenes (e.g., diopside), biotite, and garnets.

It must be underscored that the rocks affected by argillic and phyllitic alterations are characterized by extremely low permeability. In fact, the minerals typical of these two zones behave plastically under mechanic stress. Therefore, these two zones constitute the cover (or cap-rock) of the geothermal system. The hydrothermal minerals of the propylitic and thermo-metamorphic zones exhibit instead brittle behavior, permitting the development of fractures, which act as high permeability pathways for geothermal fluids. Therefore these two hydrothermal alteration zones mark the geothermal reservoirs.

On this thermal zoning of the hydrothermal alteration mineralogy are based the petrographic logs, which are generally carried out during deep geothermal drillings.

8. Geothermometric methods for geothermal waters

Water geothermometers can be classified in two groups:

- those based on temperature dependent changes in the solubility of individual minerals, such as the silica geothermometers.
- those based on temperature dependent exchange reactions, which involve at least two minerals and the aqueous solution, thus fixing the ratios of suitable dissolved constituents (e.g., the ionic solutes geothermometers).

To understand the theoretical basis of the geothermometers belonging to the first group, let us consider the quartz geothermometer, which is based on the dissolution reaction of quartz:

$$\text{quartz} + 2\ H_2O = H_4SiO_4 \qquad (8.1)$$

whose thermodynamic equilibrium constant is simply:

$$K_{qz} = a_{H4SiO4} \qquad (8.2)$$

assuming that quartz is a pure phase and water activity is unity. Besides, since the activity coefficient of neutral aqueous species, such as H_4SiO_4, is also close to unity, equations (8.2) can be rewritten as follows:

$$K_{qz} \cong m_{H4SiO4} \qquad (8.3)$$

Assuming that the temperature dependence of K_{qz} is approximated by a van't Hoff equation, then

$$\log m_{H4SiO4} = A/(T+273.15) + B \qquad (8.4)$$

from which

$$T(°C) = A/(\log m_{H4SiO4} - B) - 273.15 \qquad (8.5)$$

or, if concentrations in mg/kg SiO_2 (ppm SiO_2), are preferred, as usually done in the literature:

$$T\ (°C) = A/(\log C_{SiO2} - B - \log MW_{SiO2}) - 273.15$$
$$= A/(\log C_{SiO2} + B^*) - 273.15 \qquad (8.6)$$

where $B^* = -B - \log MW_{SiO2}$ and MW_{SiO2} stands for the molecular weight of SiO_2.

Ionic solutes geothermometers are based, instead, on temperature-dependent ion exchange reactions, such as

$$\text{albite} + K^+ = \text{K-feldspar} + Na^+ \qquad (8.7)$$

whose thermodynamic equilibrium constant is

$$K_{NaK} = (a_{K\text{-feldspar}}\ a_{Na+}) / (a_{albite}\ a_{K+}). \qquad (8.8)$$

If K-feldspar and albite are pure phases, then $a_{K\text{-feldspar}}=1$ and $a_{albite}=1$, and

$$K_{NaK} = a_{Na+}/a_{K+} \qquad (8.9)$$

Since $\gamma_{Na+}/\gamma_{K+} \cong 1$, equation (8.9) can be rewritten as follows:

$$K_{NaK} \cong m_{Na+}/m_{K+}. \qquad (8.10)$$

Following the same line of reasoning of the quartz geothermometer (see above), the following expression is obtained:

$$T(°C) = A/[\log (C_{Na+}/C_{K+}) - B - \log MW_{Na+} + \log MW_{K+}] - 273.15$$
$$= A/[\log (C_{Na+}/C_{K+}) + B^*] - 273.15 \qquad (8.11)$$

where:

$$B^* = -B - \log MW_{Na+} + \log MW_{K+} \quad (8.12)$$

As we have seen above, the temperature dependence of thermodynamic equilibrium constants is usually described by a van't Hoff equation, i.e., a relationship of this kind:

$$\log K = A/T(K) + B \quad (8.13)$$

What is the meaning of A and B ?

Remembering that:

$$\Delta G° = \Delta H° - T\,\Delta S° \quad (8.14)$$

and

$$\Delta G° = -RT \ln K \quad (8.15)$$

we have

$$\log K = -\Delta G°/2.303\,RT = (-\Delta H°/2.303\,RT) + \Delta S°/2.303\,R \quad (8.16)$$

Therefore

$$A = -\Delta H°/2.303\,R \quad (8.17)$$

and

$$B = \Delta S°/2.303\,R \quad (8.18)$$

A linear relationship between log K and 1/T(K) is obtained if $\Delta H°$ and $\Delta S°$ change little with temperature, that is if $\Delta C_P \cong 0$.

Moving from this theoretical background to the practical use of geothermometers, it must be stressed that all geothermometers are used assuming that: (1) the geothermal liquid is in equilibrium with relevant hydrothermal minerals in the reservoir; (2) the pore-fluid pressure in the reservoir is fixed by coexistence of liquid and steam; (3) the geothermal liquid cools either conductively or adiabatically, through steam separation at 100°C; (4) the geothermal liquid does not mix with cold, shallow waters during the ascent towards the surface; (5) the geothermal liquid does not precipitate any relevant mineral phase along the upflow path.

An other very important practical tip is: do not use tables but graphs to display the results of geothermometers. As discussed below, a variety of graphical techniques have been proposed to help geochemists in this exercise.

8.1. Silica geothermometers

The solubilities of all silica minerals decrease with increasing temperature. Plotting the logarithm of dissolved silica versus the inverse of the absolute temperature, the data for several silica minerals (quartz, chalcedony, α-cristobalite, opal-CT, and amorphous silica) lie along straight lines in the 20-250 °C range, even in the residual water after single-step steam separation at 100 °C. The equations of these straight lines are as follows, where S indicates silica concentration in mg/kg (from Fournier, 1973, 1991):

$$T(°C) = [1309/(5.19 - \log S)] - 273.15, \text{ for quartz;} \quad (8.19)$$

$$T(°C) = [1522/(5.75 - \log S)] - 273.15, \text{ for quartz (maximum steam loss at 100°C);} \quad (8.20)$$

$$T(°C) = [1032/(4.69 - \log S)] - 273.15, \text{ for chalcedony;} \quad (8.21)$$

$$T(°C) = [1000/(4.78 - \log S)] - 273.15, \text{ for } \alpha\text{-cristobalite;} \quad (8.22)$$

$$T(°C) = [781/(4.51 - \log S)] - 273.15, \text{ for opal-CT;} \quad (8.23)$$

$$T(°C) = [731/(4.52 - \log S)] - 273.15, \text{ for amorphous silica.} \quad (8.24)$$

The rate of quartz dissolution / precipitation depends strongly on temperature and is relatively fast at high temperatures and very slow at low temperature (Rimstidt and Barnes, 1980). This explains why: (1) in the geothermal reservoirs of constant, high temperature (generally > 180°C), liquids attain saturation with respect to quartz, after relatively long water-rock interaction, and (2) little dissolved silica polymerizes and precipitates during the relatively fast ascent of geothermal waters, even though

saturation with respect to quartz is largely exceeded. On the other hand, amorphous silica precipitates relatively fast when saturation with respect to it is exceeded, although the lack of solubility and polymerization data at high temperatures, pH and in multi-component solutions limits the understanding of amorphous silica behavior (Chan, 1989).

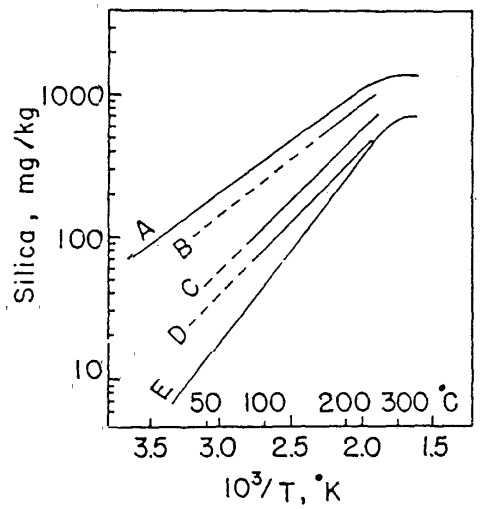

Fig. 8.1. Solubility of several silica minerals in water at the vapor pressure of the solution. A=amorphous silica, B=opal-CT, C=α-cristobalite, D=chalcedony, and E=quartz (from Fournier, 1973, 1991)

Below 300 °C and depths of some km, variations in hydrostatic pressure have small influence on the solubilities of quartz and amorphous silica (Fournier and Potter, 1982a; Fournier and Rowe, 1977). The effects of added salts are significant only for concentrations greater than 2-3 wt% approximately (Marshall, 1980; Chen and Marshall, 1982; Fleming and Crerar, 1982; Fournier and Marshall, 1983; Fournier, 1985). However, above 300°C small variations in pressure and salinity becomes very important.

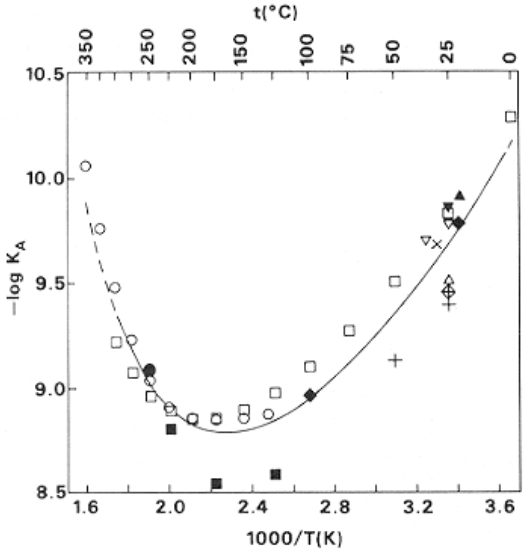

Fig. 8.2. pKa of the dissociation of silicic acid vs. 1000/T(K) for different literature data (from Fleming and Crerar, 1982)

Since the pKa of the dissociation of silicic acid:

$$H_4SiO_4° = H^+ + H_3SiO_4^- \quad (8.25)$$

varies between 10.3 and 8.8, in the 0-350°C range (Fig. 8.2), the solubility of silica is also affected by pH, for pH values above 7.8-9.3, depending on temperature. Besides, for pH < 2.5, acid-driven dissolution of Al-silicates may control dissolved silica at concentrations greater than solubilities of quartz and chalcedony, particularly for temperatures < 100-150 °C (Fournier, 1991). However, since the pH of geothermal reservoir liquids is generally constrained at values of 5-7 by water-rock reactions, corrections for pH-effects are rarely needed in geothermometric calculations.

For all these reasons, dissolved silica in solutions of near neutral pH from geothermal wells is a reliable geothermometer. The interpretation of dissolved silica from hot springs is somewhat ambiguous because of uncertainties about the mineral controlling dissolved silica and the amount of steam possibly separated (Fournier, 1991).

8.1.1. Quartz geothermometer

Fournier and Potter (1982) proposed a widely utilized formulation of the quartz geothermometer:

$$T(°C) = -42.198 + 0.28831\ S - 3.6686\ 10^{-4}\ S^2 + 3.1665\ 10^{-7}\ S^3 + 77.034 \log S, \quad (8.26)$$

where S is the silica concentration in mg/kg. Equation (8.26) can be used in the range 20-330 °C, whereas linear functions in 1/T(K), such as equations (8.19) and (8.20), cannot be applied above 250 °C, since they diverge significantly from actual quartz solubility above this temperature (Fig. 8.3).

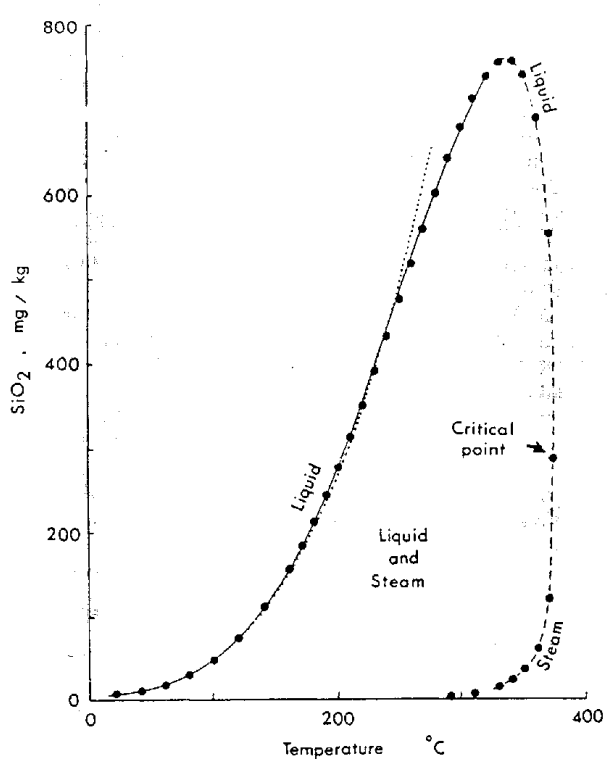

Fig. 8.3. Solubility of quartz in water at the vapor pressure of the solution (from Fournier, 1991). Dots are calculated after Fournier and Potter (1982). The solid line refers to equation (8.26) and the dashed line extends beyond its range of applicability. The dotted line represents equation (8.19).

In the absence of steam separation, quartz equilibrium temperatures can be computed from equation (8.26) or obtained from Fig. 8.3. Methods of computing quartz equilibrium temperatures when steam separation takes place are discussed below. Equation (8.26) applies to pure water and relatively dilute solutions (i.e. for salinities lower than 1-2 wt% and at temperature lower than 300°C).

8.1.2. Chalcedony geothermometer

Chalcedony is an aggregate of very tiny quartz grains. These small dimensions determine large surface energies, which make chalcedony more soluble than quartz. At T > 120-180 °C, chalcedony is unstable in contact with water and is quickly replaced by larger-sized quartz crystals. The size of quartz grains is controlled by several factors: temperature, time, fluid composition and origin, either re-crystallization of amorphous silica or direct precipitation of quartz. It turns out that in some places quartz controls dissolved silica at temperaturs as low as 100 °C, for instance where water has been in contact with rocks for comparatively long lapses of time. In other places, chalcedony governs dissolved silica up to 180 °C, especially in portions of geothermal systems recently affected by fracturing.

Therefore, it is recommendable (Fournier, 1991) to compute both quartz temperatures and chalcedony temperatures, below 180 °C, by means of equations (8.26) and (8.21). The latter is quite similar to that derived empirically by Arnorsson et al. (1983):

$$T(°C) = [1112/(4.91 - \log S)] - 273.15. \quad (8.27)$$

8.1.3. Silica vs. enthalpy diagram

Rather than inspecting a table reporting the temperatures calculated by means of the silica geothermometers, it is advisable to construct and investigate a plot of silica vs. enthalpy, where both the solubility of quartz and other silica minerals are reported together with the analyzed waters.

As already noted, most geothermal liquids have sufficiently low salinities, so that enthalpies of pure water can be used to construct the silica vs. enthalpy diagram. Fournier and Potter (1982) have proposed the following relationships to relate the enthalpies of liquid water (H_L) and vapor (H_V) to temperature (T, in °C), at the vapor pressure of the solutions, in the temperature range 50 to 340 °C:

$$H_L = 418.84 + 10.286\,T - 0.05092\,T^2 + 2.6309\,10^{-4}\,T^3 - 6.9303\,10^{-7}\,T^4 + 7.4566\,10^{-10}\,T5 - 1209.8\,T^{-1} + 11.99\,T^{-2} - 353.76 \log T \quad (8.28)$$

$$H_V = 2035 - 5.0499\,T + 0.057399\,T^2 - 3.0426\,10^{-4}\,T^3 + 7.909510^{-7}\,T^4 - 8.6968\,10^{-10}\,T5 + 1342.4\,T^{-1} - 13.298\,T^{-2} + 396.29 \log T \quad (8.29)$$

From 0 to 50°C, H_L is closely approximated by the following relationship, which must be used instead of equation (8.28):

$$H_L = 4.1868\,T. \quad (8.30)$$

The solubility of quartz in liquid water at vapor pressure of the solutions is related to enthalpy (for $H_L < 1670$ J/g) by the following function (Fournier and Potter, 1982):

$$S = -3.5532 + 0.146\,H_L - 4.927\,10^{-4}\,H_L^2 + 1.2305\,10^{-6}\,H_L^3 - 4.9421\,10^{-10}\,H_L^4 \quad (8.31)$$

Use of equations (8.28)-(8.31) allows the construction of a silica vs. enthalpy diagram such as that of Fig. 8.4.

Relating the solubility of quartz to enthalpy instead of temperature has several advantages.

(1) The solubility of quartz in water (liquid and steam) is represented by a bell-shaped symmetrical curve, which reaches a maximum of 770 mg/kg at 1595 J/g and decreases with a further increase in enthalpy. Therefore, at a given enthalpy, there is only one

value of dissolved silica, while at a given temperature there are two values of dissolved silica, one for the liquid and one for the steam (compare Fig. 8.4 with Fig. 8.3).

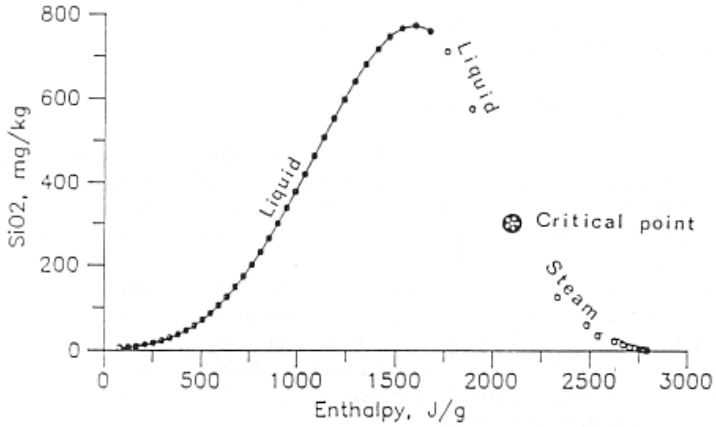

Fig. 8.4. Solubility of quartz in water at vapor pressure of the solutions as a function of enthalpy (from Fournier, 1991)

(2) If iso-enthalpic boiling occurs, the silica vs. enthalpy plot allows a quick determination of the silica concentration and enthalpy of the initial liquid before boiling assuming (1) single-stage steam loss and (2) that dissolved silica is controlled by quartz solubility. This graphical exercise, shown in Fig. 8.5, corresponds to solve a system constituted by a mass balance and an enthalpy balance; no balance can be written for temperature.

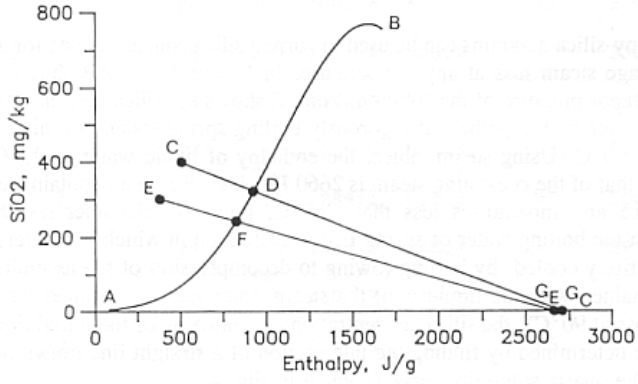

Fig. 8.5 Enthapy-silica plot showing that the enthalpy and silica content of the initial liquids (D,F) before boiling are given by the intersection of the solubility curve (B) with the line joining the steam points (G_E,G_C) and the boiled liquids (C,E), from Fournier (1991).

(3) If two waters A and B mix without loss or gain of heat, the combined enthalpies are conserved (neglecting second-order effects, such as the heat of dilution) in proportions dictated by an enthalpy balance (equation 6.2). Again, no balance can be written for temperature. Therefore, under the hypothesis stated above, enthalpy can be treated similar to mass, which makes the silica vs. enthalpy plot a good tool to investigated iso-enthalpic mixing. In fact, if iso-enthalpic mixing takes place without silica precipitation before and after mixing and without steam loss before mixing, this plot can be used to determine the temperature of the hot-water component (Truesdell and Fournier, 1977): the straight line drawn from the cold endmember (A) through the mixtures (B, D) to the intersection with the quartz solubility curve (C) gives the initial silica content and

enthalpy of the hot-water endmember (Fig. 8.6). However, if conductive cooling took place, the inferred enthalpy of the hot-water endmember will be too high.

8.1.4. Effects of pH on the solubility of silica

Geothermal liquids generally have pH value between 5 and 7 under unperturbed reservoir conditions. Decompressional boiling causes a CO_2 loss and a corresponding increase in pH, up to values of 8 to 9, which favors increased amounts of silica in solution.

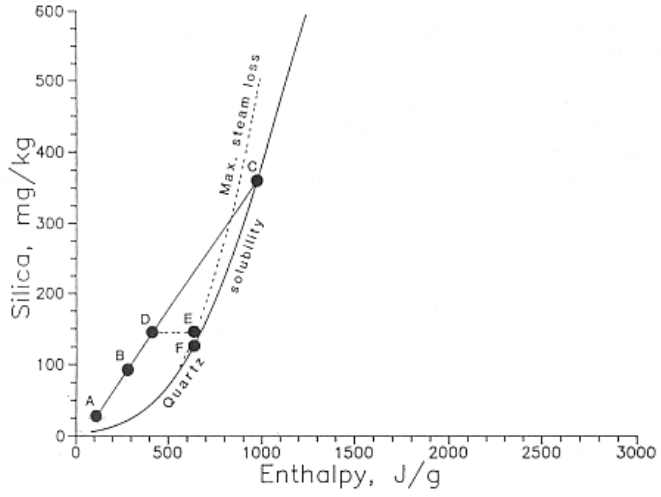

Fig. 8.6 Enthapy-silica plot illustrating the silica mixing model (from Fournier, 1991).

In order to evaluate pH effects on silica solubility, let us go back to the dissociation reaction of silicic acid:

$$H_4SiO_4° = H^+ + H_3SiO_4^- \qquad (8.25)$$

that we have already considered above. The thermodynamic equilibrium constant of equation (8.25) is:

$$K_a = (m_{H3SiO4-}\ \gamma_{H3SiO4-}\ 10^{-pH}) / (m_{H4SiO4°}\ \gamma_{H4SiO4°}). \qquad (8.32)$$

For ionic strengths < 2 mol/kg, values of the individual ionic activity coefficient of the $H_3SiO_4^-$ ion, can be calculated using an extended form of the Debye-Hückel equation (Helgeson et al., 1981):

$$-\log \gamma_i = [(A\ z_i^2\ I^{½}) / (1 + å\ B\ I^{½})] + b\ I \qquad (8.33)$$

where z is the ionic charge of the ion, I the ionic strength of the aqueous solution, A and B are characteristics parameters of the solvent (and depend on its density and dielectric constant as well as on temperature), å is the effective diameter of the ion in the solution and b is a coefficient which is specific for each ion.

For ionic strengths > 2 mol/kg other methods (e.g., Pitzer, 1981) have to be used to calculate γ.

The activity coefficient of the neutral species $H_4SiO_4°$ can be taken equal to 1. The temperature dependence of pK_a, from 0 to 300 °C, which is depicted in Fig. 8.2, is closely approximated by the following equation (T in K, Fournier, 1991):

$$-\log K_a = -631.8744 - .2967\ T + .000133266\ T^2 + 16705.03/T + 267.6478 \log T. \qquad (8.34)$$

By coupling equation (8.32) with the mass balance equation:

$$m_{SiO2,T} = m_{H3SiO4-} + m_{H4SiO4°}, \qquad (8.35)$$

where $m_{SiO2,T}$ is total silica concentration (i.e., the result of chemical analysis), the following relationship is obtained:

$$m_{SiO2,T} = m_{H4SiO4°} / \{1 - 1/[1 + (10^{-pH} \gamma_{H3SiO4-}/K_a)]\}. \quad (8.36)$$

Since $m_{H4SiO4°}$ is fixed by the equilibrium between a silica mineral and the aqueous solution, it is, to a first approximation, a simple temperature function, and it can be obtained by use of one of the equations (8.19) to (8.24), (8.26) or (8.27). Therefore we have all we need to calculate the pH effect on total silica concentration.

8.1.5. Solubility of amorphous silica

Because of conductive or adiabatic cooling, geothermal fluids may become supersaturated with respect to amorphous silica, which precipitates relatively fast. Occurrence of amorphous silica precipitation hinders the use of quartz and chalcedony geothermometers. Much more important, the consequent deposition of amorphous silica in surface installation and in reinjection circuits is a major problem in the use and disposal of geothermal liquids for electrical production. For this reason, it is very important to evaluate the temperature at which saturation with respect to amorphous silica is attained. The solubility of amorphous silica at the vapor pressure of the solution is given by equation (8.24) for temperatures between 0° and 250°C, whereas the following equations are applicable from 90° to 340°C, at the vapor pressure of the solution and at 1 kbar, respectively (Fournier and Marshall, 1983):

$$\log m_{SiO2} = -6.116 + 0.01625\ T - 1.758\ 10^{-5}\ T^2 + 5.257\ 10^{-9}\ T^3 \quad (8.37)$$

$$\log m_{SiO2} = -7.010 + 0.02285\ T - 3.262\ 10^{-5}\ T^2 + 1.730\ 10^{-8}\ T^3 \quad (8.38)$$

By use of these equations, the line expressing the solubility of amorphous silica can be easily added to the silica vs. enthalpy diagram (Fig. 8.7). On the same plot, further lines can be drawn to take into account also the pH effects on amorphous silica solubility.

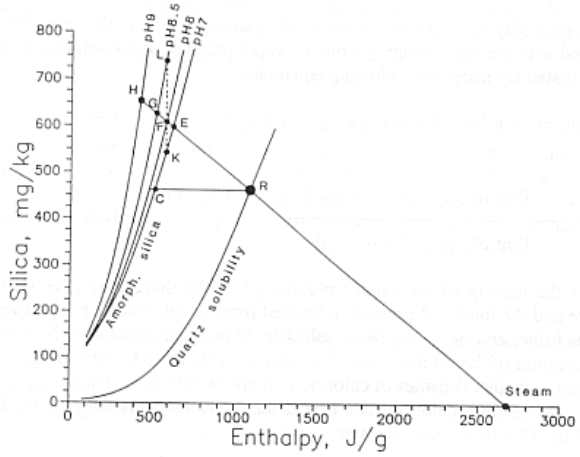

Fig. 8.7. Silica vs. enthalpy plot showing quartz solubility and the solubility of amorphous silica at various pH values, as specified (from Fournier, 1991).

Referring to Fig. 8.7, let us consider a geothermal liquid in equilibrium with quartz at 250°C, under reservoir conditions (point R, H_L = 1085 J/g, SiO_2 = 462 ppm). If this water cools conductively, such as in a low flowrate hot spring, without loss of silica, it becomes saturated with amorphous silica at point C (H_L = 520 J/g, 124°C, ad SiO_2 = 462 ppm), if pH is 7 or somewhat lower. However, if pH increases to 8, due to CO_2 loss, saturation with amorphous silica would be reached at 480 J/g (115°C).

In case of adiabatic cooling (boiling spring or discharge from a well) a pH increase is expected due to CO_2 loss. Boiling will cause an increase in silica and a decrease in enthalpy of the liquid, as indicated by the line connecting the point of steam and point R. This line intersects the amorphous silica solubility lines at decreasing enthalpies, depending on the pH of the liquid, i.e.:

- at point E for pH 7, where H_L is 620 J/g, which corresponds to a temperature of 147°C and a pressure of 4.39 bar
- at point F for pH 8, where H_L is 575 J/g, which corresponds to a temperature of 137°C and a pressure of 3.32 bar
- at point H for pH 9, where H_L is 425 J/g, which corresponds to a temperature of 102°C and a pressure of 1.09 bar.

From this discussion, it is evident that the operating pressures of well-head steam-separators must be decided considering the pH of the liquid phase to avoid silica scaling.

If the salinity of the geothermal liquid is higher than that of seawater, its effect on amorphous silica solubility has to be considered too (see Fournier, 1991).

8.2. Ionic solutes geothermometers

8.2.1. The Na-K geothermometer

A general decrease in Na/K ratios of thermal waters with increasing temperatures was observed long ago (White, 1957; Ellis and Wilson, 1960; Ellis and Mahon, 1964). The initial attempts to derive, from these observations, an empirical Na-K geothermometer led to equations (White, 1965, Ellis and Mahon, 1967) with relatively small temperature dependences, due to the inclusion in the data sets of poorly equilibrated spring waters.

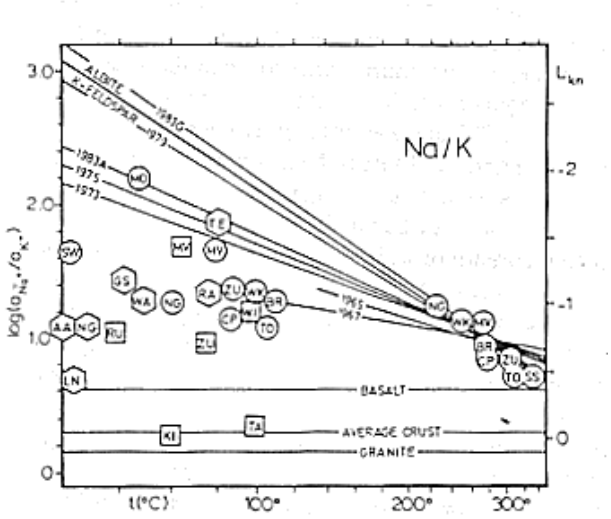

Fig. 8.8. Empirical, theoretical and analytical Na/K activity ratios of geothermal liquids as a function of temperature (from Giggenbach, 1988); squares = acid sulfate waters; hexagons = CO_2-rich bicarbonate waters (soda springs); circles= neutral chloride waters.

A calibration equation with a higher temperature dependence was proposed by Fournier and Truesdell (1973), evidently because they took into account experimental data on cation exchanges between coexisting Na- and K-feldspars (Orville, 1963; Hemley, 1967). The relationships proposed later by Truesdell (1975) and Arnorsson et al. (1983) did not led to substantial modifications (Fig. 8.8).

A step forward was done by Fournier (1979b), who carried out an empirical calibration based on well-equilibrated water discharges from deep geothermal wells and oil field brines. In fact, the equation proposed by Fournier (1979b)

$$T(°C) = \{1217/[1.483 + \log (Na/K)]\} - 273.15 \qquad (8.39)$$

closely approach that computed by means of thermodynamic data of Na- and K-feldspars (Bowers et al., 1984).

An other empirical relationship, characterized by a slightly steeper temperature dependence, was suggested by Giggenbach et al. (1983) and Giggenbach (1988):

$$T(°C) = \{1390/[1.75 + \log (Na/K)]\} – 273.15, \quad (8.40)$$

again based on well-equilibrated aqueous solutions.

In addition to the empirical formulations of the Na-K geothermometer and the theoretical albite-K-feldspar coexistence, which are representative of partial or complete equilibration with these mineral phases, three horizontal lines representative of rock dissolution (average basalt, average granite, and average crustal rock) are also given in Fig. 8.8, together with selected waters.

These were plotted converting the analytical concentrations ratios in activity ratios. Interestingly, the data from deep geothermal wells (circles, T>200°C) plot close to the theoretical albite-K-feldspar coexistence suggesting attainment of mineral-solution equilibrium. Sodium-Cl springs (circles, T<100°C) have Na-K equilibrium temperatures some 50°C lower than corresponding well discharges, suggesting that Na/K ratios are quenched at depth. This agrees with the slow kinetics, below 300°C, of the Na-K exchange between alkali feldspars and aqueous solutions, as indicated by both experiments (Orville, 1963; Hemley, 1967) and well discharges, where the Na/K ratio usually re-equilibrates more slowly than the quartz geothermometer upon temperature changes in response to production (Fournier, 1991). In Fig. 8.8, acid waters (squares) and CO_2-rich waters (hexagons) occupy positions intermediate between rock dissolution and equilibration, which might be due to preferential leaching of Na or uptake of K in alunite at low pH and in clays at higher pH, rather than attainment of equilibrium with feldspars at temperatures significantly higher than outlet temperature.

8.2.2. The K-Mg geothermometer

It was recognized long ago that Mg contents of thermal waters are strongly dependent on temperature, and this relationship was early attributed to equilibration of geothermal liquids with chlorites (Ellis, 1971) or other Mg-bearing minerals, e.g., montmorillonites and saponites. According to Giggenbach (1988), the behavior of Mg in well-equilibrated geothermal waters is described by the reactions:

$$0.8 \text{ muscovite} + 0.2 \text{ clinochlore} + 5.4 \text{ chalcedony} + 2\ K^+ = 2.8 \text{ K-feldspar} + 1.6 \text{ water} + Mg^{2+} \quad (8.41)$$

and

$$0.8 \text{ muscovite} + 0.2 \text{ clinochlore} + 5.4 \text{ chalcedony} + 2\ Na^+ = 2 \text{ albite} + 0.8 \text{ K-feldspar} + 1.6 \text{ water} + Mg^{2+} \quad (8.42)$$

The corresponding equilibrium constants are plotted in Fig. 8.9, both for activity of the solid phases equal to 1 and for different values of $AP = 0.8 \log (a_{muscovite}) + 0.2 \log(a_{clinochlore})$ to take into account the effect of the incorporation of muscovite and clinochlore into natural illites and chlorites.

The Mg/Na^2 activity ratios of liquids from geothermal wells plot close to or slightly above the theoretical lines, indicating substantial attainment of mineral-solution equilibrium (Fig. 8.9). A similar position is observed for associated spring waters, suggesting maintenance of mineral-solution equilibrium upon water ascent towards the surface. The Mg/Na^2 activity ratios of acid waters and CO_2-rich waters are controlled by rock dissolution of crustal rocks, indicating that the high Na/K activity ratios of Fig. 8.8 (with respect to crustal rock composition) are due to uptake of K in alunite or clays rather than preferential leaching of Na.

Also the Mg/K^2 activity ratios of liquids from geothermal wells plot close to the theoretical lines, indicating attainment of mineral-solution equilibrium, whereas associated springs are shifted to somewhat higher values, and have Mg-K equilibrium

temperatures some 50°C lower than corresponding well discharges, suggesting that Mg/K^2 ratios are quenched at depth.

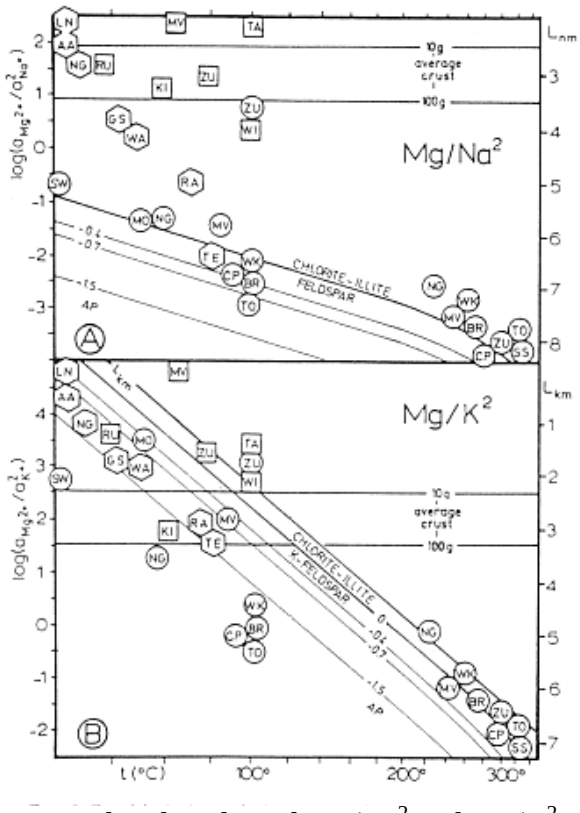

Fig. 8.9. Empirical, theoretical and analytical Mg/Na^2 and Mg/K^2 activity ratios of geothermal liquids as a function of temperature (from Giggenbach, 1988); squares = acid sulfate waters; hexagons = CO_2-rich bicarbonate waters (soda springs); circles= neutral chloride waters.

Fig. 8.9 shows that the compositional ranges of rock dissolution coincide with equilibrium compositions in the low to intermediate temperature range. Acid waters plot either in this range of Mg/K^2 ratios or above, due to precipitation of K-rich mineral phases. Bicarbonate CO_2-rich waters plot also close to the theoretical lines, indicating that the K-Mg system approaches mineral-solution equilibrium at temperatures as low as 25°C. This implies a fast response of this system upon cooling. The Mg/K^2 ratio represents, therefore, the suitable basis for a geothermometer, which was, in fact, proposed by Giggenbach et al. (1983) and later slightly revised by Giggenbach (1988), who reported the following equation (concentrations in ppm):

$$T(°C) = \{4410/[14.0 - \log (K^2/Mg)]\} - 273.15 \qquad (8.43)$$

Combining the fast-responding K-Mg geothermometer with the slowly re-equilibrating Na-K geothermometer, by means of a triangular plot, Giggenbach (1988) suggested a method to assess the degree of attainment of water-rock equilibrium (Fig. 8.10). In this Na-K-$Mg^{1/2}$ plot, the two systems are presented by two sets of lines of constant Na/K ratios and $K/Mg^{1/2}$ ratios, radiating from the $Mg^{1/2}$ vertex and the Na vertex, respectively. Since at each value of the Na/K ratio and $K/Mg^{1/2}$ ratio corresponds a unique temperature value, each of these lines is an isotherm. The intersections of the Na-K and K-Mg isotherms, referring to the same temperatures, correspond to water compositions in equilibrium with the mineral phases controlling both geothermometers and delineate the so-called “full equilibrium” curve. The compositions of waters generated through isochemical dissolution of average crustal rocks, also shown in this

triangular plot, delineate a rock dissolution area, which is well distinct from the “full equilibrium” curve.

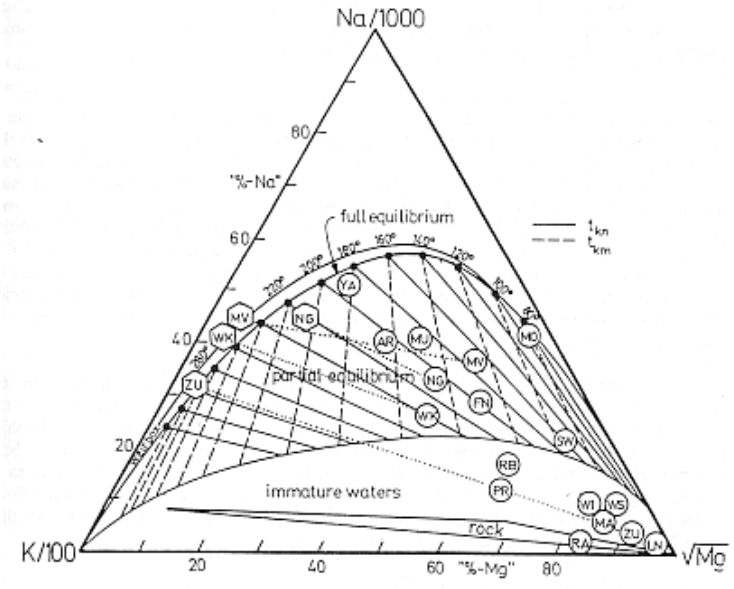

Fig. 8.10. The Na-K-$Mg^{1/2}$ triangular plot of Giggenbach (1988).

Samples from deep geothermal wells generally plot on the full equilibrium curve, at temperatures slightly higher than those physically measured in these wells. Corresponding spring waters plot below the full equilibrium curve and are shifted towards the $Mg^{1/2}$ vertex, indicating that, upon cooling, Mg acquisition by thermal waters proceeds faster than Na acquisition.

Some bicarbonate waters indicate attainment of partial equilibrium, whereas other CO_2-rich waters and acid waters are situated close to the $Mg^{1/2}$ vertex. These are the so-called “immature waters”, which provide unreliable Na-K temperatures, whereas their K-Mg temperatures may still be valid, at least for not too acid waters.

This Na-K-$Mg^{1/2}$ plot is a powerful tool as it allows:

(1) the immediate distinction between waters suitable or unsuitable for the application of ionic solute geothermometers,
(2) the assessment of deep equilibrium temperatures, and
(3) the evaluation of re-equilibration and mixing effects on a large number of water samples.

8.2.3. The Na-K-Ca geothermometer

The Na-K-Ca geothermometer (Fournier & Truesdell, 1973) is probably the most popular and used ionic solute geothermometer, although as we will see below it is not a geothermometer. The Na-K-Ca function is entirely empirical and assumes two different exchange reactions:

$$Na_{2/3}Ca_{1/6}\text{-solid} + K^+ = 1/6\ Ca^{2+} + 2/3\ Na^+ + \text{K-solid}, \qquad (8.44)$$

for T>100 °C, and:

$$Ca_{2/3}\text{-solid} + K^+ + 1/3\ Na^+ = 2/3\ Ca^{2+} + KNa_{1/3}\text{-solid} \qquad (8.45)$$

for T<100 °C.

Fournier & Truesdell (1973) do not give the temperature dependence of each of these two separate reactions, but only the following equation (concentrations in ppm):

$$T(°C) = (1647/\{\log (Na/K) + \beta\ [\log (Ca^{1/2}/Na) + 2.06] + 2.47\}) - 273.15, \qquad (8.46)$$

where β=1/3 for waters equilibrating above about 100 °C and β=4/3 for waters equilibrating below about 100 °C. However β=1/3 for waters less than 100°C when log ($Ca^{1/2}$/Na) is negative, with molal concentrations.

The Na-K-Ca function gives erratic results below 200 °C due to high partial pressures of carbon dioxide (Paces, 1975) and to the occurrence of exchange reactions involving also Mg. This led Fournier & Potter (1979) to propose a quite complex Mg-correction to the Na-K-Ca function. In addition, precipitation of calcite causes an overestimation of the equilibrium temperature obtained by means of the Na-K-Ca function.

According to Tonani (1980), the Na-K-Ca geothermometer can be split into three temperature functions, based on the Na/K, $Ca^{1/2}$/Na, and $Ca^{1/2}$/K ratios, of which only two are mutually independent.

Giggenbach (1988) summarized the results of several investigations, which were carried out for providing both theoretical and experimental justifications to this technique, and concluded that many problems in the use of the Na-K-Ca geothermometer are connected with its sensitivity to differences in the CO_2 contents of geothermal fluids (see also Chiodini et al., 1991a), especially at relatively low temperatures. Therefore, rather than representing the basis for a geothermometer, Ca may be used to formulate a P_{CO2}-indicator. Actually, Ellis (1970) had already pointed out that Ca is potential CO_2-indicator for thermal waters proposing a technique to evaluate deep P_{CO2} on the basis of Na and Ca concentrations.

8.2.4. The K-Ca P_{CO2}-indicator

According to Giggenbach (1988), it is likely that the initial CO_2 contents of deep geothermal fluids are externally controlled by variable contributions of CO_2-rich magmatic fluids and CO_2-poor meteoric waters. These fluids are expected to become reactive with respect to the conversion of Ca-Al-silicates to calcite, which involves the formation of either “acid clays”:

$$\text{Ca-Al-silicate} + CO_2 + H_2O = 2(\text{H-Al-silicate}) + \text{calcite} \qquad (8.47)$$

or K-mica:

$$\text{Ca-Al}_2\text{-silicate} + \text{K-feldspar} + CO_2 = \text{K-mica} + \text{calcite}. \qquad (8.48)$$

The temperature dependence of reaction (8.48) is described by the following equation (Giggenbach, 1984; P_{CO2} in bar, t in °C)

$$\log P_{CO2} = .0168\ t - 3.78. \qquad (8.49)$$

The univariant reaction (8.48) involves two constituents of the full equilibrium mineral assemblage, K-mica and K-feldspar, and represents the calcite/ Ca-Al_2-silicate boundary. For a given temperature, calcite is stable for P_{CO2} higher than that given by equation (8.49), whereas the Ca-Al_2-silicate mineral (either laumontite, epidote or wairakite, depending on temperature) is stable for P_{CO2} lower than that given by equation (8.49). K-mica, K-feldspar, and calcite are also involved in the following reaction:

$$3\ \text{K-feldspar} + Ca^{2+} + CO_2 = \text{K-mica} + \text{calcite} + 2\ K^+ \qquad (8.50)$$

whose equilibrium constant corresponds to $\log (a_{K+}^2/a_{Ca++}) - \log P_{CO2}$ if the solid phases are assumed to be pure. An other interesting property of this reaction is that its equilibrium constant is practically temperature independent, since it is equal to -1.66 ± 0.15 in the temperature range 50-300°C, based on the thermodynamic data of Bowers et al. (1984). Therefore the K^2/Ca ratio acts as a P_{CO2}-indicator, as described by the following equation (Giggenbach, 1988; concentrations in ppm):

$$\log (K^2/Ca) = \log P_{CO2} + 3.0. \qquad (8.51)$$

A geothermometr adjusting with speed similar to that of the K-Ca P_{CO2}-indicator is required to correlate the P_{CO2} obtained by means of equation (8.51) with temperature.

Assuming that this is the K-Mg geothermometer, Giggenbach (1988) proposed to combine the two functions in a graphical method (Fig. 8.11) permitting the determination of both CO_2 contents and temperature of "last" water-rock equilibrium.

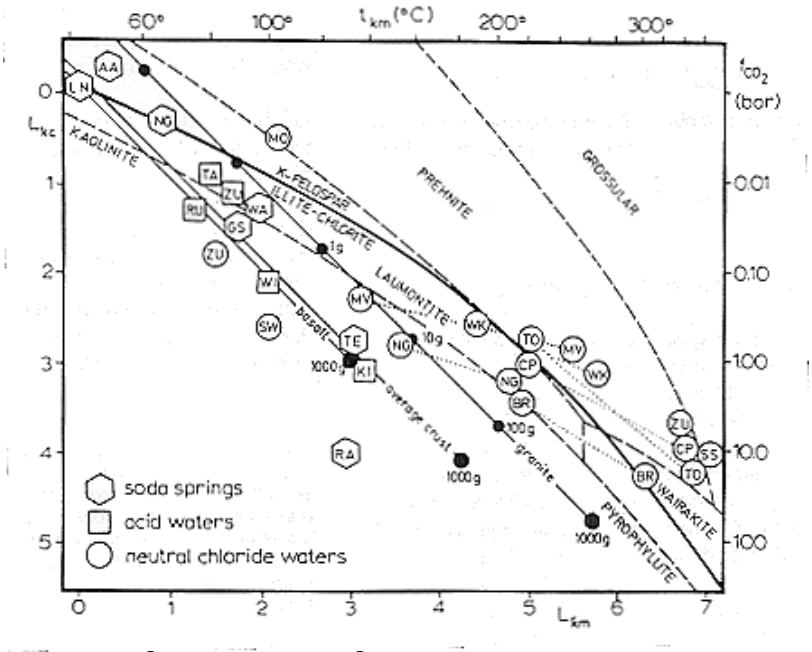

Fig. 8.11. Plot of log (K^2/Mg) vs. log (K^2/Ca), used to evaluate the P_{CO2} of geothermal liquids. The stability fields of some Ca-Al-silicates, the full equilibrium line, and the dissolution lines of basalt, granite and average crust are also shown (from Giggenbach, 1988).

The full equilibrium line, expressing coexistence of K-feldspar, illite, and chlorite is drawn in Fig. 8.11. Data points below it have P_{CO2} higher than full-equilibrium P_{CO2}, and can promote conversion of Ca-Al-silicates to calcite. On the other hand, the data points above it have low CO_2 contents, which are not sufficient to drive this reaction. All acid waters and most CO_2-rich, bicarbonate springs are situated below the full equilibrium line and their chemistry, again, appears to be controlled by rock dissolution rather than by mineral-solution equilibrium. Equation (8.51) cannot be applied to these waters. Evaluation of P_{CO2} by use of K-Ca contents is reliable only for points (either mature chloride waters or CO_2-rich, bicarbonate waters) plotting close to the full equilibrium line.

Taking into account Eqns. (8.43), (8.49), and (8.51) the full equilibrium condition can be drawn on the plot of 10 Mg/(10 Mg + Ca) vs. 10 K/(10 K + Na) (Fig.8.12). In this plot the compositions of well-equilibrated, mature waters are clearly separated from the compositions produced through isochemical dissolution of crustal rocks, such as basalt, granite and the average crust. (Giggenbach, 1988).

An other useful graphical technique is obtained combining the two chemical subsystems responding most quickly and with comparable speed to changes in temperatures, that is those based on dissolved silica and on the K^2/Mg ratio (Giggenbach, et al., 1994, Fig. 8.12).

8.2.5. Other ionic solutes geothermometers

Other ionic solutes geothermometers include:

(1) The $Li/Mg^{1/2}$ geothermometer (Kharaka and Mariner, 1989) and the Li/Na geothermometer (Fouillac & Michard, 1981), whose general utilization is questionable, because of the variable fraction of the Li-endmember in the solid-

mixtures taking part to the exchange reactions governing these geothermometers.

(2) The Ca/Mg and SO_4/F^2 geothermometers (Marini et al., 1986; Chiodini et al., 1995b), which are specific for waters coming from carbonate-evaporite reservoirs. They have stimulated the investigation of the influence of ion complexing on geothermometers and P_{CO2}-indicators.

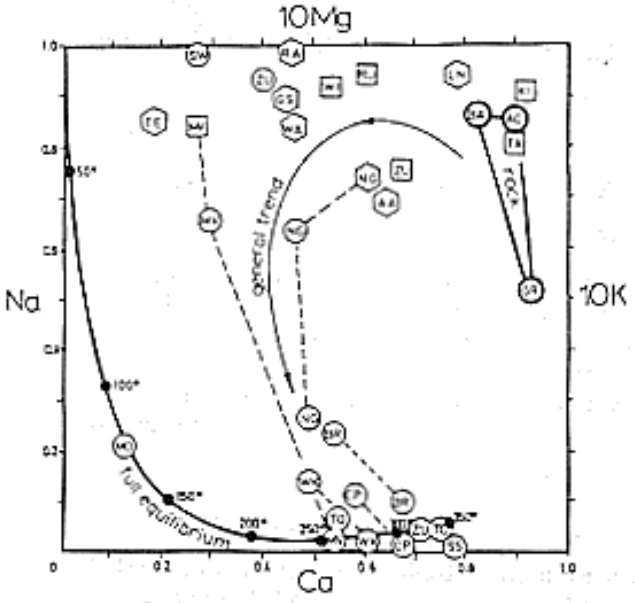

Fig. 8.12. Plot of 10 Mg/(10 Mg + Ca) vs. 10 K/(10 K + Na), above, showing the full equilibrium curve and the compositions produced through isochemical dissolution of crustal rocks (from Giggenbach, 1988) and, below, plot of log SiO_2 vs log (K^2/Mg) (from Giggenbach, et al., 1994).

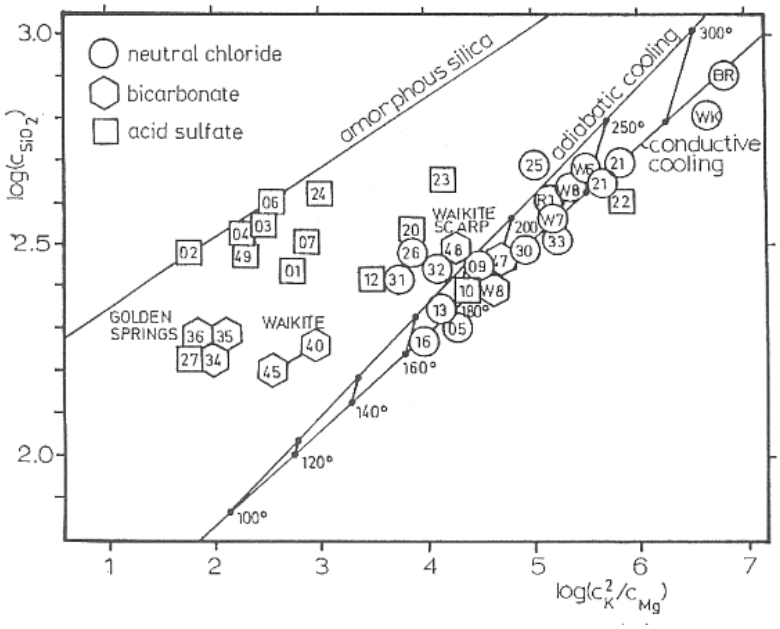

8.3. A theoretical investigation of geothermometers and P_{CO2}-indicators for high-temperature geothermal liquids

Guidi et al. (1990) and Chiodini et al. (1991a) investigated the possible geothermometers and P_{CO2}-indicators for aqueous solutions coming from high-temperature (150-300°C) geothermal systems. They used a mineral-solution equilibrium model to calculate the concentrations of dissolved compatible constituents, which are

fixed by equilibrium with a defined mineral assemblage at given T, P_{CO2} and concentrations of mobile constituents (chloride only in their approach). The mineral-solution equilibrium model has the same computational structure of the model by Michard et al. (1981) but takes into account the effects of ion complexing. The following aqueous species are considered in the model: $H_2O°$, H^+, OH^-, Na^+, $NaCl°$, $NaSO_4^-$, $NaCO_3^-$, $NaF°$, $NaOH°$, K^+, $KCl°$, KSO_4^-, $KHSO_4°$, Ca^{2+}, $CaSO_4°$, $CaCO_3°$, $CaHCO_3^+$, CaF^+, $CaOH^+$, Mg^{2+}, $MgSO_4°$, $MgCO_3°$, $MgHCO_3^+$, MgF^+, $MgOH^+$, $H_2CO_3°$, HCO_3^-, CO_3^{2-}, SO_4^{2-}, F^-, Cl^-, $H_4SiO_4°$, $H_3SiO_4^-$, $Al(OH)_4^-$, Al^{3+}, $Al(OH)^{2+}$, $Al(OH)_2^+$. The model finds the roots of a polynomial equation of H^+ activity, which is obtained considering: the electroneutrality equation, the thermodynamic constants of hydrolysis equilibria of relevant mineral phases, the Henry constant of CO_2, the thermodynamic constants of dissociation equilibria of complex aqueous species.
In the light of the available information on high-temperature geothermal systems:

- Na^+, K^+, Ca^{2+}, Mg^{2+}, $Al(OH)_4^-$, $H_4SiO_4°$, SO_4^{2-}, F^-, and HCO_3^- were chosen as compatible dissolved species;
- the hydrothermal mineral assemblage was assumed to be made up of albite, K-feldspar, either a Ca-Al-silicate and/or calcite (depending on the P_{CO2}), clinochlore, muscovite, quartz, anhydrite, and fluorite;
- P_{CO2} was considered an externally controlled parameter fixing the activity of HCO_3^-.

The expected composition of the equilibrium aqueous solutions was calculated, at different T, P_{CO2} and chloride molalities. The agreement between calculated and observed contents is generally satisfactorily (Fig. 8.13).

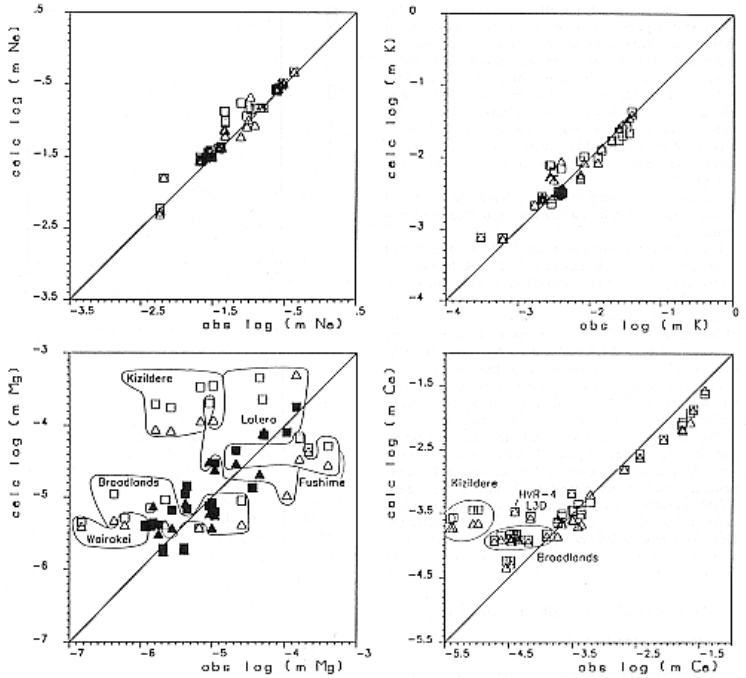

Fig. 8.13. Comparison between observed and calculated concentrations of cations (from Chiodini et al., 1991a).

8.3.1. Complexing in hydrothermal aqueous solutions.

Ion association in hydrothermal aqueous solutions has different effects mainly depending on the absolute value and sign of the ionic charge. These effects can be summarized as follows (Figs. 8.14-8.16):

Sodium and potassium: free ions, Na^+ and K^+, are always the dominant species of dissolved sodium and potassium; therefore total (analyzed) Na and K contents are always representative of free ions contents.

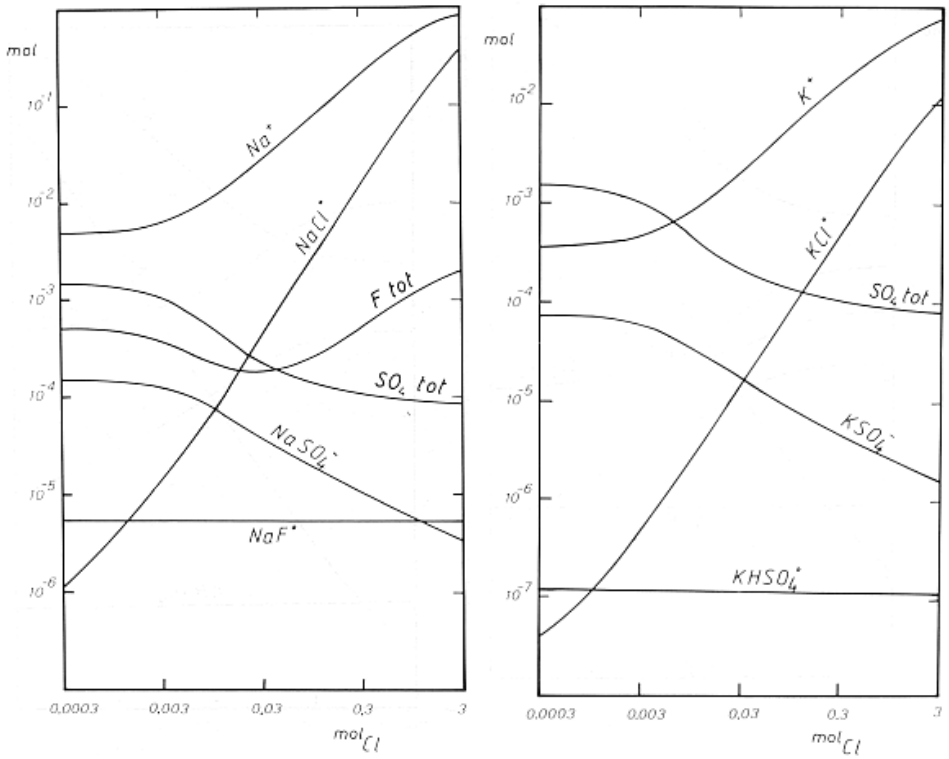

Fig. 8.14. Distribution of sodium (left) and potassium (right) species in a hydrothermal aqueous solution in equilibrium with albite, K-feldspar, clinozoisite, calcite, clinochlore, muscovite, quartz, anhydrite, and fluorite at 250°C and variable Cl concentration. P_{CO2} is fixed by coexistence of calcite and clinozoisite (from Guidi et al., 1990).

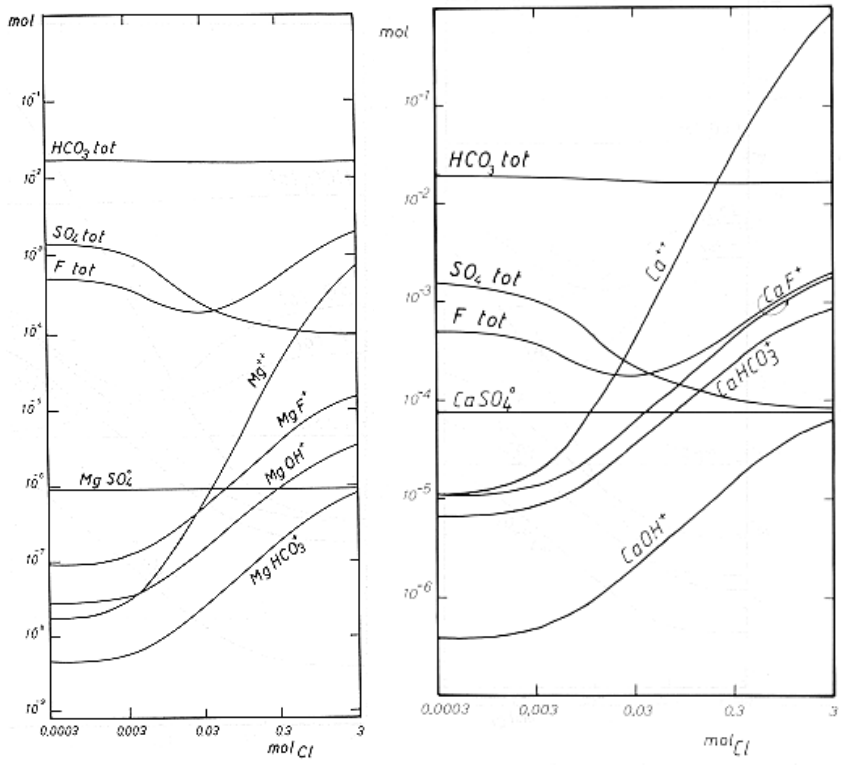

Fig. 8.15. Distribution of magnesium (left) and calcium (right) species in an hydrothermal aqueous solution in equilibrium with the stable hydrothermal mineral paragenesis at 250°C and variable Cl concentration. P_{CO2} is fixed by coexistence of calcite and clinozoisite (from Guidi et al., 1990).

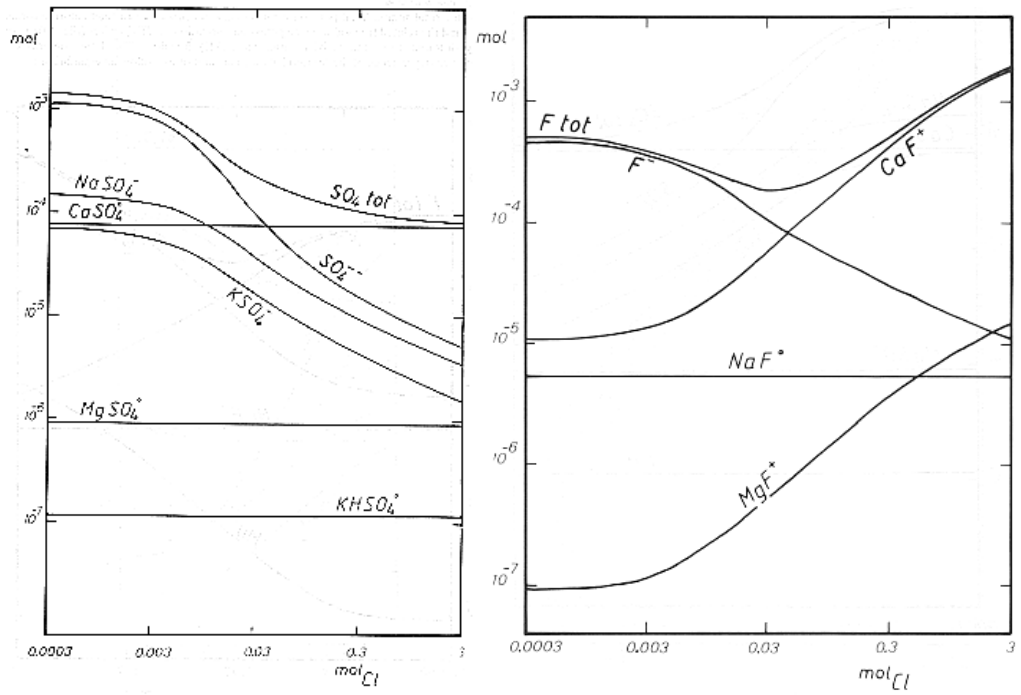

Fig. 8.16. Distribution of sulfate (left) and fluoride (right) species in an hydrothermal aqueous solution in equilibrium with the stable hydrothermal mineral paragenesis at 250°C and variable Cl concentration. P_{CO2} is fixed by coexistence of calcite and clinozoisite (from Guidi et al., 1990).

Magnesium and calcium: free ions, Mg^{2+} and Ca^{2+}, are the dominant species only in Cl-rich solutions, whereas $MgSO_4°$ and $CaSO_4°$ prevail over other Mg- and Ca-species at low Cl concentrations; it turns out that total (analyzed) Mg and Ca contents are representative of free ions contents only in Cl-rich solutions.
Sulfate and fluoride: free ions, SO_4^{2-} and F^-, are the prevailing species only in Cl-poor solutions, while $CaSO_4°$ and CaF^+ are the dominant species at high Cl concentrations; therefore total (analyzed) sulfate and fluoride contents are representative of free ions contents only in Cl-poor solutions.

Due to these effects of ion complexing, total (analytical) concentration ratios of compatible cations (Na^+, K^+, Ca^{2+} and Mg^{2+}) and compatible anions (SO_4^{2-}, F^-, and HCO_3^-) diverge, to variable amounts, from free ions activity ratios, which are uniquely fixed, at a given T or T, P_{CO2} condition, by mineral-solution equilibrium (Fig. 8.17).

Chiodini et al. (1991a) treated the logarithms of total concentrations of compatible constituents and log-ratios as dependent variables in multiple stepwise regression analysis, in which 1/T, log P_{CO2} and log Σeq (Σeq is total ionic salinity in eq/kg) were taken as independent variables. Final regression equations for total concentrations of compatible constituents are reported in Table 1, whereas those for total concentration ratios are given in Table 2.
Inspection of Tables 1 and 2 shows that:

- Na/K, K^2/Mg, and SO_4/F^2 ratios as well as SO_4 and F contents are mainly controlled by temperature and are therefore potential geothermometers;
- K^2/Ca, Ca/Mg, HCO_3/F, and $(HCO_3)^2/SO_4$ ratios as well as HCO_3 contents are largely controlled by P_{CO2} and are therefore potential P_{CO2}-indicators.
- Na^2/Mg and Na^2/Ca ratios, the concentrations of other constituents, and pH are mainly constrained by total ionic salinity and are therefore less suitable, in principle, as either geothermometers or P_{CO2}-indicators.

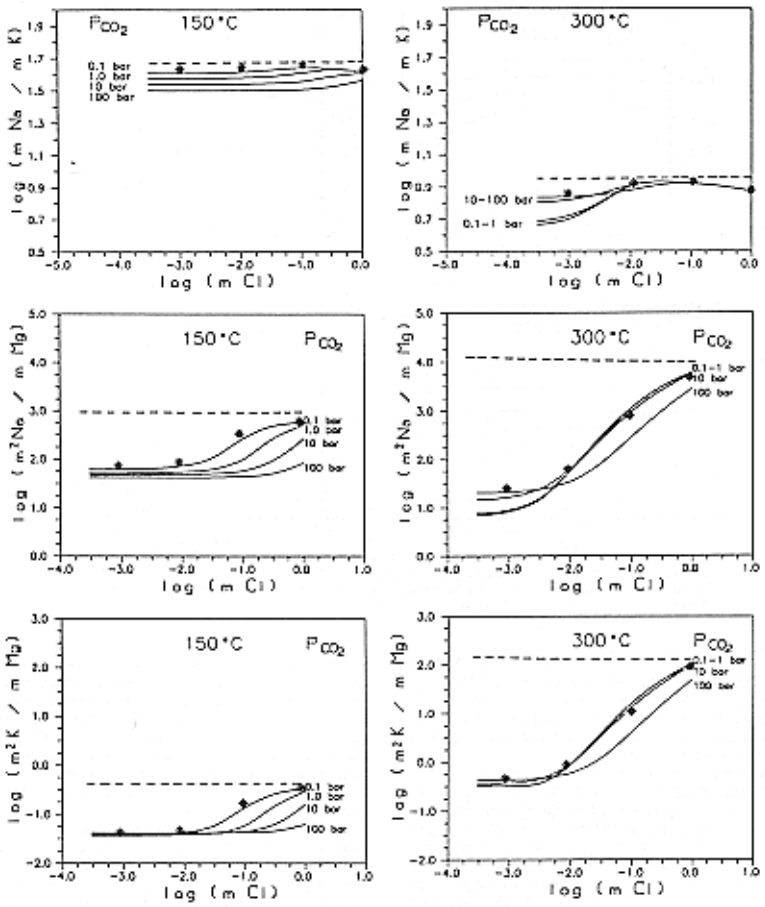

Fig. 8.17 Na/K, K^2/Mg and Na^2/Mg total (analytical) concentration ratios against total chloride concentration at different T, P_{CO2} conditions. Corresponding free ions activity ratios are represented by dashed lines. The asterisks indicate the full equilibrium values (from Chiodini et al., 1991a).

$$\log m_{Na} = -0.527 + 0.982 \log \Sigma eq + 78.9/T + 0.0119 \log P_{CO2}$$
$$\log m_{K} = 0.458 + 0.944 \log \Sigma eq - 1014/T + 0.0346 \log P_{CO2}$$
$$\log m_{Ca} = -1.116 + 1.302 \log \Sigma eq - 0.390 \log P_{CO2} - 443/T$$
$$\log m_{Mg} = -8.188 + 0.912 \log \Sigma eq + 2156/T + 0.356 \log P_{CO2}$$
$$\log m_{HCO3} = -10.004 + 0.904 \log P_{CO2} + 3223/T - 0.489 \log \Sigma eq$$
$$\log m_{SO4} = -12.503 + 4604/T + 0.501 \log P_{CO2} - 0.626 \log \Sigma eq$$
$$\log m_{F} = -5.069 + 798/T + 0.127 \log P_{CO2} - 0.0886 \log \Sigma eq$$
$$pH = 1.757 - 0.822 \log \Sigma eq + 1846/T - 0.0171 \log P_{CO2}$$

Table 1. Final regression equations for total concentrations of compatible constituents (Chiodini et al. 1991a)

These studies found a theoretical justification for ionic solutes geothermometers and P_{CO2}-indicators, which were originally derived on a purely empirical basis. In addition the functions of Table 2 allows one to investigate the behavior of each solute upon mixing and re-equilibration, as attempted by Marini et al. (1998) for the thermal waters of the San Marcos area (Guatemala). It was shown that SiO_2 and K play a key role in unravelling mixing, boiling and re-equilibration phenomena (Fig. 8.18). On the other hand, dissolved magnesium does not seem to be constrained by equilibrium with chlorites, at least in the mixed Na-Cl waters of the San Marcos area, possibly because Mg-bearing montmorillonites and saponites are more abundant than chlorites at

temperatures below 200°C. If so, the use of the K-Mg geothermometer might be in error, especially below ~175°C, as pointed out by Fournier (1991).

$$\log m_{Na}/m_K = -0.985 + 1093/T + 0.0384 \log \Sigma eq - 0.0228 \log P_{CO2}$$
$$\log (m_K^2/m_{Mg}) = 9.104 - 4184/T + 0.975 \log \Sigma eq - 0.286 \log P_{CO2}$$
$$\log (m_{SO4}/m_F^2) = -2.364 + 3007/T - 0.449 \log \Sigma eq + 0.247 \log P_{CO2}$$
$$\log (m_K^2/m_{Ca}) = 2.031 + 0.459 \log P_{CO2} + 0.585 \log \Sigma eq - 1584/T$$
$$\log (m_{Ca}/m_{Mg}) = 7.073 - 0.746 \log P_{CO2} - 2600/T + 0.390 \log \Sigma eq$$
$$\log (m_{HCO3}^2/m_{SO4}) = -7.506 + 1.307 \log P_{CO2} + 1843/T - 0.352 \log \Sigma eq$$
$$\log (m_{HCO3}/m_F) = -4.935 + 0.777 \log P_{CO2} + 2425/T - 0.401 \log \Sigma eq$$
$$\log (m_{Na}^2/m_{Mg}) = 7.134 + 1.052 \log \Sigma eq - 1999/T - 0.332 \log P_{CO2}$$
$$\log (m_{Na}^2/m_{Ca}) = 0.061 + 0.662 \log \Sigma eq + 0.414 \log P_{CO2} + 601/T$$

Table 2. Final regression equations for total concentration ratios of compatible constituents (Chiodini et al. 1991a)

8.4. Effects of mixing on the geothermometers

The effects of mixing between thermal waters and cold waters on the silica (quartz) geothermometer has been already discussed above (section 8.1.3), referring to the silica vs. enthalpy plot. The main disadvantage of that model is the possible occurrence of conductive heat losses, which determine an overestimation of the calculated temperature of the hot-water endmember.

To get rid of this possible problem, we will try to develop mixing models, which do not assume enthalpy (heat) conservation but mass conservation only. It might seem obvious, but first the occurrence of mixing must be established by means of suitable plots between mobile species. It is also useful to examine plots between the pairs of species involved in ionic solutes geothermometers, e.g., the Na-K and the K-Mg geothermometers. This exercise will probably show that, if the cold water has low salinity, the Na-K geothermometer is practically unaffected by dilution, whereas the K-Mg geothermometer is significantly influenced by mixing. In fact: (1) in the Na vs. K plot, the mixing line, as well as the different isotherms, are straight lines passing through the origin, whereas (2) in the K vs. Mg plot the mixing line is still a straight line, but the isotherms have parabolic shape.

How to calculate the equilibrium temperature of the pure thermal endmember? Some hypotheses are needed. They are: (1) existence of overall equilibrium in the reservoir; this means that different geothermometers (e.g. the Na/K and quartz geothermometers) indicate the same temperature for the pure thermal endmember; (2) neither gain nor loss of matter occur upon mixing and cooling; (3) the chemical composition of the cold component is known. Let us now select two samples which are representative of the mixed water, M, and of the cold water, C. The sodium, potassium and silica concentrations in the pure thermal endmember, T, are related to those in the mixed water and in the cold water by the following mass balances:

$$C_{Na,T}\, x = C_{Na,M} - C_{Na,C}\,(1-x) \quad (8.52)$$
$$C_{K,T}\, x = C_{K,M} - C_{K,C}\,(1-x) \quad (8.53)$$
$$C_{SiO2,T}\, x = C_{SiO2,M} - C_{SiO2,C}\,(1-x) \quad (8.54)$$

where x indicates the weight fraction of the thermal component in the mixture.

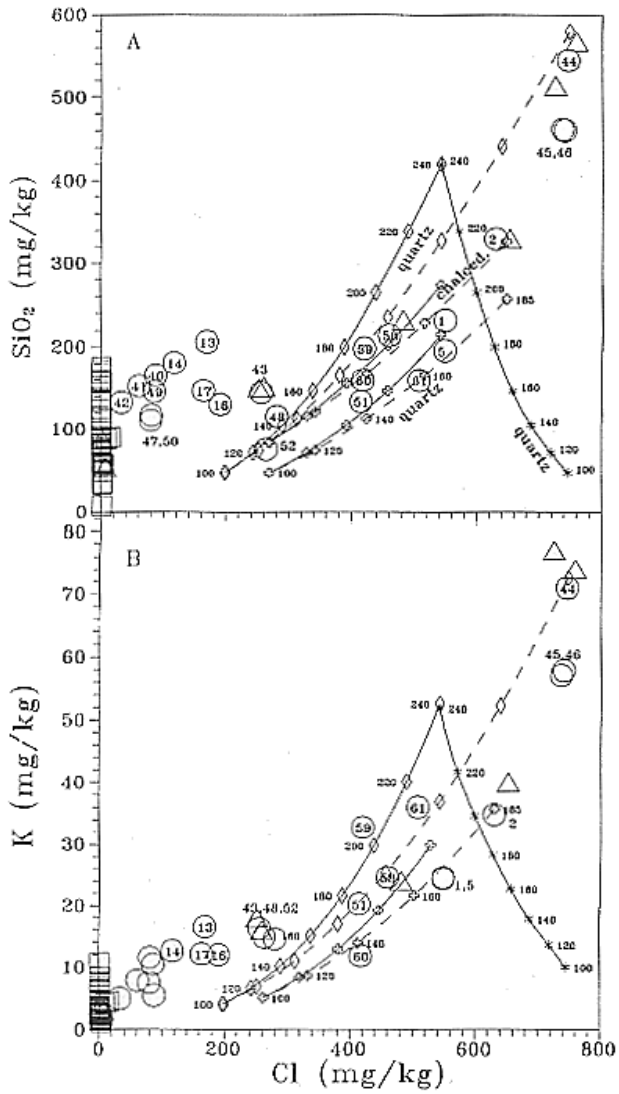

Fig. 8.18. Plots of (A) SiO_2 and (B) K vs Cl for San Marcos water discharges. Curves with small diamonds and crosses refer to the La Cimarrona (initial temperature 240°C) and La Castalia (initial temperature 185°C) geothermal endmembers, respectively; they report the compositions expected for geothermal water-groundwater isoenthalpic mixtures that are allowed to equilibrate with the hydrothermal paragenesis typical of most geothermal systems, and reach the surface after either no steam loss (solid curve) or maximum steam loss (dashed curve). The curve with asterisks represents the theoretical composition for the La Cimarrona geothermal liquid after boiling and equilibration at decreasing temperatures.

The Na/K ratio of the pure thermal endmember is obtained dividing Eqn. (8.52) by Eqn. (8.53), while the silica concentration of the thermal component is simply obtained dividing Eqn. (8.54) by x.

$$[C_{Na}/C_K]_T = [C_{Na,M} - C_{Na,C}\,(1\text{-}x)] / [C_{K,M} - C_{K,C}\,(1\text{-}x)] \qquad (8.55)$$

$$C_{SiO2,T} = [C_{SiO2,M} - C_{SiO2,C}\,(1\text{-}x)] / x \qquad (8.56)$$

Expressions (8.55) and (8.56) are then inserted in the Na/K and quartz geothermometers, obtaining a system of two equations and two unknowns (T and x), which can be solved. Once x is computed it can be inserted back in the mass balance equations to calculate the composition of the pure thermal endmember. Similar mixing models can be based upon any two geothermometers.

Alternatively the concentrations of Na, K, Mg, and SiO_2, i.e., all constituents involved in the geothermometers of interest (Na-K, K-Mg, and quartz, in this case) are regressed against Cl. If the concentrations of the considered constituents in the mixed waters are governed by mixing between a thermal water and a cold water, data should fit straight lines and simple linear equations ($C_{Na} = a_1 C_{Cl} - b_1$, $C_K = a_2 C_{Cl} - b_2$, $C_{Mg} = a_3 C_{Cl} - b_3$, $C_{SiO2} = a_4 C_{Cl} - b_4$) should be obtained. These are inserted in the Na-K, K-Mg, and quartz geothermometers (e.g., Eqns. 8.39, 8.43, and 8.19), obtaining simple T-Cl functions, such as

$$T_{Na\text{-}K}(°C) = \{1217/[1.483 + \log (a_1 C_{Cl} - b_1) - \log (a_2 C_{Cl} - b_2)]\} - 273.15 \quad (8.57)$$

$$T_{K\text{-}Mg}(°C) = \{4410/[14.0 - 2\log (a_2 C_{Cl} - b_2) - \log (a_3 C_{Cl} - b_3)]\} - 273.15 \quad (8.58)$$

$$T_{qz}(°C) = \{1309/[5.19 - \log (a_4 C_{Cl} - b_4)]\} - 273.15 \quad (8.59)$$

Then, Na-K-, K-Mg- and qz-temperatures are calculated for increasing Cl concentrations and plotted against it. If overall equilibrium is satisfied for the thermal endmember, the three functions converge, indicating the Cl concentration and overall equilibrium temperature of the thermal component. This approach has been used for the thermal waters of Plymouth, Montserrat by Chiodini et al. (1996a; Fig. 8.17).

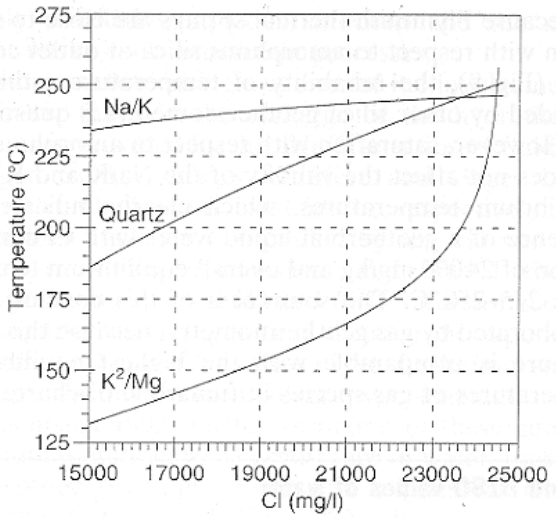

Fig. 8.17. Variations of Na/K temperatures, K^2/Mg temperatures and quartz temperatures vs. Cl contents along the mixing line of Plymouth discharges.

Ternary mixtures can be modeled by means of models involving three geothermometers (Antrodicchia et al., 1985) or two geothermometers and the conservation of enthalpy (Cioni et al., 1992).

8.5. Affinity to equilibrium and log(Q/K) vs. T diagrams

The degree of attainment of equilibrium may be monitored by using the concept of thermodynamic affinity to equilibrium: since a reaction proceeds minimizing the Gibbs free energy of the system, for a generic reaction j occurring at constant T,P, the thermodynamic affinity, A_j, is defined as follows:

$$A_j = -\left(\partial G / \partial \xi_j\right)_{P,T} = -2.303\, RT \log\left(Q_j / K_j\right) \quad (8.60)$$

where ξ_j is the progress variable for the j-th reaction, K_j is the equilibrium constant and Q_j is the corresponding activity product. The affinity has the magnitude of an energy (i.e., kJ/mole, kcal/mol) and represents the energy driving towards the equilibrium condition in a chemical potential field.

Restricting our attention to the specific case of dissolution/precipitation of a given mineral in an aqueous solution, three general situations are possible.

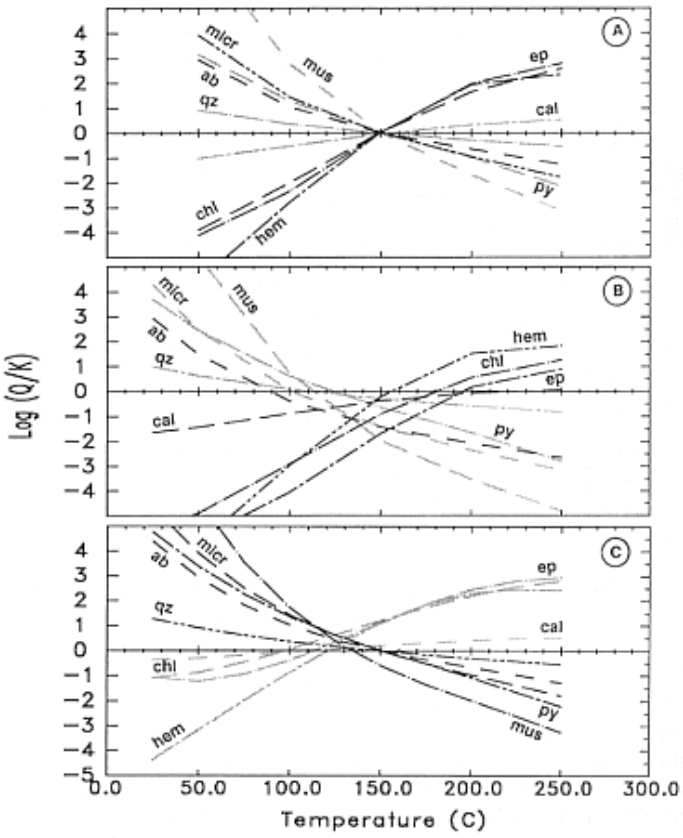

Fig. 8.17. Changes in the saturation indices of hydrothermal minerals, as a function of temperature, for a synthetic geothermal water (from Pang and Reed, 1998). Graph (A) refers to the pure geothermal water. In (B) the effects of mixing of the geothermal water with an equal volume of pure water are depicted. (C) shows the effect of 25% CO_2 loss.

If $A_j > 0$, the aqueous solution is oversaturated with respect to the solid phase. If $A_j = 0$, the aqueous solution is saturated with respect to the mineral, i.e., in equilibrium with it. If $A_j < 0$, the aqueous solution is undersaturated with respect to the solid phase. Many authors prefer to work with the adimensional variable log (Q/K), which is called saturation index, SI, rather than with thermodynamic affinity, but the two approaches are totally equivalent.

Reed and Spycher (1984) showed that calculation, for a given geothermal water, of SI's (or affinities to equilibrium) with respect to a number of plausible hydrothermal alteration minerals, at varying temperature, can be used as an effective geothermometric tool. Saturation indices are initially calculated at outlet temperature and measured pH. Temperature is then changed iteratively and the SI's recomputed. Computed SI's are then plotted against temperature, obtaining plots such as those reported in Fig. 8.17. If the geothermal water is in equilibrium with the considered minerals at a given temperature, all the SI curves converge to 0 at that temperature (150°C in Fig. 8.17 A). If the geothermal water mixes with a water of low salinity, all the SI curves are shifted downward into the undersaturation field, but the intersection cluster remains, indicating the approximate temperature of equilibrium (Fig. 8.17 B). If loss of CO_2 takes place, the SI curves for minerals sensitive to changing pH are shifted to lower values (Fig. 8.17 C). In spite of these perturbations brought about by mixing and CO_2 loss, the SI vs. T plot is a powerful tool to investigate the equilibrium temperature of geothermal waters.

In order to calculate the SI's, the chemical speciation in the aqueous solution have to be reconstructed first, taking into account all ion complexes. This is a great step forward with respect to simple geothermometers. Of course, calculations have to be carried out with the aid of a computer program. The most suitable is SOLVEQ (Reed, 1982), which was specifically implemented for this purpose (Reed and Spycher, 1984), and can be obtained from Mark H. Reed, Department of Geological Sciences, 1272 University of Oregon, Eugene, OR 97403-1272 USA, mhreed@oregon.uoregon.edu.

Since most hydrothermal minerals are Al-silicates, the aluminum concentration in the aqueous solution has to be introduced in the computations. Unfortunately, Al concentrations are rarely measured in geothermal liquids and sometimes poorly representative values are obtained, because finely dispersed Al-oxyhydroxides pass through the membrane filters, as already recalled. However, the absence or the poor analytical quality of Al data is not a major problem and it can be circumvented assuming that aluminum concentrations are constrained by equilibrium with a given Al-silicate (Pang and Reed, 1998).

9. Geothermal gases

In general, the major component of geothermal gases is H_2O, which is followed by CO_2 and H_2S in order of decreasing importance. Other gas species present in lower concentrations are N_2, H_2, CH_4, CO, NH_3, Ar and He. Strongly acid gases, i.e., SO_2, HCl and HF, which are typical of fluids degassed from magma bodies (Giggenbach, 1987; Chiodini et al, 1993), are virtually absent in geothermal fluids (Giggenbach, 1980). Sulfur dioxide was detectable only in some fumarolic discharges from active volcanic areas, such as Guagua Pichincha crater, Ecuador (Marini et al., 1991) and Forgia Vecchia of Vulcano, Italy (Chiodini et al., 1995a). Besides, geothermal gases are characterized by CH_4 contents much greater than CO concentrations (Chiodini et al., 1992).

Similar to what is done for waters, for which a first classification step is needed before investigating mineral-solution equilibria, also for gases it is convenient to carry out an initial evaluation involving the less reactive constituents, with the aim to get information on the possible origin of fluid components, on the main processes controlling their distribution and on the secondary processes possibly interfering with gas equilibria evaluations. The most obvious constituents to use are N_2, Ar, and He, as suggested by Giggenbach (1991a).

9.1. Relative concentrations of He, Ar, and N_2

Ar and He are chemically inert noble gases. Although N_2 is reactive (see below), in general its contents are not perturbed by chemical reactions since it is by far the predominant nitrogen species. Considering a large number of gas analyses coming from different tectonic settings, Giggenbach (1991a, 1992b) showed that the relative concentrations of He, Ar, and N_2 delineate the following major source components.

A *meteoric* component represented by air-saturated groundwater (asw), which is characterized by N_2/Ar ratios of ~38 or somewhat higher due to possible entrainment of air bubbles. The He/Ar ratio is less than 0.001.

A *magmatic "andesitic"* component with N_2/Ar ratios of 800-2000, which are typical of gas discharges from geothermal and volcanic centers along convergent plate boundaries (see also Giggenbach, 1997a and references therein). These relatively high N_2/Ar ratios were attributed to addition of N_2, mostly from the thermal decomposition of organic material contained in subducted sediments (Matsuo et al., 1978).

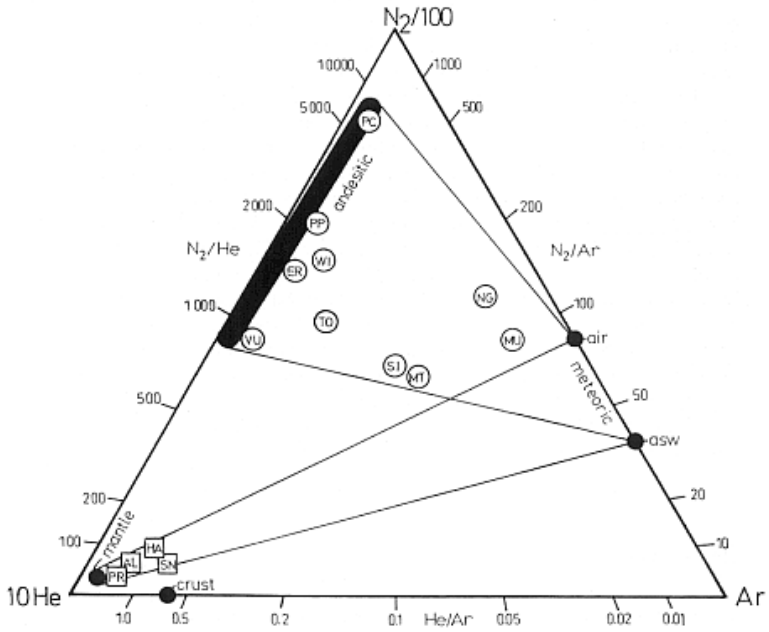

Fig. 9.1. Relative concentrations of He, Ar, and N_2 in several geothermal gases coming from different tectonic settings (from Giggenbach, 1996)

However, this ratio is highly variable, possibly due to differences in the amounts of marine sediments reaching the zones where andesitic magmas are generated (Kita et al., 1993). Some systems situated along convergent plate boundaries (e.g., the volcanic islands of Nisyros, Milos and Kos belonging to the Hellenic island arc, Giggenbach, 1997a; La Ruffa et al., 1999; Kavouridis et al., 1999; Brombach et al., 2000a) have low N_2/Ar ratios, comparable to those of mantle-derived gases, probably due to low contributions of N_2 from the subduction slab.

A *magmatic "basaltic"* component, characterized by a helium content significantly higher than that of the meteoric component (He/Ar ≥ 0.1). Gases rich in this component, labeled mantle in Fig. 9.1, are typically found along divergent plate boundaries (sample PR) and in hot spot areas (e.g., SN and AL from the Galapagos and HA from the Hawaii).

A *crustal* component, which is also rich in helium, because of addition of radiogenic He, i.e., ^{4}He from radioactive decay of crustal U and Th. In principle, the ^{3}He/^{4}He ratios could be used to discriminate the contributions of mantle and crustal gases. The ^{3}He/^{4}He ratio of mantle gases, normalized to air, is usually close to 8 R_A in mid-ocean ridge gases, but may exceed 20 R_A in some hot spot gases. On the other hand, crustal gases usually have ^{3}He/^{4}He ratios < 0.1 R_A. However, since the present understanding of the processes governing the ^{3}He/^{4}He ratios in volcanic and geothermal fluids is still at a very qualitative-descriptive stage, inferences based on He isotopes are highly speculative in our opinion.

In spite of the care in sampling natural gas discharges, atmospheric air contamination cannot always be avoided, for instance when air is entrained in the upflow path of deep fluids upstream of the surface discharge. Air contamination might be indicated by the presence of O_2, but this is not a general rule, since O_2 is rapidly consumed through reaction with the reducing gas species (mainly H_2S) initially present in deep gases. In turn, air contamination may lead to partial or complete oxidation of reducing gas species. The occurrence of this process, therefore, invalidates the geothermometric-geobarometric techniques involving either reducing gas species or atmospheric gases (e.g., Ar).

9.2. Geothermal gas equilibria in the H_2O-H_2-CO_2-CO-CH_4 system

Geothermal gas equilibria have been extensively investigated (e.g., Hulston and McCabe, 1962; Ellis, 1962; Glover, 1970; Tonani 1973; Seward, 1974; D'Amore and Nuti, 1977; Giggenbach, 1980, 1991a, 1993; D'Amore and Panichi, 1980; D'Amore and Celati, 1983; Nehring and D'Amore, 1984; Arnorsson and Gunnlaugsson, 1985; Bertrami et al., 1985; Arnorsson, 1987, 1990; Chiodini and Cioni 1989; Arnorsson et al., 1990; D'Amore, 1991; Chiodini et al., 1991b, 1992; Chiodini, 1994).

Based on earlier findings by Hulston and McCabe (1962), Giggenbach (1980) incorporated vapor-liquid gas distribution coefficients into equilibrium relationships, showing that the contents of CO_2, H_2S, NH_3, H_2, N_2, and CH_4 in the fluids discharged from the deep geothermal wells of the Wairakei, Kawerau, and Broadlands (New Zealand) and Manikaran (India) are closely approximated by two theoretical processes, either addition to or removal from an equilibrium liquid phase of an equilibrium vapor phase, defined as "vapor gain" and "vapor loss", respectively. Giggenbach (1980) took into account the following three reactions:

$$CH_4 + 2H_2O = 4\ H_2 + CO_2 \qquad (9.1)$$

$$2\ NH_3 = N_2 + 3\ H_2 \qquad (9.2)$$

$$FeS_2 + H_2 + [H_2O] = [FeO] + 2\ H_2S \qquad (9.3)$$

and described the effects of vapor gain or loss with respect to the composition expected for the discharge of a pure equilibrium liquid phase by means of simple mass balances. These mass balances were suitably readjusted, referring to the vapor-liquid distribution coefficient of each gas species, B_i, which was defined above (Eqn. 6.6). The following equation was thus obtained for the theoretical concentration quotient of reaction (9.1):

$$K'_C = (K_C\ P_{H2O}^2\ D_{CO2}^{\pm 1}\ D_{H2}^{\pm 4}\ B_{CH4}) / (B_{CO2}\ B_{H2}^4\ D_{CH4}^{\pm 1}) \qquad (9.4)$$

where:

- K_C is the equilibrium constant of reaction (9.1), and its logarithm can be expressed as a linear function of 1/T(K):

$$\log K_C = 10.76 - 9323/T(K); \qquad (9.5)$$

- P_{H2O} is the partial pressure of water, and its logarithm is also a linear function of 1/T(K) for liquid-vapor coexistence:

$$\log P_{H2O} = 5.51 - 2048/T(K); \qquad (9.6)$$

- log B_i's are linear functions of T(°C), as expressed by equations (6.7)-(6.12);
- D_i is equal to $(1 - y + yB_i)$, with y expressing the fraction of equilibrium vapor either added to or separated from the deep liquid phase.

Instead of comparing these theoretical concentration quotients with the analytical counterparts

$$K'_C = x_{d,CO2}\ x_{d,H2}^4\ P_t^4 / x_{d,CH4} \qquad (9.7)$$

where $x_{d,i}$ is the total (well discharge) mol fraction of the i-th species, Giggenbach preferred to get rid of total pressure, by means of the following approximated expression:

$$P_t = P_{H2O} / (1 - x_g\ y_s\ B_{CO2,280°}) \qquad (9.8)$$

where x_g is the gas fraction and y_s is the steam fraction, thus obtaining:

$$K''_C = K'_C / P_{H2O}^4 =$$
$$= x_{d,CO2}\ x_{d,H2}^4 / x_{d,CH4}\ (1 - x_g\ y_s\ B_{CO2,280°}) \qquad (9.9)$$

These concentration quotients are shown in Fig. 9.2.

The approach by Giggenbach (1980), and other similar models (e.g., D'Amore and Celati, 1983; Arnorsson et al., 1990; D'Amore, 1991) are based on total fluid composition. It is also required that total fluid composition measured at the surface is fully representative of reservoir conditions (e.g., absence of gas-slip effects).

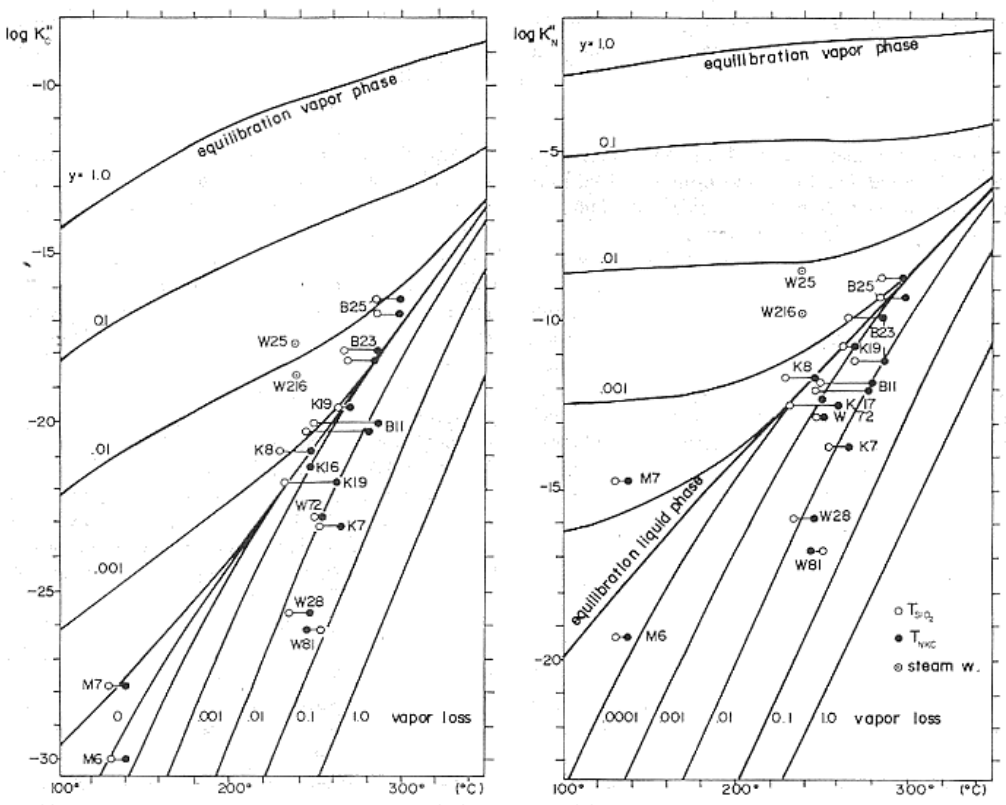

Fig. 9.2. Values of log K"$_C$ and log K"$_N$ as a function of temperature and y, which is the fraction of equilibrium vapor either added to or separated from the deep liquid phase. The corresponding analytical quotients for some geothermal wells of Wairakei (W), Broadlands (B) , Kawerau (K), and Manikaran (M) are also plotted (from Giggenbach, 1980).

These "vapor gain" models cannot be applied to vapors discharged by fumaroles, which are usually generated through steam separation from boiling liquids. "Vapor gain" models cannot be applied also to geothermal wells of which only the composition of the separated vapor phase is known. Recently, the geochemical techniques proposed by Giggenbach (1980) have been adapted to fumarolic gas discharges by Chiodini and Marini (1998). Besides, Chiodini et al. (2000c) investigated the effects of gas solubility in aqueous solutions of high salinity on relevant gas equilibria.

Following Chiodini and Marini (1998), this presentation is largely based on the equilibria in the H_2O-H_2-CO_2-CO-CH_4 system, which plays a pivotal role for geothermal gas discharges. First, the theoretical compositions of gaseous mixtures in chemical equilibrium under fixed temperature-pressure-redox or temperature-pressure conditions are computed. The results of these calculations are expressed in suitable graphics, also showing the effects of possible processes (boiling and steam condensation) experienced by deep fluids during the upflow towards the surface. Then, the analytical data are compared with theoretical data.

9.2.1. Variables controlling gas equilibria

To calculate the theoretical composition of geothermal gases, the fugacity of H_2O and, depending on the approach, the fugacities of CO_2 and O_2 as well, have to be known at the temperatures of interest.

Depending on P, T conditions, the main component of geothermal fluids, H_2O, can be present in different physical states, i.e., liquid, gas (called here ‘superheated vapor’ to avoid misunderstanding) and saturated liquid + vapor. For coexisting vapor

and liquid water, changes of log f_{H2O} with temperature are closely approximated by equation (9.6), from Giggenbach (1980). Water fugacity is not constrained by temperature alone, and becomes an additional external variable, both for a single liquid phase at pressures higher than saturation and for a single vapor phase at pressures lower than saturation.

As discussed above, CO_2 fugacity in "full equilibrium" geothermal systems is fixed, at any given temperature, by univariant reactions involving calcite, a Ca-Al-silicate, K-feldspar, K-mica and chalcedony (Giggenbach, 1984, 1988). Fugacity of CO_2 and temperature are linked by Eqn. (8.49). Also Arnorsson and Gunnlaugsson (1985) recognized that f_{CO2} is governed, above ~230 °C, by a buffer comprising calcite, epidote, prehnite and quartz and proposed an empirical geothermometer that agrees closely with expression (8.49).

According to Giggenbach (1987) the most suitable parameter describing redox potentials of most natural fluids is:

$$R_H = \log r_H = \log(f_{H2}/f_{H2O}) \cong \log(X_{H2}/X_{H2O}) \quad (9.10)$$

He proposed that the redox potentials of geothermal systems are governed by the (FeO)-($FeO_{1.5}$) couple, which controls also the redox state of basaltic and andesitic magmas as earlier recognized by Fudali (1965). Referring to the (FeO)-($FeO_{1.5}$) buffer, R_H-values are fixed by the reaction:

$$H_2O + 2(FeO) = H_2 + 2(FeO_{1.5}) \quad (9.11)$$

the equilibrium constant of which is equal to R_H and is practically temperature independent at -2.82 ± 0.02. Considering formation of water from H_2 and O_2, reaction (9.11) can be rewritten as:

$$2(FeO) + ½\ O_2 = 2(FeO_{1.5}) \quad (9.12)$$

and log f_{O2} can be linked to temperature through the following equation:

$$\log f_{O2} = 10.736 - 25414/T. \quad (9.13)$$

Similar equations relating f_{O2}'s and temperatures in geothermal environments were proposed by many authors (e.g., Tonani, 1973; D'Amore and Nuti, 1977; D'Amore and Panichi, 1980; D'Amore and Gianelli, 1984). For the purpose of the following discussion, we report here the empirical relationships of D'Amore and Panichi (1980):

$$\log f_{O2} = 8.20 - 23643/T \quad (9.14)$$

and D'Amore and Gianelli (1984):

$$\log f_{O2} = -3.808 - 13708.31/T - 2074882/T^2 \quad (9.15)$$

9.2.2. Attainment of chemical equilibrium in a single vapor phase

It is initially assumed that the considered gas species attain chemical equilibrium in a single vapor phase. The following three reactions provide the equilibrium constraints in the H_2O-H_2-CO_2-CO-CH_4 system:

$$H_2O = H_2 + ½\ O_2 \quad (9.16)$$

$$CO_2 = CO + ½\ O_2 \quad (9.17)$$

$$CO_2 + 2H_2O = CH_4 + 2O_2 \quad (9.18)$$

Production of CH_4 could take place also through reaction of elemental C and H_2. Although elemental C (graphite) may be present in some natural geothermal systems such as Cerro Prieto, Mexico (Nehring and D'Amore, 1984) and in Northern Latium, Italy (Chiodini, 1994), these are probably peculiar cases rather than the general situation. The most general approach, i.e., equation (9.18) is preferred here.

The equilibrium constants of reactions (9.16)-(9.18) can be written as:

$$\log f_{H2} = \log K_{H2} - ½\log f_{O2} + \log f_{H2O} \quad (9.19)$$

$$\log f_{CO} = \log K_{CO} - ½\log f_{O2} + \log f_{CO2} \quad (9.20)$$

$$\log f_{CH4} = \log K_{CH4} - 2\log f_{O2} + 2\log f_{H2O} + \log f_{CO2} \quad (9.21)$$

The temperature dependence of the thermodynamic constants K_{H2}, K_{CO} and K_{CH4} is given by the following equations, based on the thermodynamic data by Stull et al. (1969):

$$\log K_{H2} = -12707/T + 2.548 \quad (9.22)$$

$$\log K_{CO} = -14955/T + 5.033 \quad (9.23)$$

$$\log K_{CH4} = -42007/T + 0.527 \quad (9.24)$$

Theoretical fugacities of H_2, CO and CH_4. To solve equations (9.19) to (9.21) fugacities of H_2O, CO_2 and O_2 have to be known at the temperatures of interest. Assuming that f_{CO2} is constrained by equation (8.49), f_{O2} is governed by a suitable buffer, e.g., equations (9.13) or (9.14), and treating f_{H2O} as either a simple temperature function, for coexisting liquid plus vapor (Eqn. 9.5), or an externally fixed parameter, for single phase environments, equations (9.19) to (9.21) allow one to compute fugacities of H_2, CO and CH_4 at different temperatures (Fig. 9.3).
Use of the two O_2-buffers of Giggenbach (1987) and D'Amore and Panichi (1980) leads to different theoretical fugacities of H_2, CO and CH_4. Carbon monoxide shows the largest changes with temperature, and it is, therefore, the best geothermometer. However, since fugacities of single gas species are practically impossible to be determined for fumarolic effluents and only with limited accuracy for well discharges, Fig. 9.3 cannot be used to compare theoretical and analytical compositions.

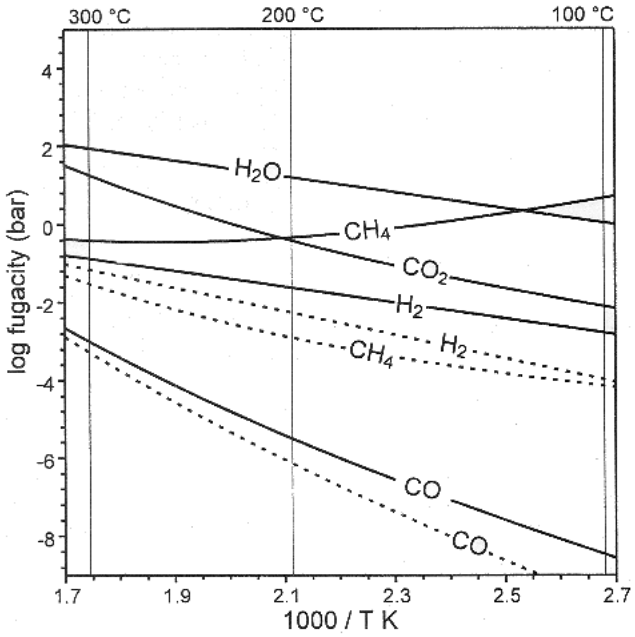

Fig. 9.3. Fugacities of H_2, CO and CH_4 at different temperatures, for a vapor phase coexisting with an infinitesimally small amount of liquid water, calculated assuming that f_{CO2} is constrained by the full equilibrium function of Giggenbach (1984, 1988), and f_{O2} is governed by either the FeO-$FeO_{1.5}$ hydrothermal buffer of Giggenbach (1987, solid lines) or the f_{O2}-buffer of D'Amore and Panichi (1980, dashed lines). Fugacities of H_2O and CO_2, which are simple temperature functions, are also shown (from Chiodini and Marini, 1998).

Theoretical log-ratios H_2/H_2O, CO/CO_2, and CH_4/CO_2. Most of the disadvantages of referring to fugacities of single gas species are overcome by working with isomolar concentration ratios, which can be analytically determined on both fumarolic fluids and

well discharges. In order to meet these requirements, the equilibrium constants of reactions (9.16)-(9.18) can be re-formulated as:

$$\log(f_{H2}/f_{H2O}) = \log K_{H2} - \tfrac{1}{2}\log f_{O2} = \log(X_{H2}/X_{H2O}) \quad (9.25)$$

$$\log(f_{CO}/f_{CO2}) = \log K_{CO} - \tfrac{1}{2}\log f_{O2} = \log(X_{CO}/X_{CO2}) \quad (9.26)$$

$$\log(f_{CH4}/f_{CO2}) = \log K_{CH4} - 2\log f_{O2} + 2\log f_{H2O} = \log(X_{CH4}/X_{CO2}) \quad (9.27)$$

For gas phases largely made up of water vapor, i.e., when $X_{H2O} > 0.8$, the ratios of fugacity coefficients Γ_{H2}/Γ_{H2O}, Γ_{CO}/Γ_{CO2}, and $\Gamma_{CH4}/\Gamma_{CO2}$ do not deviate significantly from 1, in the typical P,T range of geothermal systems, 100-374 °C and 1-220 bar (Ryzhenko and Volkov, 1971; Ryzhenko and Malinin, 1971; Naumov et al., 1974). Therefore use of ratios of mole fractions in the vapor phase, Xi's, introduces negligible errors (Giggenbach, 1987). The theoretical values obtained from equations (9.25)-(9.27) are reported as vapor lines and superheated vapor grids in Figs. 9.4 and 9.5. It must be underscored that equilibrium values of $\log(X_{H2}/X_{H2O})$ and $\log(X_{CO}/X_{CO2})$ depend upon the temperature and the redox potential in the gas equilibration zone only, whereas theoretical $\log(X_{CH4}/X_{CO2})$ ratios are also controlled by water fugacity. As a consequence, $\log(X_{H2}/X_{H2O})$ and $\log(X_{CO}/X_{CO2})$ in pure saturated vapors are equal to those in superheated vapors at any T and redox condition (vapor lines in Fig. 9.4), whereas $\log(X_{CH4}/X_{CO2})$ in pure saturated vapors (vapor lines in Fig. 9.5) are different from those in superheated vapors (superheated vapor grids in Fig. 9.5).

Theoretical sums of log-ratios H_2/H_2O, CO/CO_2, and CH_4/CO_2. Geoindicators independent on the redox potential can be derived summing reactions (9.16) to (9.18) in order to eliminate O_2. This exercise produces the following 5 reactions, each including 4 and excluding 1 of the considered 5 constituents:

$$CO_2 + H_2 = CO + H_2O \quad (9.28)$$

$$CH_4 + 2H_2O = 4\,H_2 + CO_2 \quad (9.29)$$

$$3CO_2 + CH_4 = 4CO + 2H_2O \quad (9.30)$$

$$CH_4 + H_2O = 3H_2 + CO \quad (9.31)$$

$$CH_4 + CO_2 = 2H_2 + 2CO \quad (9.32)$$

Only 2 of these 5 reactions are mutually independent, as all the 5 constituents are involved in any 2 of these reactions. Let us consider, for instance, reactions (9.28) or water-gas shift reaction WGS and (9.30) here indicated with the acronym CCC. Their equilibrium constant expressions are:

$$\log(f_{CO}/f_{CO2}) - \log(f_{H2}/f_{H2O}) = \log K_{WGS} = \cong \log(X_{CO}/X_{CO2}) - \log(X_{H2}/X_{H2O}) \quad (9.33)$$

$$3\log(f_{CO}/f_{CO2}) + \log(f_{CO}/f_{CH4}) = \log K_{CCC} - 2\log f_{H2O} = \cong 3\log(X_{CO}/X_{CO2}) + \log(X_{CO}/X_{CH4}) \quad (9.34)$$

The temperature dependence of the thermodynamic constants K_{WGS} and K_{CCC} is given by the following equations:

$$\log K_{WGS} = -2248/T + 2.485 \quad (9.35)$$

$$\log K_{CCC} = -17813/T + 19.605 \quad (9.36)$$

Equilibrium values of $\log(X_{CO}/X_{CO2}) - \log(X_{H2}/X_{H2O})$ depend upon the temperature in the gas equilibration zone only, whereas theoretical values of $3\log(X_{CO}/X_{CO2}) + \log(X_{CO}/X_{CH4})$ are also controlled by water fugacity. Theoretical values of these sums of log-ratios are shown as vapor lines and superheated vapor grids in Fig. 9.6.

9.2.3. Attainment of chemical equilibrium in a single saturated liquid phase

Equilibrium gas contents in a single saturated liquid phase are conveniently computed using the vapor-liquid distribution coefficient. The temperature dependence of vapor-liquid distribution coefficients for the gas species of interest is described, in the 100-340 °C range, by equations (6.9)-(6.11) and (6.13). Above the upper temperature limit, Bi's

are obtained interpolating between the value at 340 °C and 1, i.e., the theoretical value at 374°C for all gas species.

Insertion of Eqn. (6.6) in equations (9.25), (9.26), (9.27), (9.33), and (9.34) leads to the following relationships:

$$\log(X_{H2}/X_{H2O})_L = \log K_{H2} - ½ \log f_{O2} - \log B_{H2} \quad (9.37)$$

$$\log(X_{CO}/X_{CO2})_L = \log K_{CO} - ½ \log f_{O2} - \log(B_{CO}/B_{CO2}) \quad (9.38)$$

$$\log(X_{CH4}/X_{CO2})_L = \log K_{CH4} - 2 \log f_{O2} + 2 \log f_{H2O} - \log(B_{CH4}/B_{CO2}) \quad (9.39)$$

$$\log(X_{CO}/X_{CO2})_L - \log(X_{H2}/X_{H2O})_L = \log K_{WGS} - \log(B_{CO}/B_{CO2}) + \log B_{H2} \quad (9.40)$$

$$3\log(X_{CO}/X_{CO2})_L + \log(X_{CO}/X_{CH4})_L = \\ = \log K_{CCC} - 2 \log f_{H2O} - 3\log(B_{CO}/B_{CO2}) - \log(B_{CO}/B_{CH4}) \quad (9.41)$$

Compositions described by equations (9.37)-(9.41) can be reached in fumaroles and steam wells only through complete isothermal evaporation of an equilibrated liquid. This process requires a considerable supply of heat from an external source and it is possible under peculiar situations only, usually absent in most ‘normal’ geothermal systems. Nevertheless they represent a useful reference, and would be applicable to any unflashed samples of a deep liquid phase. The theoretical values of $\log(X_{H2}/X_{H2O})_L$, $\log(X_{CO}/X_{CO2})_L$, $\log(X_{CH4}/X_{CO2})_L$, $\log(X_{CO}/X_{CO2})_L - \log(X_{H2}/X_{H2O})_L$, and $3\log(X_{CO}/X_{CO2})_L + \log(X_{CO}/X_{CH4})_L$ are reported as liquid lines in Figs. 9.4-9.6.

9.2.4. Steam produced through boiling of an equilibrated liquid phase

To compare theoretical and measured data, the effect of secondary phenomena affecting rising geothermal fluids have to be taken into account. Since it is not possible to separate the effects of two or more secondary phenomena for a given sample, we implicitly assume that only one of these phenomena is important in each case. Among these secondary phenomena, boiling and steam condensation (for computing the effects of the latter process see Chiodini and Marini, 1998), can bring about large chemical changes, due to distribution of different gas species between separating liquid and vapor phases. To calculate the effects of boiling on the theoretical values of $\log(X_{H2}/X_{H2O})_L$, $\log(X_{CO}/X_{CO2})_L$, $\log(X_{CH4}/X_{CO2})_L$, $\log(X_{CO}/X_{CO2})_L - \log(X_{H2}/X_{H2O})_L$, and $3\log(X_{CO}/X_{CO2})_L + \log(X_{CO}/X_{CH4})_L$, it is assumed attainment of chemical equilibrium in a single saturated liquid phase at initial (equilibrium) temperature To, followed by adiabatic single-step steam separation at temperature Ts. Under these assumptions, the mole fractions of the gas species of interest in the separated vapor phase are constrained by simple mass balances (e.g., Eqn. 6.15) and enthalpy balance (Eqn. 6.4). The following relations are obtained inserting expression (6.15) into equations (9.25), (9.26), (9.27), (9.33) and (9.34):

$$\log(X_{H2}/X_{H2O})_{Ts} = \log K_{H2} - ½ \log f_{O2} - \log(y+(1-y)/B_{H2,Ts}) - \log B_{H2,To} \quad (9.42)$$

$$\log(X_{CO}/X_{CO2})_{Ts} = \log K_{CO} - ½ \log f_{O2} - \log(y+(1-y)/B_{CO,Ts}) + \log(y+(1-y)/B_{CO2,Ts}) \\ - \log B_{CO,To} + \log B_{CO2,To} \quad (9.43)$$

$$\log(X_{CH4}/X_{CO2})_{Ts} = \log K_{CH4} - 2 \log f_{O2} + 2 \log f_{H2O} - \log(y+(1-y)/B_{CH4,Ts}) \\ - \log B_{CH4,To} + \log(y+(1-y)/B_{CO2,Ts}) + \log B_{CO2,To} \quad (9.44)$$

$$\log(X_{CO}/X_{CO2})_{Ts} - \log(X_{H2}/X_{H2O})_{Ts} = \log K_{WGS} - \log(y+(1-y)/B_{CO,Ts}) - \log B_{CO,To} \\ + \log(y+(1-y)/B_{CO2,Ts}) + \log B_{CO2,To} \\ + \log(y+(1-y)/B_{H2,Ts}) + \log B_{H2,To} \quad (9.45)$$

$$3\log(X_{CO}/X_{CO2})_{Ts} + \log(X_{CO}/X_{CH4})_{Ts} = \log K_{CCC} - 2 \log f_{H2O} - 4\log(y+(1-y)/B_{CO,Ts}) \\ - 4\log B_{CO,To} + \log(y+(1-y)/B_{CH4,Ts}) + \log B_{CH4,To} \\ + 3\log(y+(1-y)/B_{CO2,Ts}) + 3\log B_{CO2,To} \quad (9.46)$$

The theoretical log ratios and sums of log ratios values in the vapor phase separated at different temperatures from a liquid phase initially at 150°, 200°, 250°, 300° and 350 °C are shown in Figs. 9.4-9.6 as single-step vapor separation lines (SSVS lines). In Figs.

9.4 and 9.6 the theoretical values of vapor separated at 100° and 200°C starting from any initial temperature are represented as Ts lines.

9.2.5. Comparison between theoretical and analytical compositions

Analytical data spread throughout the theoretical grids in the $\log(X_{CO}/X_{CO2})$ vs $\log(X_{H2}/X_{H2O})$ plot (Fig. 9.4), which is slightly affected by the choice of redox buffer.

In the $\log(X_{CH4}/X_{CO2})$ vs $\log (X_{CO}/X_{CO2})$ plot (Fig. 9.5), the field of saturated vapors overlaps that of superheated vapors, thus complicating the interpretation of measured data. In addition, a large number of analytical data plot outside the theoretical grid, using either the redox buffer by Giggenbach (1987) or that of D'Amore and Panichi (1980). As the CH_4/CO_2 ratio is strongly affected by redox conditions in the gas equilibration zone, this disagreement between measured and theoretical values suggests that no unique redox buffer is active in all the geothermal environments. Alternatively, CH_4 might be out of equilibrium with the other gases due to kinetic reasons. An attempt to quantify the kinetics of chemical equilibration between CO_2 and CH_4 was presented by Giggenbach (1997b). Assuming that the conversion of CO_2 to CH_4 may be described by a pseudo-first order reaction, the reaction half-time would be about 12a at 300°C, 500a at 200°C and 160ka at 100°C. However, these are very preliminary estimates based on limited experimental data and further researches are needed to clarify the kinetics of conversion of CO_2 to CH_4 in the presence of catalysts occurring in natural environments (Giggenbach, 1997b).

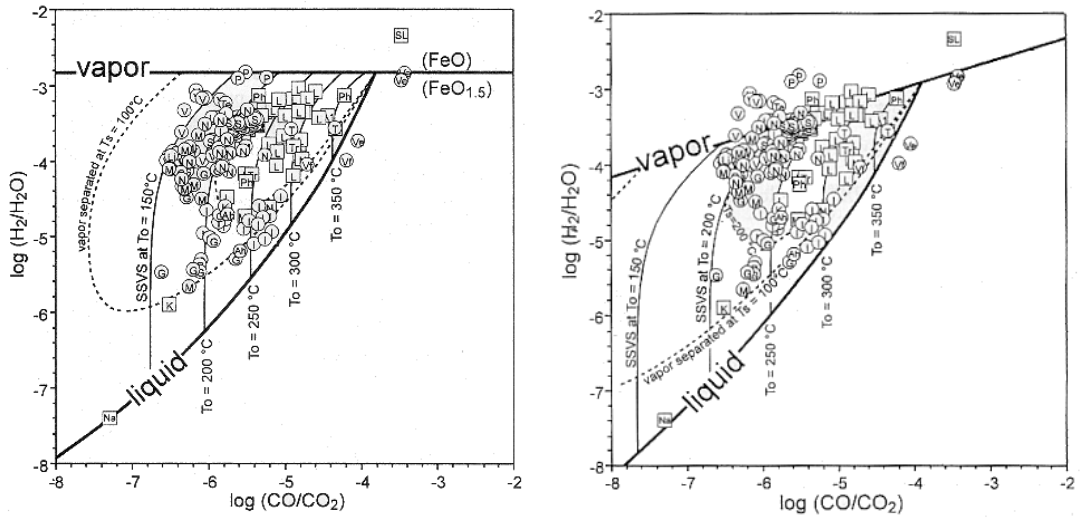

Fig. 9.4. Plot of $\log(X_{H2}/X_{H2O})$ vs $\log(X_{CO}/X_{CO2})$. The theoretical grid assumes that redox conditions in the gas equilibration zone are controlled either by the FeO-$FeO_{1.5}$ hydrothermal buffer of Giggenbach (left) or by the f_{O2}-buffer of D'Amore and Panichi (right). Compositions of both the vapor and liquid phases (thick solid lines) are shown. Compositions of the vapor phase separated in a single-step (SSVS) at different temperatures from a liquid phase initially at To = 150°, 200°, 250°, 300° and 350 °C are also shown (thin solid lines) as well as the compositions resulting from single-step vapor separation at two fixed Ts temperatures (100° and 200°C) starting from any initial temperature (dashed lines). Circles = fumarolic vapors; squares = vapors from geothermal wells (from Chiodini and Marini, 1998).

The diagrams that make use of 2 sums of log-ratios [e.g., $\log(X_{CO}/X_{CO2})$ - $\log(X_{H2}/X_{H2O})$, and $3\log(X_{CO}/X_{CO2}) + \log(X_{CO}/X_{CH4})$, Fig. 9.6] are independent of redox conditions. In addition, the weight of CH_4 on these functions is relatively small and these sums of log-ratios are mainly controlled by the CO/CO_2 and H_2/H_2O ratios. These

functions gave reasonable estimates of the equilibrium temperature and, therefore, can be used as effective geoindicators in most geothermal systems.

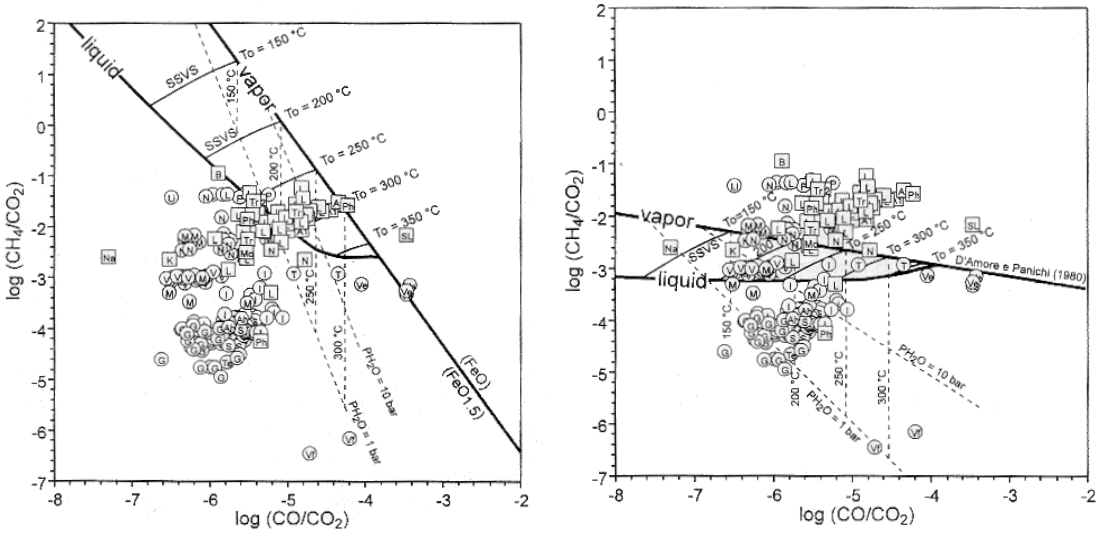

Fig. 9.5. Plot of $\log(X_{CH4}/X_{CO2})$ vs $\log(X_{CO}/X_{CO2})$. Theoretical grids for coexisting liquid plus vapor phases (solid lines) and superheated vapors (dashed lines) are calculated assuming that redox potentials in the gas equilibration zone are controlled by the either the FeO-$FeO_{1.5}$ hydrothermal buffer (left) or the f_{O2}-buffer of D'Amore and Panichi (right). Symbols as in Fig. 9.4 (from Chiodini and Marini, 1998).

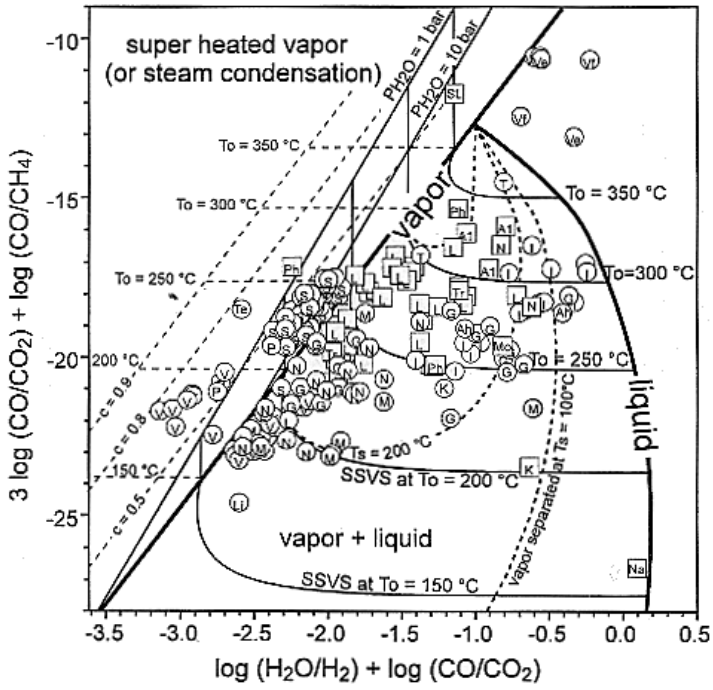

Fig. 9.6. Plot of $3\log(X_{CO}/X_{CO2}) + \log(X_{CO}/X_{CH4})$ vs. $\log(X_{CO}/X_{CO2}) - \log(X_{H2}/X_{H2O})$. Phase lines and symbols as in Fig. 9.4. The compositions of superheated vapors equilibrated at different temperature-P_{H2O} values (solid lines), and the compositions of equilibrated, single vapor phases affected by steam condensation at Tc = 100°C (dashed lines) are also shown. The curves labelled c = 0.5, c = 0.8 and c = 0.9 refer to different fractions of condensed steam (from Chiodini and Marini, 1998).

9.3. Geothermal gas equilibria in the H_2O-H_2-H_2S system

Giggenbach (1980) showed that the H_2S fugacity in hydrothermal environments is controlled by coexisting pyrite, an unspecified Fe-Al-silicate (here indicated as [FeO], probably chlorite or epidote in natural systems) and the corresponding Al-silicate in its protonated, Fe-free form, [H_2O], as expressed by the following reaction (after Giggenbach, 1980, modified):

$$FeS_2 + H_2O + [H_2O] = [FeO] + 1/2\ O_2 + 2\ H_2S, \quad (9.47)$$

whose equilibrium constant is conveniently written as:

$$\log (X_{H2S}/X_{H2O}) = ½ \log K_S – ¼ \log f_{O2} - ½ \log f_{H2O}. \quad (9.48)$$

As indicated by Eqn. (9.48), equilibrium X_{H2S}/X_{H2O} ratios depend upon temperature, redox potential and water fugacity in the gas equilibration zone. The temperature dependence of the thermodynamic constant K_S is given by the following equation:

$$\log K_S = 2.388 - 13211.8/T(K), \quad (9.49)$$

which is based on an empirical correlation by Giggenbach (1980) and on the thermodynamic constant of water formation from elements (Stull et al., 1969). Assuming that redox conditions in the gas equilibration zone are fixed by either Eqns. (9.13) or (9.14) and water fugacity is constrained by Eqn. (9.6), the temperature dependence of the theoretical X_{H2S}/X_{H2O} ratio in a single saturated vapor phase can be easily computed.

9.4. Geothermal gas equilibria in the H_2O-H_2-N_2-NH_3 system

Ammonia and N_2 are involved in the following redox reaction (Giggenbach, 1980, modified):

$$N_2 + 3\ H_2O = 2\ NH_3 + 3/2\ O_2 \quad (9.50)$$

whose equilibrium constant can be written as

$$L_N = \log (X_{NH3}/X_{N2}) + \log (X_{NH3}/X_{H2O}) = \log K_N - 3/2 \log f_{O2} + 2 \log f_{H2O}. \quad (9.51)$$

Eqn. (9.51) indicates that theoretical L_N values are controlled by temperature, redox conditions and water fugacity in the gas equilibration zone. On the basis of the thermodynamic data of Stull et al. (1969), the temperature dependence of the thermodynamic constant K_N is described by:

$$\log K_N = -3.996 - 32863/T(K). \quad (9.52)$$

Again, assuming that redox conditions in the gas equilibration zone are fixed by suitable f_{O2}-buffers, e.g., Eqns. (9.13) or (9.14), and water fugacity is constrained by Eqn. (9.6), the temperature dependence of the theoretical L_N values in a single saturated vapor phase can be easily computed.

9.5. The H_2-Ar geoindicator

Giggenbach (1991a) derived a H_2-Ar geoindicator which is based on the strong dependence of f_{H2} on temperature and on the assumption that the Ar content of hydrothermal fluids derives almost entirely from air-saturated meteoric waters involved in the recharge of these systems. A derivation slightly different from that of Giggenbach (1991a) is presented hereunder.

First of all, it is convenient to test the Giggenbach's hypothesis, i.e., to verify if the Ar contents of fumarolic fluids are equal to those of air-saturated groundwaters or not. This exercise is conveniently carried out by means of a H_2O-N_2-Ar triangular plot (Fig. 9.7), where the fumarolic samples are plotted together with the points representative of atmospheric air and air-saturated groundwaters at 5, 10, 15 and 20°C. The composition air-saturated groundwaters is easily computed referring to the solubility data of Wilhelm et al. (1977) and considering that the average atmospheric partial pressures of Ar and N_2 are 0.00934 bar and 0.7808 bar, respectively. For

instance, at 12°C $K_{H,Ar}$ = 31289 and $K_{H,N2}$ = 69013 bars (mole fraction)$^{-1}$; therefore log X_{Ar} = -6.52 and log X_{N2} = -4.95.

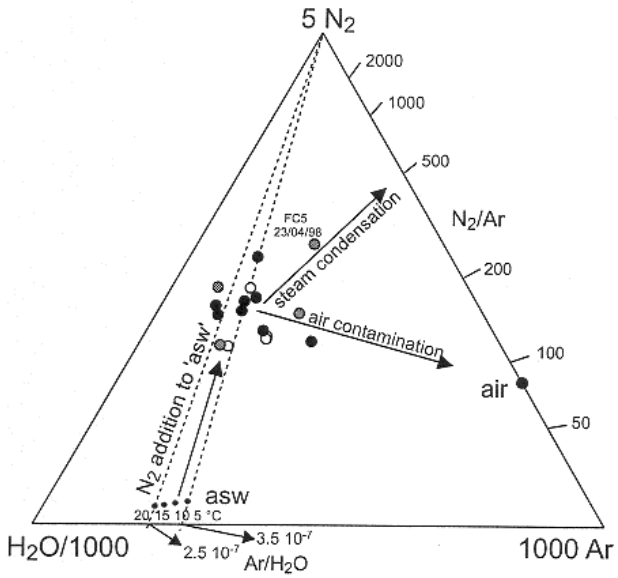

Fig. 9.7. Triangular plot H_2O-N_2-Ar, showing analytical data of Vesuvius fumaroles and the compositions of atmospheric air and of air-saturated groundwater at 5-20°C (from Chiodini et al., 2000c).

According to Giggenbach (1987), the log $(f_{H2}/f_{H2O}) \cong$ log $(X_{H2}/X_{H2O})_V$ of hydrothermal fluids is buffered by the (FeO) – ($FeO_{1.5}$) redox buffer of the rock system at –2.82, at any temperature of interest. Assuming that the X_{Ar}/X_{H2O} ratio in the liquid phase is equal to that of average air saturated groundwater, and admitting that X_{H2O} is close to unity, both in the liquid and vapor phases, the X_{Ar}/ X_{H2O} ratio in the vapor phase is given by:

$$\log (X_{Ar}/ X_{H2O})_V = \log B_{Ar} + \log (X_{Ar}/ X_{H2O})_L = \log B_{Ar} - 6.52. \quad (9.53)$$

The theoretical X_{H_2}/X_{Ar} ratio in the vapor phase is readily obtained as follows:

$$\log (X_{H2}/X_{Ar})_V = \log (X_{H2}/X_{H2O})_V - \log (X_{Ar}/X_{H2O})_V =$$
$$= 3.7 - \log B_{Ar} . \quad (9.54)$$

The vapor-liquid distribution coefficient of Ar is related to temperature by the following linear equation (data from Naumov et al., 1974; T is in °C):

$$\log B_{Ar} = 6.4822 - 0.0160\ T. \quad (9.55)$$

Therefore, the H_2/Ar ratio in the vapor phase is linked to temperature by this equation:

$$\log (X_{H2}/X_{Ar})_V = -2.78 + 0.016\ T. \quad (9.56)$$

A similar expression holds true for the liquid phase, as already observed by Giggenbach (1991a):

$$\log (X_{H2}/X_{Ar})_L = -2.53 + 0.014\ T. \quad (9.57)$$

The similarity of the two expressions is not surprising because the vapor-liquid distribution coefficients of H_2 and Ar are quite similar.

These two equilibrium relationships are compared with some analytical data of geothermal and volcanic discharges in Fig. 9.8 (data from Giggenbach, 1991a, 1996, 1997a). Most points distribute close to the theoretical relationships, even at temperatures lower than 100°C. For the points situated to the left of the equilibrium lines, it is possible to hypothesize quenching of H_2/Ar ratio upon cooling.

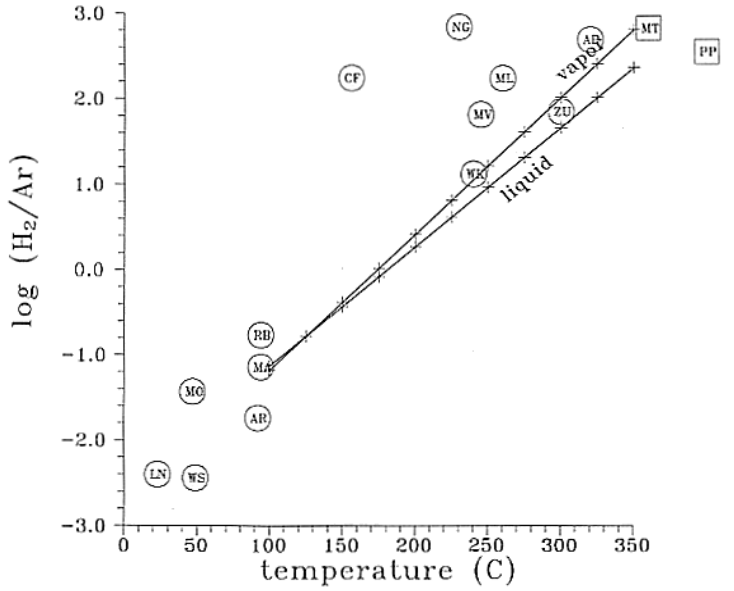

Fig. 9.8. Comparison of analytical (data from Giggenbach, 1991a, 1996, 1997a) and theoretical H_2/Ar ratios.

9.6. Gas solubilities in NaCl solutions

All the expressions considered above for describing the temperature dependence of the vapor-liquid distribution coefficient of gas species are valid for pure water and can be extended to low salinity aqueous solutions. Expressions valid for aqueous solutions of relatively high salinity can be obtained based on the experimental data available for CO_2 and H_2S (Chiodini et al., 2000c).

Gas solubilities of CO_2 in pure water and in 0.5, 1, and 2 m NaCl solutions were measured, at temperatures of 172-334°C, by Ellis and Golding (1963), whereas the solubility of H_2S in pure water and in NaCl solutions up to 2.5 m were determined, at temperatures up to 320°C, by Suleimenov and Krupp (1994). These are the most complete datasets on the solubility of these two gases in high-temperature NaCl solutions. Unfortunately, no experimental data are available on the solubilities of other geothermal-volcanic gases in high-temperatures NaCl solutions. Solubility of H_2S in pure water at high temperatures was also investigated by Drummond (1981) and Kozintseva (1964).

Gas solubilities in salt solutions are usually expressed through the salting out coefficient of Sechënov (or Setchenov, or Setschenow). This is a useful generalization for gas species of known solubilities, both in pure water and salt solutions, but they cannot be used to predict the behavior of other gases.

To this purpose, Chiodini et al. (2000c) found a tight linear relation between the logarithm of the vapor-liquid distribution coefficient of CO_2 and H_2S, both in pure water and in NaCl aqueous solutions, (which have been calculated from available experimental data) and the following parameter:

$$L_\rho = \log (\rho_V / \rho_L) - \log \rho_C, \qquad (9.58)$$

where ρ_L is the density of the salt solution (Ellis and Golding, 1963), ρ_V is the density of the vapor phase and ρ_C is the critical density (Knight and Bodnar, 1989). The density of the vapor phase in equilibrium with NaCl solutions has been taken equal to the that of pure steam at the same P,T conditions (data from Keenan et al., 1969). As suggested by Tanger and Pitzer (1989), this is an acceptable approximation because the fraction of NaCl present in the vapor phase is very small.

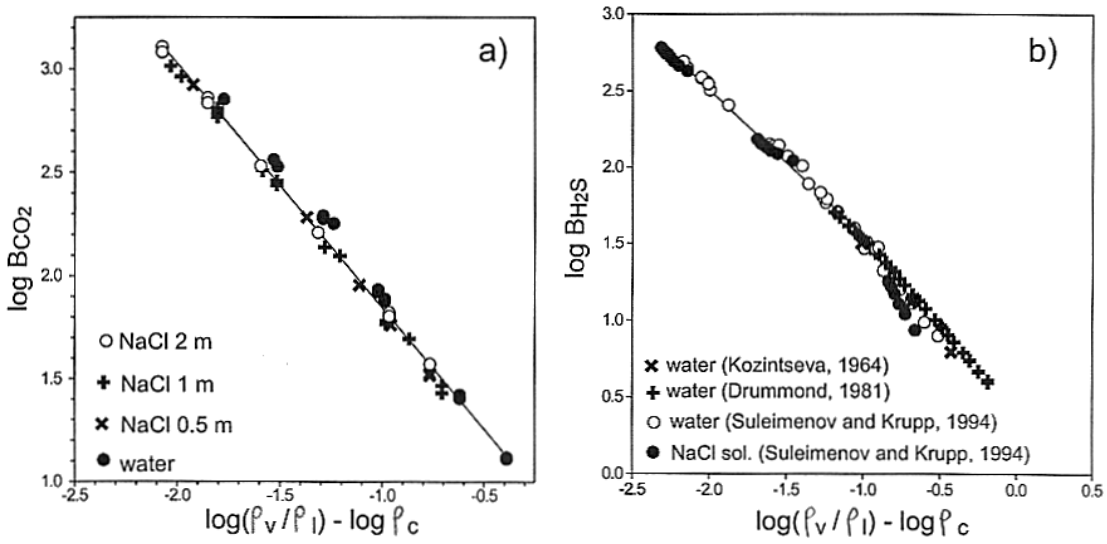

Fig. 9.9. Correlation plots between the logarithm of the vapor-liquid distribution coefficient B_i, for (a) CO_2 and (b) H_2S, and the L_ρ parameter, which is equal to log (ρ_V / ρ_L) - log (ρ_C) (from Chiodini et al., 2000c)

Inspection of Fig. 9.9 shows that all the log B_{CO_2} values, for pure water and salt solutions, define a unique alignment, which is described by the following linear regression equation (R=-0.997):

$$\log B_{CO_2} = 0.66566 (\pm 0.00701) - 1.1807 (\pm 0.0132) L_\rho. \quad (9.59)$$

A similar linear regression equation is obtained for H_2S, at least for $L_\rho < -0.9$, corresponding to T < 275°C (R=-0.997):

$$\log B_{H_2S} = 0.6058 (\pm 0.0110) - 0.9503 (\pm 0.0108) L_\rho. \quad (9.60)$$

For $L_\rho > -0.9$ (T > 275°C) experimental solubility data, both in pure water and NaCl solutions deviate from the linear trend depicted by Eqn. (9.60). Besides, at $L_\rho > -0.9$, the B_{H_2S} in NaCl solutions are significantly lower than in pure water for the same L_ρ values. These discrepancies might be due to experimental problems (perhaps due to the strongly corrosive nature of the mixed sulfide-chloride solutions; Kozintseva, 1965), which are probably more severe at higher temperatures. Therefore, we prefer to rely on the measurements carried out at T < 275°C.

Coupling Eqns. (9.59) and (9.60) with the linear equation linking L_ρ and T(°C) for a specified NaCl concentration, log B_{CO_2} - T and log B_{H_2S} - T relationships are easily obtained for this NaCl concentration. Equations linking log B_i and L_ρ have been derived for other geothermal-volcanic gases from solubilities in pure water (Giggenbach, 1980; Naumov et al., 1974) and corresponding L_ρ values. Assuming that these equations hold true also for NaCl solutions, as documented above for CO_2 and H_2S, log B_i - T relationship for 1, 2, and 3 m NaCl solutions have been obtained through substitution of L_ρ - T equations in log B_i - L_ρ equations (Chiodini et al., 2000c).

However, it must be stressed that Eqns. (9.59) and (9.60), and consequently all the similar relationships for other gas constituents, are expected to give erratic results close to the critical point of any NaCl-H_2O solution. In fact, approaching this condition, log $B_i \rightarrow 0$ and $L_\rho \rightarrow$ log ρ_C. Since the critical density of NaCl-H_2O solutions varies with the NaCl concentration, these equations lose their validity approaching critical conditions.

10. The δD and $\delta^{18}O$ values of geothermal fluids

The δD and $\delta^{18}O$ values of liquids circulating in deep, high-temperature geothermal systems are controlled by several processes, including (Giggenbach, 1991b): (1) rock-water ^{18}O exchange, (2) mixing of different waters (meteoric waters, marine waters, connate waters, magmatic waters, ...), and (3) steam separation (boiling).

10.1. The rock-water ^{18}O exchange

The ^{18}O exchange between a geothermal liquid and a given mineral is governed, at equilibrium, by the fractionation factors $\alpha_{m\text{-}w}$, which is defined as follows:

$$\alpha_{m\text{-}w} = (^{18}O/^{16}O)_m / (^{18}O/^{16}O)_w \qquad (10.1)$$

Equilibrium isotope fractionation factors can be computed through the partition functions, i.e., mathematical relationships coming from statistical mechanics (e.g., Richet and Bottinga, 1976; Richet al al., 1977; Kieffer, 1982; O'Neil, 1986).

The $\alpha_{m\text{-}w}$ values increase with increasing strength of the chemical bonds holding oxygen atoms into a given mineral lattice. Quartz and calcite have high $\alpha_{m\text{-}w}$ values, whereas feldspars have low $\alpha_{m\text{-}w}$ values (see insert in Figure 10.1, where $\varepsilon_{m\text{-}w} = 1000 \ln\alpha_{m\text{-}w}$ is reported against temperature). In general, equilibrium isotope fractionation factors are temperature dependent and approach 1 (which means small fractionation) with increasing temperature. However, the $\alpha_{m\text{-}w}$ values of quartz, calcite, and feldspars are significantly >1 ($\varepsilon_{m\text{-}w}$ >0) for temperatures lower than 400°C.

The decrease in temperature brings about also a quick decrease in the kinetics of the ^{18}O exchange between minerals and water. Therefore, ^{18}O enrichments in Na-Cl geothermal liquids with respect to meteoric waters (usually called "shifts") have been traditionally considered as indicators of high temperatures (>150 °C) in the geothermal reservoirs of provenance (e.g., Truesdell and Hulston, 1980 and references therein). However, the ^{18}O shifts depend also on the initial isotope composition of the liquid and solid phases involved in the exchange process as well as on the water/rock ratio, or on system dynamics (Giggenbach, 1991b, see below).

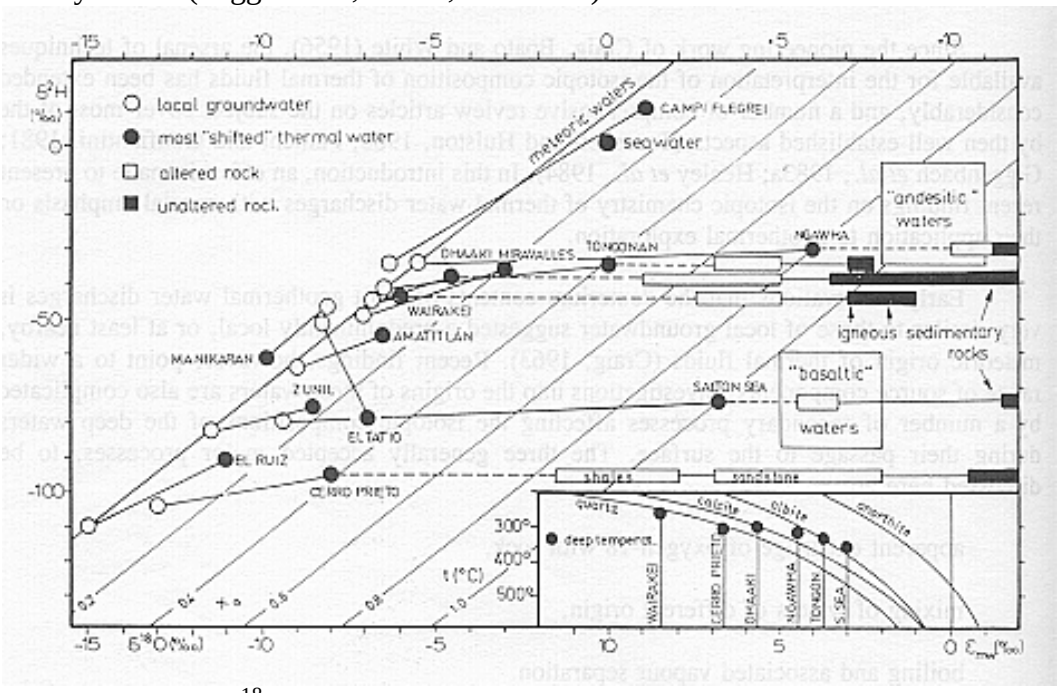

Figure 10.1. δD and $\delta^{18}O$ values of shallow and deep thermal waters and altered and unaltered rocks form different geothermal systems. In the insert the equilibrium fractionation factors between minerals and water are compared with those observed in some geothermal systems (from Giggenbach, 1991b).

These ^{18}O shifts are not accompanied by hydrogen isotope shifts because (1) rock minerals contain little hydrogen and (2) water/rock ratios are usually relatively high and, consequently, the hydrogen of rock minerals is not a significant fraction of the total hydrogen of the water-rock system, which is dominated by water.

Referring to the geothermal systems of New Zealand, Giggenbach (1991b) underscored the differences between Ngawha and Wairakei.

At Ngawha (temperatures up to 320°C), the least diluted water is remarkably enriched in ^{18}O with respect lo local meteoric waters and it is only 5‰ lighter than rocks. Besides altered rocks have $\delta^{18}O$ values, which are not much different from those of unaltered rocks. Water approaches isotopic equilibrium with rocks, since the system is almost stagnant and rock-dominated.

At Wairakei (temperatures close to 260°C) the ^{18}O enrichment of the geothermal liquids with respect lo local meteoric waters is small, ~1.2 ‰, and altered rocks are, with $\delta^{18}O$ values of 2.5 to 5 ‰, much lighter than unaltered rocks, whose $\delta^{18}O$ values range from 7 to 9 ‰. Wairakei appears to be a dynamic, water-dominated geothermal system, i.e., flushed by large water flows.

This distinction between stagnant, rock-dominated systems and dynamic, water-dominated (Giggenbach, 1991b) is more reasonable than that based on the water/rock ratio.

10.2. Mixing of different waters

A second type of processes affecting the δD and $\delta^{18}O$ values of geothermal liquids is mixing between local meteoric waters and waters of different origin, such as: (1) marine waters (e.g. Campi Flegrei in Fig. 10.1); (2) high-salinity waters or connate waters, especially in sedimentary basins; examples of this class of waters are represented by the brines circulating in the geothermal systems of Salton Sea and Cerro Prieto, whose high salinity is ascribable to leaching of evaporite rocks; the interaction of these stagnant brines with fine grained sediments at temperatures close to 350°C explains their enrichment in ^{18}O; (3) magmatic waters, as anticipated in the Introduction.

The andesitic or arc-type magmatic water, which is characterized by δD values of -10 to -30 ‰, is found in all the geothermal areas located along convergent plate boundaries as well as in areas which were affected by subduction in a geologically recent past (e.g., Tyrrhenian Central-Southern Italy). In some of these volcanic areas (e.g., Amatitlan and Zunil, Guatemala, and Miravalles, Costa Rica), if the involvement of andesitic water is ruled out, dilution trends would imply that geothermal waters derived from rain waters infiltrating at low elevations mix with shallow groundwaters infiltrating at high elevations, which is a rather queer hydrogeological model.

It must be recalled that the isotopic ratios of any binary mixture made of, for instance, a thermal endmember and a cold endmember are constrained by the following general binary mixing equation (Faure, 1986):

$$\delta_M = [\delta_T C_T x + \delta_F C_F(1-x)]/C_M \qquad (10.2)$$

where subscripts M, T, and F identify the binary mixture, the thermal endmember and the cold endmember and x is the fraction of the thermal component in the mixture. If $C_T \neq C_F \neq C_M$ the binary mixing line is a hyperbola in δ - C and δ - δ spaces, but it becomes a straight line in the δ - (1/C) space. Since water is by far the major component of any aqueous solution, $C_T = C_F = C_M$, and Eqn. (10.2) reduces to:

$$\delta_M = \delta_T x + \delta_F (1-x) \qquad (10.3)$$

which is equivalent to Eqn. (6.1). As a consequence, mixing lines are straight lines in the δ - C and δ - δ spaces, but this is the exception, not the rule, a fact which cannot be

forgotten when working with isotope ratios of chemical constituents different from water.

10.3. Steam separation

Steam separation (boiling) takes place when the vapor pressure (plus the sum of the partial pressures of dissolved gases) of high-temperature (>>100 °C) geothermal waters uprising towards the surface exceeds the hydrostatic burden. This process brings about isotopic fractionation, with heavy isotopes concentrating in the liquid (at any temperature for ^{18}O and at temperatures below 229°C for deuterium in a pure water system) whereas the vapor phase is obviously depleted in heavy isotopes.

The isotopic fractionation factor decreases approaching the critical point both for ^{18}O and D. It is recalled that the critical point is 374°C, 221 bar for pure water, but depending on the salt content of the NaCl-H_2O system (which is the obvious, simplest analogue of the complex, natural geothermal liquids), the critical point is shifted to pressures and temperatures significantly higher than those of pure water (e.g., Bischoff and Pitzer, 1989; Knight and Bodnar, 1989). Liquid-vapor fractionation factors of O and H isotopes for pure water from 0°C to the critical temperature are given by the following relationships (Horita and Wesolowski, 1994, T in K):

$$1000 \ln \alpha_{L\text{-}V}(D) = 1158.8(T^3/10^9) - 1620.1(T^2/10^6) + 794.84(T/10^3) - 161.04 + 2.9992(10^9/T^3) \quad (10.4)$$

$$1000 \ln \alpha_{L\text{-}V}(^{18}O) = -7.685 + 6.7123(10^3/T) - 1.6664(10^6/T^2) + 0.35041\,(10^9/T^3). \quad (10.5)$$

Computed values of 1000 ln $\alpha_{L\text{-}V}$ are approximated to ±1.2 ‰ (1 σ) for D and ±0.11 ‰ (1 σ) for ^{18}O. Liquid-vapor fractionation factors for NaCl solutions from 0 to 5 m NaCl, are computed by means of the following equations (Horita et al., 1995):

$$1000 \ln \Gamma(D) = m\,(0.01680\,T - 13.79 + 3255/T) \quad (10.6)$$

$$1000 \ln \Gamma(^{18}O) = m\,(-0.033 + 8.93\times10^{-7}\,T^2 - 2.12\times10^{-9}\,T^3) \quad (10.7)$$

where

$$1000 \ln \Gamma = 1000 \ln \alpha_{L\text{-}V(\text{pure water})} - 1000 \ln \alpha_{L\text{-}V(\text{salt soln.})} \quad (10.8)$$

m is the molality of the NaCl solution and T is in K. Computed values of 1000 ln $\alpha_{L\text{-}V}$ are approximated to ±0.9 ‰ (1 σ) for D and ±0.12‰(1 σ) for ^{18}O. At temperatures above 350°C, the fractionation factors can be obtained interpolating between the value at 350 °C and 0 ‰, i.e., the theoretical value at the critical temperature. Since at these high temperatures the fractionation factors are relatively small (-10 to 0 ‰ for H isotopes and +1 to 0 ‰ for O isotopes), uncertainties in this interpolation have negligible effects on boiling calculations.

Fractionation of O and H isotopes between liquid water and vapor attains equilibrium almost immediately, even at temperatures close to 100°C. Isotopic fractionation depends also on the fraction of separated steam and the kind of separation (single step, multistep or continuous). In general, natural steam separation processes are satisfactorily approximated by the single step model (Truesdell et al, 1977; Giggenbach, 1978; Giggenbach and Stewart, 1982). In this case, the δ values of the separated vapor and liquid, δ_V e δ_L, are related to that of the initial liquid, δ_T, by the following mass balance:

$$\delta_T = \delta_L\,(1\text{-}y) + \delta_V\,y \quad (10.9)$$

and by the approximate relationship:

$$1000 \ln\alpha_{L\text{-}V} = \delta_L - \delta_V. \quad (10.10)$$

For isoenthalpic steam separation y is calculated through Eqn. (6.5). The following relationships are easily obtained from Eqns. (10.9) and (10.10):

$$\delta_L = \delta_T + y\,1000 \ln\alpha_{L\text{-}V} \quad (10.11)$$

$$\delta_V = \delta_T - (1-y)\ 1000\ \ln\alpha_{L\text{-}V} \qquad (10.12)$$

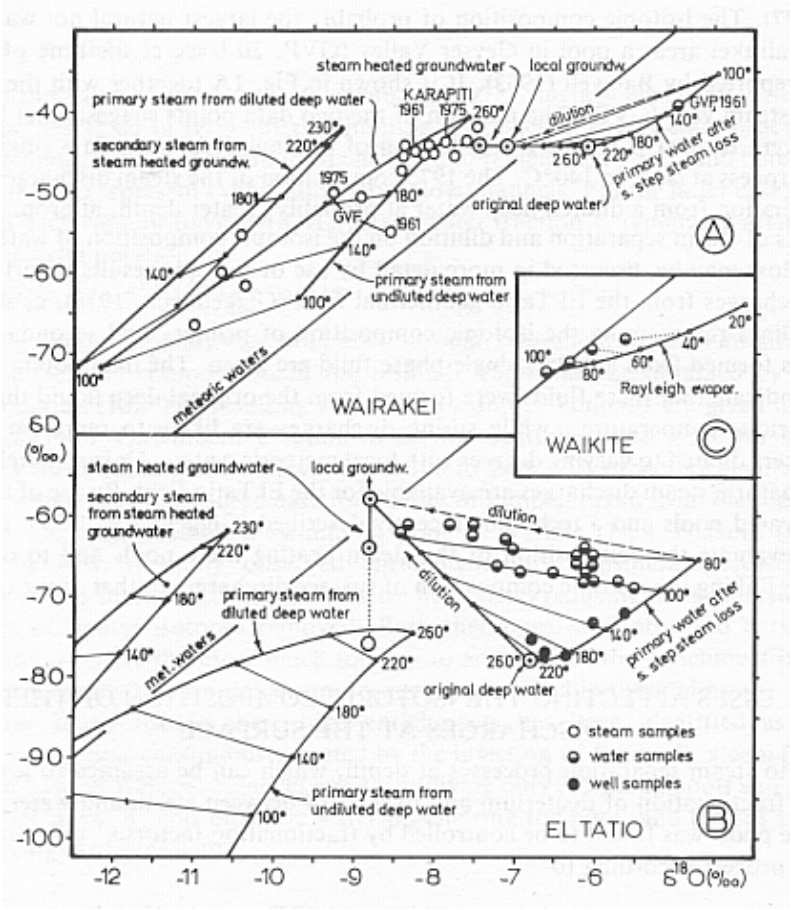

Fig. 10.2. δD vs. $\delta^{18}O$ plot comparing observed and theoretical isotope values of vapor and liquid produced through boiling of a parent geothermal liquid (from Giggenbach and Stewart, 1982).

They allow one to compute the theoretical δD and $\delta^{18}O$ values of the separated vapor and liquid during the evolution of the process. Further theoretical models involve boiling of diluted waters, absorption of maximum enthalpy steam in local groundwater (Giggenbach and Stewart, 1982), and condensation (Brombach et al., 2000c). Theoretical values can be compared with observed values in a δD vs. $\delta^{18}O$ plot (Fig. 10.2).

The isotope composition of acid sulfate waters of steam-heated pools (which are produced through input of steam in very shallow or stagnant surface waters) reflects instead non-equilibrium surface evaporation (Giggenbach and Stewart, 1982). This process brings about dramatic enrichments in heavy isotopes, with respect to local meteoric waters (Fig. 10.3). The slope of the straight line connecting data poins from steam-heated pools is given by:

$$\sigma_P = (\delta D_{si} - \delta D_{wi} + \varepsilon_D) / (\delta^{18}O_{si} - \delta^{18}O_{wi} + \varepsilon_{18O}) \qquad (10.13)$$

where the subscripts si and wi refer to the steam entering the pool and to local groundwater, respectively, whereas ε_i is the average kinetic isotope fractionation factor, which is close to 50 ‰ for D and 16‰ for ^{18}O, according to Giggenbach and Stewart (1982).

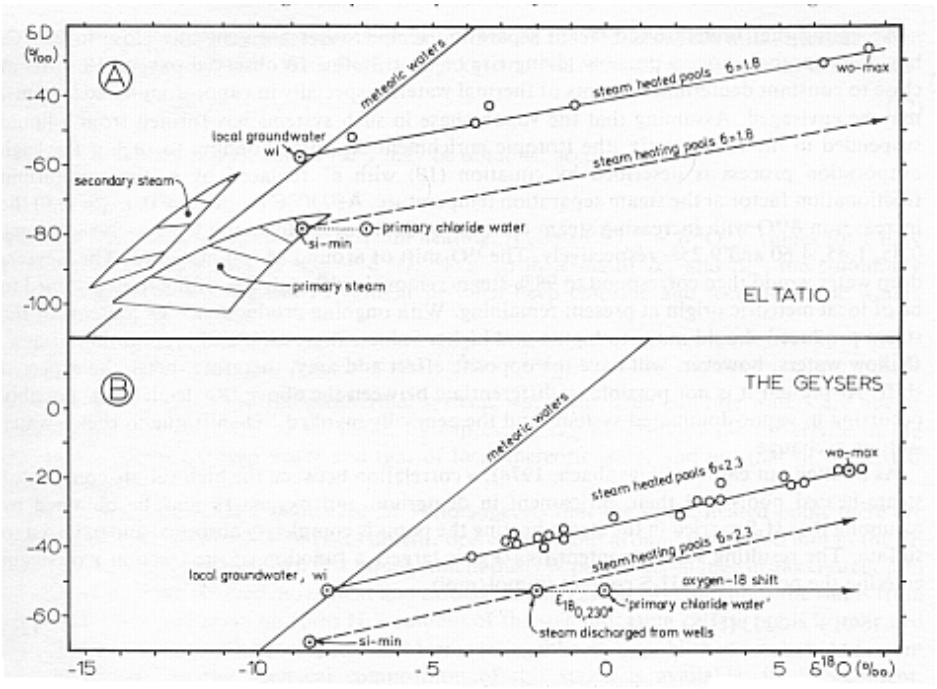

Fig. 10.3. δD vs. $\delta^{18}O$ plot showing the non-equilibrium surface evaporation effects of steam-heated pools (from Giggenbach and Stewart, 1982).

In the previous discussion it was implicitly assumed that analytical δD and $\delta^{18}O$ values of water vapor are fully representative of its isotopic composition at any P,T condition. However, this is not always true.

Chiodini et al. (2000a) showed that the $\Delta^{18}O_{CO2\text{-}H2O}$ for geothermal and volcanic vapors is very close to the theoretical oxygen isotope fractionation factor between $CO_{2(g)}$ and $H_2O_{(g)}$ at outlet temperatures, suggesting that these two species are in isotopic equilibrium at outlet conditions (Fig. 10.4). This implies that the oxygen isotope exchange between $CO_{2(g)}$ and $H_2O_{(g)}$ is a quick process. Therefore the correct interpretation of the $\delta^{18}O$ values of geothermal vapors demands to correct the analytical $\delta^{18}O$ values of H_2O for the isotopic exchange with CO_2. Obviously, this correction is important for CO_2-rich vapors. The initial $\delta^{18}O$ value of water, $\delta^{18}O_{H2O,i}$ (i.e., in the geothermal reservoir), is calculated from the final $\delta^{18}O$ value of water, $\delta^{18}O_{H2O,f}$ (i.e., at the surface discharge), combining a simple oxygen isotope mass balance with the oxygen isotope fractionation factors under both initial and final conditions, thus obtaining the following relationship:

$$\delta^{18}O_{H2O,i} = \delta^{18}O_{H2O,f} - [2\ X_{CO2}/(1+X_{CO2})]\ [1000\ \ln\alpha_i - 1000\ \ln\alpha_f], \qquad (10.14)$$

Here α identifies the oxygen isotope fractionation factor between $CO_{2(g)}$ and $H_2O_{(g)}$, whose temperature dependence is satisfactorily explained by this third order polynomial equation (Chiodini et al., 2000a):

$$1000\ \ln\alpha = -5.7232 + 20.303(10^3/T) - 11.977(10^6/T^2) + 3.7432(10^9/T^3) \qquad (10.15)$$

that closely fit the theoretical fractionation factors of Richet et al. (1977) below 400°C and those of Friedman and O'Neil (1977) at higher temperatures, up to 1000°C.

More information is needed to evaluate the possible fractionation effects between H_2O and other H-species, mainly H_2S.

11. How much water and heat can be extracted from a geothermal system ?

At this point you have probably realized that there are many geochemical techniques, more or less sophisticated, to estimate the temperature and other intensive properties of fluids circulating in geothermal systems.

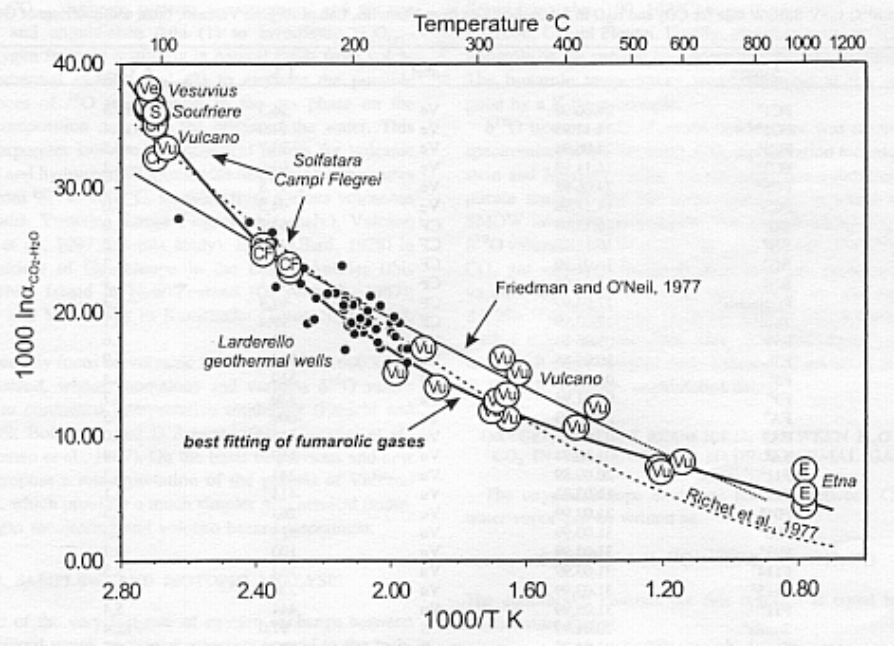

Fig. 10.4. The $\Delta^{18}O_{CO2\text{-}H2O}$ of vapors discharged from Italian volcanic and hydrothermal areas is plotted against outlet temperatures. Theoretical equilibrium fractionation factors according to Friedman and O'Neil (1977) and Richet et al. (1977) are shown for comparison.

The title of this section is, instead, a question which is difficult to be answered, but of crucial importance in the development of geothermal exploration-exploitation programs. Again, geochemistry can play a fundamental role.

11.1. Total natural discharge based on Cl balance

It is common practice to estimate the total natural discharge (the fluxes of water and heat) of geothermal systems, by measuring the flowrate and chloride content of all the thermal springs present in the surveyed area (Ellis and Mahon, 1977). The natural heat discharge represents the minimum recoverable energy flow from the geothermal system, assuming that the system is close to steady state conditions, i.e., that there is a sort of balance between discharge and recharge.

First the chloride content and enthalpy of the parent geothermal liquid, Cl_T and H_T, respectively, are reconstructed, by means of the enthalpy- chloride plot and other geothermometric techniques. The following step is the calculation of the flow of thermal component, q_T, contributed by each discharge of flowrate q_M:

$$q_T = q_M\, x, \qquad (11.1)$$

where the fraction of the thermal component x is given by Eqn. (6.1):

$$x = (Cl_M - Cl_F)/(Cl_T - Cl_F), \qquad (11.2)$$

which reduces to $x = Cl_M / Cl_T$, if $Cl_M >> Cl_F$. The total natural fluxes of water, Q_T, and heat, Φ_T, are then obtained by means of the simple equations:

$$Q_T = \Sigma\, q_T \qquad (11.3)$$

$$\Phi_T = H_T\, Q_T. \qquad (11.4)$$

In general the results of these calculations underestimate the potential of the geothermal systems, and this is particularly true for concealed systems.

11.2. The distribution of leakage indicators in groundwaters

A completely different approach was suggested by Tonani (1970), largely based on mining exploration strategy and on the transport of ammonia and boric acid in the

vapor phase, which were described and explained by him at Larderello and The Geysers. Tonani proposed to study the distribution of these substances, which he called leakage indicators, in groundwaters, in order to detect processes of steam leakage from deep-seated geothermal systems and determine thereby their presence and extension. After application of this methodology to many systems throughout the world, it turned out that (1) ammonia is often controlled by fortuitous leaching of organic-rich sediments and (2) boric acid anomalies caused by geothermal steam input are sometimes detectable in steam-heated pools but never in groundwaters.

On the other hand, a good correspondence was observed, in Tyrrhenian Central Italy (Marini and Chiodini, 1994; Chiodini et al., 1995c), between (1) surface areas of high CO_2 fluxes, outlined on the basis of P_{CO2} distribution in shallow waters and (2) areal extension of geothermal reservoirs of high enthalpy (Monte Amiata and Latera), medium enthalpy (Torre Alfina) and low enthalpy (Viterbo). These geothermal reservoirs, which are mainly made up of permeable carbonate rocks and are covered by impervious fine grained clastic rocks, act as traps of deeply originated CO_2. Gases rich in CO_2 are released towards the surface even through the relatively impervious layers of the cover rocks: these gases dissolve in part in shallow waters, and in part reach the atmosphere mainly through diffuse soil degassing. Therefore, high P_{CO2} values in groundwaters are effective indicators of the presence of geothermal reservoirs at depth and can be used to map their extension.

11.3. Diffuse CO_2 degassing through soil

Both laboratory tests and field surveys have proven that the best method to measure the soil CO_2 flux in geothermal and volcanic areas is the accumulation chamber method, which allows one to obtain reliable values of φCO_2 in the range 0.2 to over 10,000 g m^{-2} d^{-1}, i.e., from the low φCO_2 values sustained by decay of organic matter to the high φCO_2 values typical of steaming grounds (Chiodini et al., 1998).

The average run time for a φCO_2 measurement is about 1 minute. Thus detailed maps of φCO_2 can be obtained in a relatively short time. The φCO_2 is largely variable in space as shown by these maps that give prominence to active faults and fractures acting as uprising routes of deep CO_2-rich geothermal or magmatic gases. Maps of φCO_2 can be used to estimate the total diffuse CO_2 output from the entire system provided that a sufficiently large numbers of measurements are performed. Moreover these maps allow one to select restricted areas where repeated measurements of φCO_2 can be carried out to investigate the temporal evolution of the system.

Recent measurements of diffuse CO_2 degassing through soil in the fumarolic areas of the Lakki plain, Nisyros Island, Greece (Brombach, 2000; Brombach et al., 2000b), and Solfatara di Pozzuoli, Campi Flegrei, Italy (Chiodini et al., 2000b), coupled with temperature measurements at 10 cm depth, have shown that there is a good correspondence between high φCO_2 and high temperature areas (Fig. 11.1).

This suggests that both upflow of hot fluids from the underlying boiling hydrothermal reservoir and steam condensation in the subsoil are responsible for the high φCO_2 values and the elevated soil temperatures. At Nisyros, a total hydrothermal CO_2 flux of ~ 68 t d^{-1} was calculated for the surveyed area of 1.3 km^2 in 1997. Assuming that the diffuse gas is derived from hydrothermal fluids having the same chemical composition of those discharged by nearby fumaroles and that their chemistry is not biased by steam condensation, it turns out that this hydrothermal CO_2 is accompanied by a flux of steam of 2200 t d^{-1}, corresponding to a heat flux of ~ 58 MW. Following the same approach, a heat flux of 88 MW was obtained for the Solfatara of Pozzuoli (Chiodini et al., 2000b), where the diffuse degassing area is ~0.5 km^2, the hydrothermal CO_2 flux is 1520 t d^{-1} and the steam flux is 3350 t d^{-1}.

Both at Nisyros and Solfatara, the heat flux was also computed from thermal gradient measurements in the soil (0-40 cm), assuming a reasonable value for the thermal conductivity of soil. The fluxes of thermal energy computed from φCO_2 data agree with those obtained from thermal gradient measurements, supporting the hypothesised conceptual model.

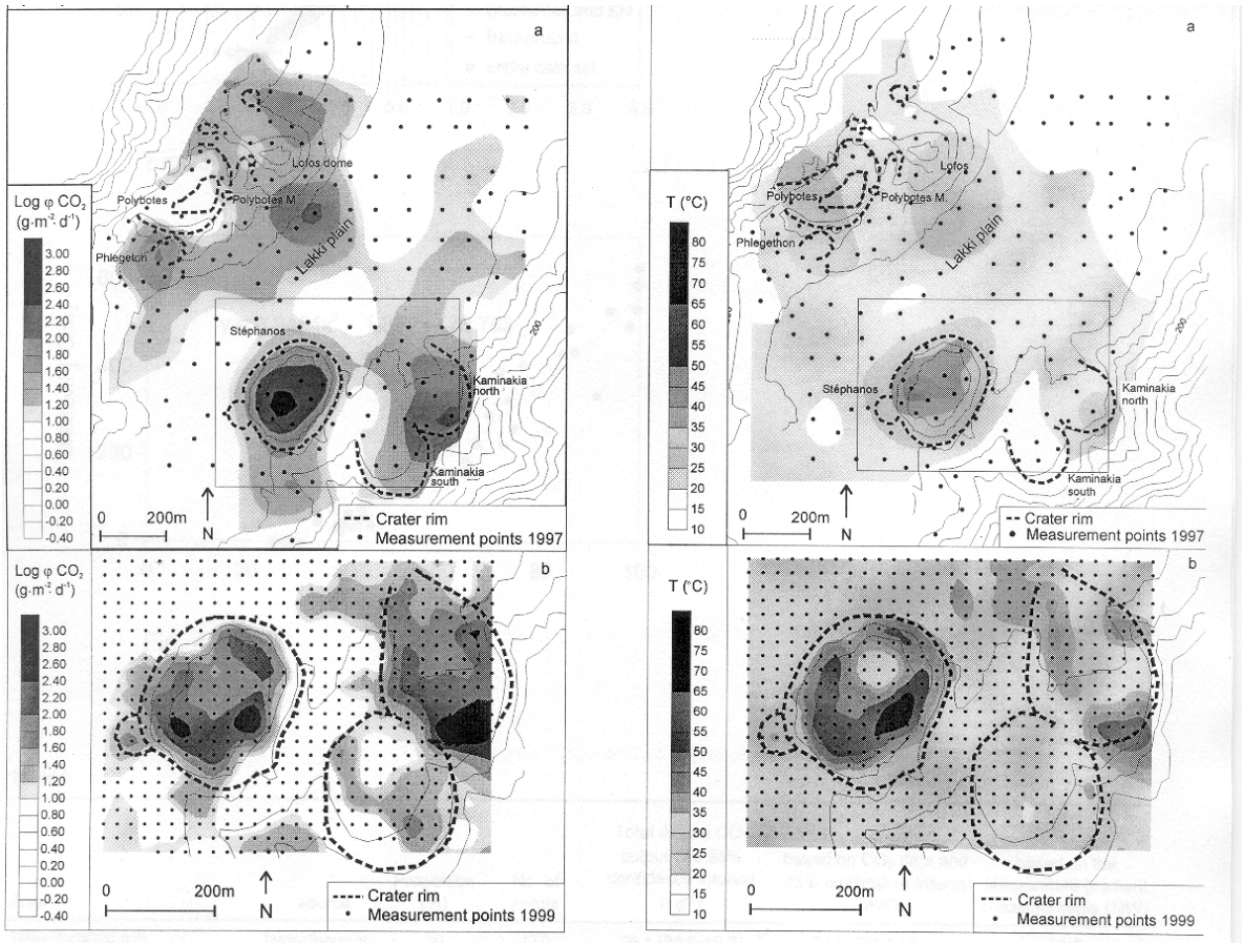

Fig. 11.1 Contour maps of log φCO_2 (left) and temperature at 10 cm depth (right) for the southern part of the Lakki plain, Nisyros Island, Greece (from Brombach, 2000; Brombach et al., 2000b)

These first results obtained at Nisyros and Solfatara show that the direct expulsion of hydrothermal gases from relatively small diffuse degassing areas is the main process through which these volcanic-hydrothermal systems dissipate thermal energy. CO_2 flux measurements constitute, therefore, a powerful tool to quantify these phenomena, which are of upmost importance in geothermal exploration.

References

Aguilera E., Chiodini G., Cioni R., Guidi M., Marini L., Raco B. (2000). Water chemistry of Lake Quilotoa (Ecuador) and assessment of natural hazards. *Journal of Volcanology and Geothermal Research* **97**, 271-285

Antrodicchia E., Cioni R., Chiodini G., Gagliardi R., Marini L. (1985). Geochemical temperatures of the thermal waters of Phlegraean Fields (Naples, Italy). *Geotherm. Res. Counc. Trans*. **9**, 287-292.

Arnórsson S. (1987) Gas chemistry of the Krísuvík geothermal field, Iceland, with special reference to evaluation of steam condensation in upflow zones. *Jökull* **37**, 32-47.

Arnórsson S. (1990) Gas chemistry of geothermal systems. In *Geochemistry of Gaseous Elements and Compounds* (S.S. Augustithis Ed.), Theophrastus, Athens, 187-222.

Arnórsson S. and Gunnlaugsson E. (1985) New gas geothermometers for geothermal exploration - Calibration and application. *Geochim. Cosmochim. Acta* **49**, 1307-1325.

Arnórsson S., Björnsson S., Muna Z.W., Bwire-Ojiambo S. (1990) The use of gas chemistry to evaluate boiling processes and initial steam fractions in geothermal reservoirs with an example from the Olkaria field, Kenya. *Geothermics* **19**, 497-514.

Arnorsson S., Gunnlaugsson E., Svavarsson (1983) The chemistry of geothermal waters in Iceland. III. Chemical geothermometry in geothermal investigations. *Geochim Cosmochim Acta* **47**, 567-577

Barbier E. (1997) Nature and technology of geothermal energy: a review. *Renewable and Sustainable Energy Reviews*, **1**, 1-69.

Bertrami R., Cioni R., Corazza E., D'Amore F., Marini L. (1985). Carbon monoxide in geothermal gases. Reservoir temperature calculations at Larderello (Italy). *Geotherm. Res. Counc. Trans*. **9**, 299-303.

Bischoff J.L. and Pitzer K.S. (1989) Liquid-vapor relations for the system NaCl-H_2O: summary of the P-T-X surface from 300°C to 500°C. *Am. J. Sci.* **289**, 1217-1248.

Bonham H.R. (1986) Models for volcanic-hosted epithermal precious metal deposits:a review. *Proc, 5th Int, Volcanology Cong*., Auckland, NZ, 13-17.

Bowers T.S., Jackson K.J., Helgeson H.C. (1984). *Equilibrium activity diagrams for coexisting minerals and aqueous solutions at pressures and temperatures to 5 kb and 600 °C*. Springer, 397 pp.

Brantley S.L., Borgia A., Rowe G., Fernandez J.F., Reynolds J.R. (1987) Poás volcano acts as a condenser for acid metal-rich brine. *Nature* **330**, 470-472.

Brombach T. (2000) *Fluid geochemistry of hydrothermal systems in volcanic island arcs: Guadeloupe (Lesser Antilles) and Nisyros (Greece).* Ph. D. Thesis. Université de Lausanne.

Brombach T., Cardellini C., Chiodini G., Cioni R., Hunziker J.C., Marini L. (2000a) Origin of the fumarolic fluids of Nisyros, Greece, and isotopic evidence for a magmatic contribution. *Bull. Volcanol.* (submitted)

Brombach T., Cardellini C., Chiodini G., Hunziker J.C., Marini L. (2000b) Soil diffuse degassing and thermal energy fluxes from the southern Lakki plain, Nisyros (Greece). *Geophys. Res. Lett.* (submitted)

Brombach T., Marini L., Hunziker J.C. (2000c) Geochemistry of the thermal springs and fumaroles of Basse-Terre island, Guadaloupe, Lesser Antilles. *Bull. Volcanol* **61**, 477-490.

Browne P.R.L. (1970) Hydrothermal alteration as an aid in investigating geothermal fields. *Geothermics*, Spec. Issue **2**, 564-570.

Browne P.R.L. (1977) *Hydrothermal alteration in active geothermal fields*. N. Z. Geol. Surv., unpublished report M58, 57 pp.

Browne P.R.L. (1982) Mapping of geothermal discharge features. In *Introduction to geothermal prospecting* (M.P. Hochstein Ed.) Univ. of Auckland Publ., 67-69.

Casadevall T.J., De La Cruz-Reyna S., Rose W.I., Bagley S., Finnegan D.L., Zoller W.H. (1984) Crater lake and post-eruption hydrothermal activity, El Chichón volcano, Mexico. *J. Volcanol. Geotherm. Res*. **23**, 169-191.

Chan S.H. (1989) A review on solubility and polymerization of silica. *Geothermics* **18**, 49-56.

Chen C.T. and Marshall W.L. (1982) Amorphous silica solubilities – IV. Behavior in pure water and aqueous sodium chloride, sodium sulfate, magnesium chloride, magnesium sulfate solutions up to 350°C. *Geochim. Cosmochim. Acta* **46**, 279-287.

Chiodini G. (1994) Temperature, pressure and redox conditions governing the composition of the cold CO_2 gases discharged in north Latium (Central Italy). *Appl. Geochem*. **9**, 287-295.

Chiodini G. and Cioni R. (1989) Gas geobarometry for hydrothermal systems and its application to some Italian geothermal areas. *Appl. Geochem*. **4**, 465-472.

Chiodini G and Marini L (1998) Hydrothermal gas equilibria: The H_2O-H_2-CO_2-CO-CH_4 system. *Geochim. Cosmochim. Acta* **62**, 2673-2687.

Chiodini, G., Cioni, R., Guidi, M., Marini, L. (1991a) Chemical geothermometry and geobarometry in hydrothermal aqueous solutions: a theoretical investigation based on a mineral-solution equilibrium model. *Geochim. Cosmochim. Acta* **55**, 2709-2727.

Chiodini G., Cioni R., Raco B., Scandiffio G. (1991b) Carbonyl sulphide (COS) in geothermal fluids: an example from the Larderello field (Italy). *Geothermics* **20**, 319-327.

Chiodini G., Cioni R., Guidi M., Marini L., Raco B., Taddeucci G. (1992) Gas geobarometry in boiling hydrothermal systems: a possible tool to evaluate the hazard of hydrothermal explosions. *Acta Vulcanologica, Marinelli Vol.* **2**, 99-107.

Chiodini G., Cioni R., Marini L. (1993) Reactions governing the chemistry of crater fumaroles from Vulcano Island, Italy, and implications for volcanic surveillance. *Appl. Geochem.* **8**, 357-371.

Chiodini G., Cioni R., Marini L., Panichi C. (1995a) Origin of the fumarolic fluids of Vulcano Island, Italy, and implications for volcanic surveillance. *Bull. Volcanol.* **57**, 99-110.

Chiodini G., Frondini F., Marini L. (1995b) Theoretical geothermometers and geobarometers for aqueous solutions coming from hydrothermal systems of medium-low temperature hosted into carbonate-evaporite rocks. Application to the thermal springs of the Etruscan Swell, Italy. *Appl. Geochem.* **10**, 337-346.

Chiodini G., Frondini F., Ponziani F. (1995c) Deep structures and carbon dioxide degassing in Central Italy. *Geothermics* **24**, 81-94

Chiodini G., Cioni R., Frullani A., Guidi M., Marini L., Prati F., Raco B. (1996a). Fluid geochemistry of Montserrat Island, West Indies. *Bull. Volcanol.* **58**, 380-392.

Chiodini G., Cioni R., Guidi M., Magro G., Marini L., Panichi C., Raco B., Russo M. (1996b). Chemical and isotopic variations of Bocca Grande fumarole (Solfatara volcano, Phlegrean Fields). *Acta Vulcanologica* **8**, 228-232

Chiodini G., Cioni R., Guidi M., Raco B., Marini L. (1998) Soil CO_2 flux measurements in volcanic and geothermal areas. *Appl. Geochem.* **13**, 543-552.

Chiodini G., Allard P., Caliro S., Parello F. (2000a) ^{18}O exchange between steam and carbon dioxide in volcanic and hydrothermal gases: isotopic and genetic implications. *Geochim. Cosmochim. Acta* **64**, 2479-2488

Chiodini G., Frondini F., Cardellini C., Granieri D., Ventura G., Marini L. (2000b) CO_2 degassing and energy release at Solfatara volcano, Campi Flegrei, Italy. *J. Geophys. Res.* (submitted)

Chiodini G., Marini L., Russo M. (2000c). Geochemical evidences of a high-temperature hydrothermal brines at Vesuvius volcano (Italy). *Geochim. Cosmochim. Acta* (submitted).

Christenson B.W. and Wood C.P. (1993) Evolution of a vent-hosted hydrothermal system beneath Ruapehu Crater Lake, New Zealand. *Bull. Volcanol*. **55**, 547-565.
Cioni R., Fanelli G., Guidi M., Kinyariro J.K., Marini L. (1992). Lake Bogoria hot springs (Kenya): geochemical features and geothermal implications. *J. Volcanol. Geotherm. Res.* **50**, 231-246.
Craig H. (1963) The isotopic geochemistry of water and carbon in geothermal areas. In *Nuclear geology in geothermal areas* (E. Tongiorgi, Ed.), Spoleto, 17-53.
D'Amore F. (1991) Gas geochemistry as a link between geothermal exploration and exploitation. In *Application of Geochemistry in Geothermal Reservoir Development*. (F. D'Amore, co-ordinator), UNITAR, 93-117.
D'Amore F. and Celati R. (1983) Methodology for calculating steam quality in geothermal reservoir. *Geothermics* **12**, 129-140.
D'Amore F. and Gianelli G. (1984) Mineral assemblages and oxygen and sulfur fugacities in natural water-rock interaction processes. *Geochim. Cosmochim. Acta* **48**, 847-857.
D'Amore F. and Nuti S. (1977) Notes on the chemistry of geothermal gases. *Geothermics* **6**, 39-45.
D'Amore F. and Panichi C. (1980) Evaluation of deep temperature of hydrothermal systems by a new gas-geothermometer. *Geochim. Cosmochim. Acta* **44**, 549-556.
Davis JC (1986) *Statistics and data analysis in geology*. 2nd Ed. Wiley.
Delfin Jr F.G., Sussman D., Ruaya R.G., Reyes A.G. (1992) Hazard assessment of the Pinatubo volcanic-geothermal system: clues prior to the June 15, 1991 eruption. *Geotherm. Res. Counc. Trans*. **16**, 519-527.
Delmelle P. and Bernard A. (1994) Geochemistry, mineralogy, and chemical modeling of the acid crater lake of Kawah Ijen Volcano, Indonesia. *Geochim. Cosmochim. Acta* **58**, 2445-2460.
Dittman G.L. (1977) *Calculation of brine properties*. Lawrence Livermore Laboratory. Report UCID-17406.
Drummond S.E. (1981) *Boiling and mixing of hydrothermal fluids: chemical effects on mineral precipitation*. Ph.D. thesis, Pennsylvania State University.
Ellis A.J. (1962) Interpretation of gas analyses from the Wairakei hydrothermal area. *N.Z.J.Sci.* **5**, 434-452.
Ellis A.J. (1970) Quantitative interpretation of chemical characteristics of hydrothermal systems. *Geothermics*, Spec. Issue **2**, 516-528.
Ellis A.J. (1971) Magnesium ion concentrations in the presence of magnesium chlorite, calcite, carbon dioxide, quartz. *Amer. J. Sci*. **271**, 481-489.
Ellis A.J. and Golding R.M. (1963) The solubility of carbon dioxide above 100°C in water and in sodium chloride solutions. *Amer. J. Sci.* **261**, 47-60.
Ellis A.J. and Mahon W.A.J. (1964) Natural hydrothermal systems and experimental hot water/rock interactions. *Geochim. Cosmochim. Acta* **28**, 1323-1357.
Ellis A.J. and Mahon W.A.J. (1967) Natural hydrothermal systems and experimental hot water/rock interactions (Part II). *Geochim. Cosmochim. Acta* **31**, 519-538.
Ellis A.J. and Mahon W.A.J. (1977) *Chemistry and Geothermal Systems*, Academic Press, 392 pp.
Ellis A.J. and Wilson S.H. (1960) The geochemistry of alkali metal ions in the Wairakei hydrothermal system. *N.Z.J. Geol. Geophys.* **3**, 593-617.
Faure G. (1986) *Principles of Isotope Geology*. 2nd Ed. Wiley, New York.
Fleming B.A. and Crerar D.A. (1982) Silicic acid ionization and calculation of silica solubility at elevated temperature and pH. Application to geothermal fluid processing and reinjection. *Geothermics* **11**, 15-29.

Fouillac C. and Michard G. (1981) Sodium/lithium ratios in water applied to geothermometry of geothermal reservoirs. *Geothermics* **10**, 55-70.
Fournier R.O. (1973) Silica in thermal waters: laboratory and field investigations. *Proc. Int.l Symp. Hydrogeochemistry and Biogeochemistry, Tokyo*, pp. 122-139.
Fournier R.O. (1979a) Geochemical and hydrological considerations and the use of enthalpy-chloride diagrams in the prediction of underground conditions in hot-spring systems. *J. Volcanol. Geotherm. Res*. **5**, 1-16.
Fournier R.O. (1979b) A revised equation for the Na/K geothermometer. *Geotherm. Res. Counc. Trans*. **5**,1-16.
Fournier R.O. (1985) The behavior of silica in hydrothermal solutions. In *Geology and Geochemistry of Epithermal Systems* (B.R. Berger and P.M. Bethke, Eds) *Rev. Econ. Geol.* **2**, 45-61.
Fournier R.O. (1991) Water geothermometers applied to geothermal energy. In *Application of Geochemistry in Geothermal Reservoir Development.* (F. D'Amore, co-ordinator), UNITAR, 37-69.
Fournier R.O. and Marshall W.L. (1983) Calculation of amorphous silica solubilities at 25° to 300°C and apparent cation hydration numbers in aqueous salt solutions using the concept of effective density of water. *Geochim. Cosmochim. Acta* **47**, 587-596.
Fournier R.O. and Potter R.W. (1979) Magnesium correction to the Na-K-Ca chemical geothermometer. *Geochim. Cosmochim. Acta* **43**, 1543-1550.
Fournier R.O. and Potter R.W.II (1982) A revised and expanded silica (quartz)geothermometer. *Geothermal Resources Council Bulletin* **11**, 3-12.
Fournier R.O. and Rowe J.J. (1977) The solubility of amorphous silica in water at high temperatures and high pressures. *Am. Min*. **62**, 1052-1056.
Fournier R.O. and Truesdell A.H. (1973) An empirical Na-K-Ca geothermometer for natural waters. *Geochim. Cosmochim. Acta* **37**, 1255-1275.
Friedman I. and O'Neil J.R. (1977) *Compilation of stable isotope fractionation factors of geochemical interest.* U.S. Geological Survey Professional Paper 440.44.
Fudali R.F. (1965) Oxygen fugacities of basaltic and andesitic magmas. *Geochim. Cosmochim. Acta* **29**, 1063-1075.
Fytikas M., Kavouridis T., Leonis C., Marini L. (1989). Geochemical exploration of the three most significant geothermal areas of Lesbos Island, Greece. *Geothermics* **18**, 465-475.
Giggenbach W.F. (1975a) A simple method for the collection and analysis of volcanic gas samples. *Bull. Volcanol.* **39**, 132-145.
Giggenbach W.F. (1975b) The chemistry of Crater Lake, Mt. Ruapehu (New Zealand) during and after the 1971 active period. *N.Z.J. Sci*. **17**, 33-45.
Giggenbach W.F. (1978) The isotopic composition of waters from the El Tatio geothermal field, northern Chile. *Geochim. Cosmochim. Acta* **42**, 979-988
Giggenbach W.F. (1980) Geothermal gas equilibria. *Geochim. Cosmochim. Acta* **44**, 2021-2032.
Giggenbach W.F. (1984) Mass transfer in hydrothermal alterations systems. *Geochim. Cosmochim. Acta* **48**, 2693-2711.
Giggenbach W.F. (1987) Redox processes governing the chemistry of fumarolic gas discharges from White Island, New Zeland. *Appl. Geochem.* **2**, 143-161.
Giggenbach W.F. (1988) Geothermal solute equilibria. Derivation of Na-K-Mg-Ca geoindicators. *Geochim. Cosmochim. Acta* **52**, 2749-2765.
Giggenbach W.F. (1991a) Chemical techniques in geothermal exploration. In *Application of Geochemistry in Geothermal Reservoir Development.* (F. D'Amore, co-ordinator), UNITAR, 119-144.

Giggenbach W.F. (1991b) Isotopic composition of geothermal water and steam discharges. In *Application of Geochemistry in Geothermal Reservoir Development*. (F. D'Amore, co-ordinator), UNITAR, 253-273.

Giggenbach WF (1992a) Isotopic shifts in waters from geothermal and volcanic systems along convergent plate boundaries and their origin. *Earth Planet. Sci. Lett.* **113**, 495-510

Giggenbach W.F. (1992b) The composition of gases in geothermal and volcanic systems as a function of tectonic setting. In *Proc. 7th Int. Symp. Water-Rock Interaction*, Park City, Utah, 873-878

Giggenbach W.F. (1993) Redox control of gas compositions in Philippine volcanic-hydrothermal systems. *Geothermics* **22**, 575-587.

Giggenbach W.F. (1996) Chemical composition of volcanic gases. In: *Monitoring and Mitigation of Volcano Hazards* (R. Scarpa and R.I. Tilling, Eds.) Springer, 221-256

Giggenbach W.F. (1997a) The origin and evolution of fluids in magmatic-hydrothermal systems. In: *Geochemistry of hydrothermal ore deposits, 3d Edition* (H. L. Barnes, Ed.), Wiley, 737-796.

Giggenbach W.F. (1997b) Relative importance of thermodynamic and kinetic processes in governing the chemical and isotopic composition of carbon gases in high-heatflow sedimentary basins. *Geochim. Cosmochim. Acta* **61**, 3763-3785.

Giggenbach W.F. and Stewart M.K. (1982) Processes controlling the isotopic composition of steam and water discharges from steam vents and steam-heated pools in geothermal areas. *Geothermics* **11**, 71-80.

Giggenbach W.F. and Goguel R.L. (1989) *Collection and analysis of geothermal and volcanic water and gas discharges*. Report No. CD 2401. Department of Scientific and Industrial Research. Chemistry Division. Petone, New Zealand.

Giggenbach W.F. and Corrales Soto R. (1992) The isotopic and chemical composition of water and steam discharges from volcanic-magmatic-hydrothermal systems of the Guanacaste Geothermal Province, Costa Rica. *Appl. Geochem*. **7**, 309-332.

Giggenbach W.F. and Matsuo S. (1991) Evaluation of results from second and third IAVCEI field workshop on volcanic gases, Mt Usu, Japan, and White Island, New Zealand. *Appl. Geochem*. **6**, 125-141

Giggenbach W.F. and Poreda R.J. (1993) Helium isotopic and chemical composition of gases from volcanic-hydrothermal systems in the Philippines. *Geothermics* **22**, 369-380.

Giggenbach W.F., Gonfiantini R., Jangi B.L., Truesdell A.H. (1983) Isotopic and chemical composition of Parbati Valley geothermal discharges, NW-Himalaya, India. *Geothermics* **12**, 199-222.

Giggenbach W.F., Sheppard D.S., Robinson B.W., Stewart M.K., Lyon G.L. (1994) Geochemical structure and position of the Waiotapu geothermal field, New Zealand. *Geothermics* **23**, 599-644

Glover R.B. (1970) Interpretation of gas compositions from the Wairakei field over 10 years. *Geothermics,* Spec. Issue **2**,1355-1366.

Goguel R.L. (1983) The rare alkalies in hydrothermal alteration at Wairakei and Broadlands geothermal fields, NZ. *Geochim. Cosmochim. Acta* **47**, 429-437.

Guidi M., Marini L., Scandiffio G., Cioni R. (1990). Chemical geothermometry in hydrothermal aqueous solutions: the influence of ion complexing. *Geothermics*, **19**, 415-441.

Heald P., Foley N.K., Hayba D.O. (1987) Comparative anatomy of volcanic-hosted epithermal deposits: acid-sulfate and adularia-sericite deposits. *Econ. Geol*. **82**, 1-26.

Hedenquist J.W. (1986) Geothermal systems in the Taupo volcanic zone; their characteristics and relation to volcanism and mineralisation. In: *Late Cenozoic volcanism in New Zealand* (I.E.M. Smith, Ed.) *Bulletin – Royal Society of New Zealand* **23**, 134-168.

Hedenquist J.W. (1987) Mineralisation associated with volcanic-related hydrothermal systems in the Circum-Pacific Basin. *Trans. 4th Circum-Pacific Energy and Mineral Resources Conference*, Singapore, 513-524.

Hedenquist J.W. and Lowenstern J.B. (1994) The role of magmas in the formation of hydrothermal ore deposits. *Nature* **370**, 519-526

Helgeson H.C., Kirkham D.H., Flowers G.C. (1981) Theoretical prediction of the behavior of aqueous electrolytes at high pressures and temperatures: Calculation of activity coefficients, osmotic coefficients, and apparent molal, and standard and relative partial molal properties to 600°C and 5kb. *Am. J. Sci.* **281**, 1249-1516

Hemley J.J. (1967) Aqueous Na/K ratios in the system K_2O-Na_2O-Al_2O_3-SiO_2-H_2O. *Program, 1967 Ann. Meeting Geol. Soc. Amer. New Orleans*, 94-95.

Henley, R.W. and Ellis, A.J. (1983) Geothermal systems, ancient and modern: a geochemical review. *Earth Science Review* **19**, 1-50.

Henley R.W., Truesdell A.H., Barton P.B.Jr, Whitney J.A. (1984) Fluid-mineral equilibria in hydrothermal systems. *Reviews in Economic Geology* **1**, 267 pp.

Horita J. and Wesolowski D.J. (1994) Liquid-vapor fractionation of oxygen and hydrogen isotopes of water from the freezing to the critical temperature. *Geochim. Cosmochim. Acta* **58**, 3425-3437.

Horita J., Cole D.R., Wesolowski D.J. (1995) The activity-composition relationship of oxygen and hydrogen isotopes in aqueous salt solutions: III. Vapor-liquid water equilibration of NaCl solutions to 350°C. *Geochim. Cosmochim. Acta* **59**, 1139-1151.

Hulston J.R. and McCabe W.J. (1962) Mass spectrometer measurements in the thermal areas of New Zealand. *Geochim. Cosmochim. Acta* **26**, 383-397.

Janik C.J., Truesdell A.H., Goff F., Shevenell L., Stallard M.L., Trujillo P.E. Jr., Counce D. (1991) A geochemical model of the Platanares geothermal system, Honduras. *J. Volcanol. Geotherm. Res*. **45**, 125-146.

Kavouridis T., Kuris D., Leonis C., Liberopoulou V., Leontiadis, J., Panichi C., La Ruffa G., Caprai A. (1999) Isotope and chemical studies for a geothermal assessment of the island of Nisyros (Greece). *Geothermics* **28**, 219-239.

Keenan J.H., Keyes F.G., Hill P.G., Moore J.G. (1969) Steam tables. Thermodynamic properties of water including vapor, liquid, and solid phases (international system of units-S.I.). Wiley, 162 pp.

Kennedy, V.C. and Zellweger, G.W., 1974. Filter pore-size effects on the analysis of Al, Fe, Mn, and Ti in water. *Water Resour. Res*. **10**, 785-790.

Kharaka Y.K. and Mariner R.H. (1989) Chemical geothermometers and their application to formation waters from sedimentary basins. In: *Thermal History of Sedimentary Basins* (N.D. Naeser and T.H. McCollon, Eds.), Springer, 99-117.

Kieffer S.W. (1982) Thermodynamics and lattice vibrations of minerals: 5. Applications to phase equilibria, isotopic fractionation, and high pressure thermodynamic properties. *Rev. Geophys. Space Phys.* **20**, 827-849.

Kita I., Nitta K., Nagao K., Taguchi S., Koga A. (1993) Difference in N_2/Ar ratio of magmatic gases from northeast and southwest Japan: New evidence for different states of plate subduction. *Geology* **21**, 391-394

Knight C.L. and Bodnar R.J. (1989) Synthetic fluid inclusions: IX. Critical properties of NaCl-H_2O solutions. *Geochim. Cosmochim. Acta* **53**, 3-8.

Kozintseva T.N. (1964) Solubility of hydrogen sulphide in water at elevated temperatures. *Geochem. Intl.*, 750-756.

Kozintseva T.N. (1965) Solubility of hydrogen sulphide in water and in salt solutions at elevated temperatures. In: *Geochemical investigation in the field of higher temperatures and pressures* (N.I. Khitarov, Ed.), Nauka, Moscow, 121-134

Laxen, D.P.H. and Chandler, I.M., 1982. Comparison of filtration techniques for size distribution in freshwater. *Anal. Chem*. **54**, 1350-1355.

La Ruffa G., Panichi C., Kavouridis T., Liberopoulou V., Leontiadis J., Caprai A. (1999) Isotope and chemical assessment of geothermal potential of Kos Island, Greece. *Geothermics* **28**, 205-217.

Marini L. and Chiodini G. (1994). The role of carbon dioxide in the carbonate-evaporite geothermal systems of Tuscany and Latium (Italy). *Acta Vulcanologica* **5**, 95-104.

Marini L. and Cioni R. (1985). A chloride method for the determination of the enthalpy of steam/water mixtures discharged from geothermal wells. *Geothermics* **14**, 29-34

Marini L., Agostini A., Cioni R., Guidi M., Leon O. (1991) Guagua Pichincha volcano, Ecuador: fluid geochemistry in volcanic surveillance. *J. Volcanol. Geotherm. Res.* **46**, 21-35.

Marini L., Bonaria V., Guidi M., Hunziker J.C., Ottonello G., Vetuschi Zuccolini M. (2000) Fluid geochemistry of the Acqui Terme-Visone geothermal area (Piemonte, Italy). *Appl. Geochem.* **15**, 917-935.

Marini L., Chiodini G., Cioni R. (1986). New geothermometers for carbonate-evaporite geothermal reservoirs. *Geothermics* **15**, 77-86.

Marshall W.L. (1980) Amorphous silica solubilities - III. Activity coefficient relations and predictions of solubility behavior in salt solutions, 0-350°C. *Geochim. Cosmochim. Acta* **44**, 925-931.

Martinotti G., Marini L., Hunziker J.C., Perello P., Pastorelli S. (1999). Geochemical and geothermal study of springs in the Ossola-Simplon region. *Eclogae Geol. Helv.*, **92**, 295-305.

Marty B, Jambon A, Sano Y (1989) Helium isotopes and CO_2 in volcanic gases of Japan. *Geology* **76,** 25-40.

Matsuo S., Suzuki M., Mizutani Y. (1978) Nitrogen to agron ratio in volcanic gases. *Adv. Earth Planet. Sci.* **3**, 17-25

Michard G., Fouillac C., Grimaud D., Denis J. (1981) Une méthode globale d'estimation des températures des resérvoirs alimentant les sources thermales. Exemple du Massif Central Français. *Geochim. Cosmochim. Acta* **45**, 1199-1207.

Murray C. and Cubicciotti D. (1983) Thermodynamics of aqueous sulfur species to 300°C and potential-pH diagrams. *J. Electrochem. Soc*. **38**, 863-869.

Naumov G.B., Ryzhenko B.N., Khodakovsky I.L. (1974) *Handbook of thermodynamic data*. Report No. USGS-WRD-74-001. U.S. Geological Survey. Water Resources Division, Menlo Park, California.

Nehring N.L. and D'Amore F. (1984) Gas chemistry and thermometry of the Cerro Prieto, Mexico, geothermal field. *Geothermics* **13**, 75-89.

O'Neil J.R. (1986) Theoretical and experimental aspects of isotopic fractionation. In: *Stable isotopes in high temperature geological processes* (J.W. Valley, H.P. Taylor, Jr., J.R. O'Neil, Eds.) *Reviews in Mineralogy* **16**, 1-40.

Orville P.M. (1963) Alkali ion exchange between vapor and feldspar phases. *Amer. J. Sci.* **261**, 201-237

Paces T. (1975) A systematic deviation from Na-K-Ca geothermometer below 75°C and above 10^{-4} atm P_{CO2}. *Geochim. Cosmochim. Acta* **39**, 541-544.

Pang Z.-H. and Reed M. (1998) Theoretical chemical thermometry on geothermal waters: Problems and methods. *Geochim. Cosmochim. Acta* **62**, 1083-1091.

Pastorelli S., Marini L., Hunziker J.C. (1999). Water chemistry and isotope composition of the Acquarossa thermal system, Ticino, Switzerland. *Geothermics*, **28**, 75-93.

Pastorelli S., Marini L., Hunziker J.C. (2000). Chemistry, isotope values (δD, $\delta^{18}O$, $\delta^{34}S_{SO4}$) and temperatures of the water inflows in two Gotthard tunnels, Swiss Alps. *Appl. Geochem.* (in press).

Perello P., Marini L., Martinotti G., Hunziker J.C. (2000). The thermal circuits of the Argentera Massif (western Alps, Italy): an example of low-enthalpy geothermal resources controlled by Neogene alpine tectonics. *Eclogae Geol. Helv.* (submitted)

Pitzer K.S. (1981) Characteristics of very concentrated solutions. In: Chemistry and *Geochemistry of Solutions at High Temperatures and Pressures* (D.T. Rickard and F.E. Wickman Eds.), Pergamon, 249-264.

Poorter R.P.E., Varekamp J.C., van Bergen M.J., Kreulen B., Siriwana T., Vrool P.Z., Wirakusumah A.D. (1989) The Sirung volcanic boiling spring: an extreme chloride-rich, acid brine on Pantar (Lesser Sunda Islands, Indonesia). *Chem. Geol*. **76**, 215-228.

Reed M.H. (1982) Calculation of multicomponent chemical equilibria and reaction processes in systems involving minerals, gases and an aqueous phase. *Geochim. Cosmochim. Acta* **46**, 513-528.

Reed M.H. (1997) Hydrothermal alteration and its relationship to ore fluid composition. In: G*eochemistry of hydrothermal ore deposits, 3d Edition* (H. L. Barnes, editor), Wiley, 517-611.

Reed M.H. and Spycher N.F. (1984) Calculation of pH and mineral equilibria in hydrothermal waters with application to geothermometry and studies of boiling and dilution. *Geochim. Cosmochim. Acta* **48**, 1479-1492.

Reyes A.G. (1990) Petrology of Philippine geothermal systems and the application of alteration mineralogy to their assessment. . *J. Volcanol. Geotherm. Res*. **43**, 279-309.

Reyes A.G. and Giggenbach W.F. (1992) Petrology and fluid chemistry of magmatic-hydrothermal systems in the Philippines. In: *Water-Rock Interaction* (Y.K. Kharaka and A.S. Maest, Eds.) A.A. Balkema, Rotterdam, 1341-1344.

Richet P. and Bottinga Y. (1976) L'energie de zero des molecules et le fractionnement des isotopes stables. *C. R. Acad. Sci. Paris*, B, 425-428.

Richet P., Bottinga Y., Javoy M. (1977) A review of H, C, N, O, S and Cl stable isotope fractionation among gaseous molecules. *Ann Rev. Earth Planet. Sci. Lett*. **5**, 65-110.

Rimstidt J.D. and Barnes H.L. (1980). The kinetics of silica-water reactions. *Geochim. Cosmochim. Acta* **44**, 1683-1699.

Rowe Jr G.L., Ohsawa S., Takano B., Brantley S.L., Fernandez J.F., Barquero J. (1992) Using crater lake chemistry to predict volcanic activity at Poas volcano, Costa Rica. *Bull. Volcanol*. **54**, 494-503.

Ryzhenko B.N. and Malinin S.D. (1971) The fugacity rule for the systems CO2-H2O, CO2-CH4, CO2-N2, and CO2-H2. *Geochem. Int.* 562-574.

Ryzhenko B.N. and Volkov V.P. (1971) Fugacity coefficients of some gases over a broad range of temperatures and pressures. *Geochem. Int.* 468-481.

Sano Y. and Marty B. (1995) Origin of carbon in fumarolic gas from the island arcs. *Chem. Geol*. **119**, 265-274.

Seward T.M.S. (1974) Equilibrium and oxidation potential in geothermal waters at Broadlands, New Zealand. *Am. J. Sci.* **274**, 190-192.

Steiner A. (1977) The Wairakei geothermal area, North Island, New Zealand. *N. Z. Geol. Surv. Bull.*, **90**, 136 pp.
Stolper E.M. and Newman S. (1994) The role of water in the petrogenesis of Mariana Trough magmas. *Earth Planet. Sci. Lett.* **121**, 293-325.
Stull D.R., Westrum E.F., Sinke G.G. (1969) *The chemical thermodynamics of organic compounds*. Wiley.
Suleimenov O.M. and Krupp R.E. (1994) Solubility of hydrogen sulfide in pure water and in NaCl solutions, from 20 to 320°C and at saturation pressures. *Geochim. Cosmochim. Acta* **58**, 2433-2444.
Sussman D., Javellana S.P., Benavidez P.J. (1993) Geothermal energy development in the Philippines: an overview. *Geothermics* **22**, 353-367.
Takano B. and Watanuki K. (1990) Monitoring of volcanic eruptions at Yugama crater lake by aqueous sulfur oxyanions. *J. Volcanol. Geotherm. Res*. **40**, 71-87.
Tanger J.C. IV and Pitzer K.S. (1989) Thermodynamics of NaCl-H_2O: a new equation of state for the near-critical region and comparison with other equations for adjoining regions. *Geochim. Cosmochim. Acta* **53**, 973-987.
Tonani F. (1970) Geochemical methods of exploration for geothermal energy. *Geothermics,* Spec. Issue **2**, 492-515.
Tonani F. (1973) Equilibria that control the hydrogen content of geothermal gases. *Unpublished Phillips Petroleum Co. report*.
Tonani F. (1980) Some remarks on the application of geochemical techniques in geothermal exploration. *Proc. Adv. Eur. Geoth. Res., 2nd Symp*, Strasbourg, 428-443.
Truesdell A.H. (1975) Geochemical techniques in exploration. *Proc. 2nd UN Symp. Development and Use of Geothermal Resources* **1**, 53-86.
Truesdell A.H. (1991) Origins of acid fluids in geothermal reservoirs. *Geotherm. Res. Counc. Trans*. **15**, 289-296.
Truesdell A.H. and Fournier R.O. (1977) Procedure for estimating the temperature of a hot-water component in a mixed water by using a plot of dissolved silica versus enthalpy. *U.S. Geol. Surv. J. Res*. **5**, 49-52.
Truesdell A.H. and Hulston J.R. (1980) Isotopic evidence on environments of geothermal systems. In: *Handbook of Environmental Isotope Geochemistry* (P. Fritz and J.Ch. Fontes, Eds) The Terrestrial Environment, A, Elsevier **1**, 179-226
Truesdell A.H., Nathenson M., Rye R.O. (1977) The effects of subsurface boiling and dilution on the isotopic compositions of Yellowstone thermal waters. *J. Geophys. Res.* **82**, 3694-3703
Varekamp JC, Kreulen R, Poorter RPE, Van Bergen MJ (1992) Carbon sources in arc volcanism, with implications for the carbon cycle. *Terra Nova* **4**, 363-373.
White D.E. (1957) Magmatic, connate, and metamorphic waters. *Geol. Soc. Amer. Bull.* **69**, 1659-1682.
White D.E. (1965) Saline waters of sedimentary rocks. In *Fluids in Subsurface Environments.* Symp. Amer. Assoc. Petroleum Geologists, 342-366.
White N.C. and Hedenquist J.W. (1990) Epithermal environments and styles of mineralisation: variations and their causes, and guidelines for exploration. *J. Geochem. Explor.* **36**, 445-474.
Wilhelm E., Battino R., Wilcock R.J. (1977) Low-pressure solubility of gases in liquid water. *Chemical Reviews* **77**, 219-262.